



NTNU – Trondheim
Norwegian University of
Science and Technology

Numerical Study of Wave Characteristics during Density Wave Oscillations in a horizontal, heated Channel

Jørn Lian

Master of Energy and Environmental Engineering

Submission date: July 2014

Supervisor: Maria Fernandino, EPT

Norwegian University of Science and Technology
Department of Energy and Process Engineering



Norwegian University
of Science and Technology

Department of Energy
and Process Engineering

EPT-M-2014-62

MASTER THESIS

for

Student Jørn Lian

Spring 2014

Numerical study of wave characteristics during density wave oscillations in a horizontal, heated channel

Numerisk studie av bølgekarakteristikk for oscillerende massetetthetsbølger i et oppvarmet, horisontalt rør

Background and objective

Density wave oscillations (DWO) are of common occurrence in industrial thermohydraulic systems. Such oscillations result from multiple feedback effects between the flow rate, vapour generation rate and pressure drop and they can be observed for instance in heat exchangers, boilers and gas lifted wells. Density wave oscillations can induce reduced efficiency, production losses and possible facility damages. For this reason, characterizing DWOs is of special interest for the design of industrial systems and equipment involving vapour generation.

In this work, numerical simulations of density wave oscillations in a heated, horizontal channel will be performed. The work will focus on wave characteristics (i.e. amplitude and period) for different pressure, subcooling and heating conditions.

The following tasks are to be considered:

1. Literature review on DWO phenomenon, with particular focus on wave characteristics for different operating conditions. Both experimental and numerical results should be included here.
2. Simulation of DWO and characterization of the effect of pressure, inlet subcooling and applied heat on the amplitude and period of the oscillations.
3. Comparison of results with experimental data.

-- ” --

Within 14 days of receiving the written text on the master thesis, the candidate shall submit a research plan for his project to the department.

When the thesis is evaluated, emphasis is put on processing of the results, and that they are presented in tabular and/or graphic form in a clear manner, and that they are analyzed carefully.

The thesis should be formulated as a research report with summary both in English and Norwegian, conclusion, literature references, table of contents etc. During the preparation of the text, the candidate should make an effort to produce a well-structured and easily readable report. In order to ease the evaluation of the thesis, it is important that the cross-references are correct. In the making of the report, strong emphasis should be placed on both a thorough discussion of the results and an orderly presentation.

The candidate is requested to initiate and keep close contact with his/her academic supervisor(s) throughout the working period. The candidate must follow the rules and regulations of NTNU as well as passive directions given by the Department of Energy and Process Engineering.

Risk assessment of the candidate's work shall be carried out according to the department's procedures. The risk assessment must be documented and included as part of the final report. Events related to the candidate's work adversely affecting the health, safety or security, must be documented and included as part of the final report. If the documentation on risk assessment represents a large number of pages, the full version is to be submitted electronically to the supervisor and an excerpt is included in the report.

Pursuant to "Regulations concerning the supplementary provisions to the technology study program/Master of Science" at NTNU §20, the Department reserves the permission to utilize all the results and data for teaching and research purposes as well as in future publications.

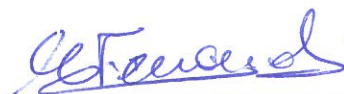
The final report is to be submitted digitally in DAIM. An executive summary of the thesis including title, student's name, supervisor's name, year, department name, and NTNU's logo and name, shall be submitted to the department as a separate pdf file. Based on an agreement with the supervisor, the final report and other material and documents may be given to the supervisor in digital format.

- Work to be done in lab (Water power lab, Fluids engineering lab, Thermal engineering lab)
 Field work

Department of Energy and Process Engineering, 14. January 2014



Olav Bolland
Department Head



Maria Fernandino
Academic Supervisor

Research Advisor: Carlos A. Dorao, EPT, NTNU

Abstract

Boiling flow in steam generators, water cooled reactors and other multiphase processes can be subject to instabilities. One of the main types of instabilities is DWO, a low amplitude and high frequency phenomenon. DWO can lead to system control problems, affect heat transfer characteristics and induce mechanical vibration of components. The need to predict the occurrence of such instabilities and know how affecting system parameters may be adjusted to control the oscillation is of high importance. In this report DWO is investigated by adding heat to a single horizontal channel. The changes in amplitude and period caused by heat-, pressure-, inlet subcooling and mass flux variations are studied numerically and compared with experimental results. The wave characteristics are also studied through a literature study. The literature review reveals that most studies for DWO are performed for vertical channels, even though horizontal channels are encountered more often in industrial applications. A hypothesis for changes in amplitude and period based on former studies mainly executed in horizontal channels is made, even though some contradicting results are found in literature regarding wave characteristics.

A method of extracting the amplitude and period of the oscillations for both the numerically modeled results and the recreated experimental results are proposed, and a method to reduce the amount of simulations needed to find the marginally stable operating conditions by using the model is established. Stability maps based on dimensionless parameters that relate the inlet subcooling and applied heat to the unstable and stable operating conditions are found in literature. The model shows converging behavior of the oscillations when operating in the stable area and diverging behavior when operating in the unstable area. Compared to experimental results from literature, the numerically obtained stability boundary is predicted to be to the left of experimentally obtained stability boundary, making the modeled diverging DWOs to appear at lower equilibrium phase change numbers. The experimental results show marginally stable oscillations when operating in the unstable area.

The effect of increasing applied heat is found to increase the amplitude and reduce the period of the oscillations by both the numerical and the experimental results. The modeled results predict the increased inlet subcooling to increase the amplitude and the period. However, the experimental results displays a small decrease in amplitude for increased inlet subcooling for the set operating conditions, while the period shows the same effect as the modeled results. The increased pressure is by the model shown to decrease the amplitude, but the opposite is shown by the experimental results for different operating conditions. The effects of mass flux can be caused by both heat variations and change of the mass flux so no conclusion can be made from the model. Similarly, the change of the period when increasing the pressure can also be caused by both the pressure change and the change of applied heat. The studied experiments shows increased amplitude with increased pressure and decreased mass flux, while the period remains unaffected by pressure and mass flux variations. Possible reasons for the differences between the model and the experiments are discussed throughout the report.

Sammendrag

Diverse ustabiliteter kan oppstå i kokende strømming i dampgeneratorer, vannkjølte reaktorer og andre flerfaseprosesser. En av de vanligste typene ustabilitet er oscillerende masstetthetsbølger som kjennetegnes av en lav amplitude og høy frekvens. Massetetthetsbølgene kan forårsake problemer med kontrollen av systemet, påvirke varmeoverføringen og forårsake mekaniske vibrasjoner. Nødvendigheten av å kunne forutse denne typen ustabilitet og ha kjennskap til hvordan systemparametere påvirker oscillasjonene er derfor viktig. I denne rapporten er massetetthetsbølger undersøkt ved å tilføre varme til et enkelt horisontalt liggende rør. Endringene i amplitude og periode forårsaket av endringer i anvendt varme, trykk, underkjøling inn i røret eller massefluks er studert numerisk og sammenlignet med eksperimentelle resultater. Parametriske effekter er også studert gjennom en litteraturstudie som avslører at hovedvekten av disse studiene omhandler vertikale systemer, på tross av at horisontale rør oftest er brukt i industrien. En hypotese for endring i amplitude og periode ved endring i systemparametere er gjort på bakgrunn av artikler som hovedsakelig omhandler horisontale systemer.

En metode for å finne amplituden og perioden for både de numeriske og de eksperimentelle resultatene er foreslått og en metode for å minske antallet simuleringer for å finne systemparametere som gir marginalt stabile oscillasjoner er etablert. Stabilitetskart som benytter dimensjonsløse parametere som relaterer anvendt varme og underkjøling i inngangen av røret til stabile og ustabile områder er funnet i litteraturen. Modellen viser konvergerende oppførsel av oscillasjonene i det stabile området og divergerende i det ustabile området. Sammenlignet med en eksperimentell stabilitetsgrense funnet i litteraturen blir den predikerte stabilitetsgrensa liggende slik at massetetthetsbølger oppstår ved lavere terskelverdi for anvendt varme. De eksperimentelle resultatene viser marginalt stabile oscillasjoner i det ustabile området.

Effekten av økende anvendt varme er funnet å øke amplituden og redusere perioden av både numeriske og eksperimentelle resultater. De modellerte resultatene viser at økt underkjøling i inngangen av røret øker amplituden og perioden. De eksperimentelle resultatene viser en liten reduksjon av amplituden for økt underkjøling, mens perioden viser samme effekt som de modellerte resultatene. Økt trykk er av modellen vist å minske amplituden, mens det motsatte er vist av de eksperimentelle resultatene for andre gitte systemparametere. Effekten av endring i massefluks kan stamme fra både endring av anvendt varme og den justerte massefluksen så ingen konklusjon kan bli gjort på bakgrunn av modellen. Det samme er tilfellet for endringen av perioden ved endring av trykk. De rekonstruerte eksperimentelle resultatene viser økt amplitude med økt trykk og redusert massefluks, mens perioden er upåvirket av både trykk og massefluks. Mulige grunner til forskjellen mellom modellen og eksperimentene er diskutert i rapporten.

Contents

1 Introduction	8
1.1 Background and motivation.....	8
1.2 Objective.....	8
1.3 Scope of work	9
2 Review on two-phase flow	10
2.1 Flow regimes and heat transfer.....	10
2.2 Principles of two-phase flow	11
2.2.1 Vapor quality and void fraction	11
2.2.2 Velocities	12
2.3 Flow models	13
2.3.1 Homogeneous Equilibrium Model (HEM)	13
2.3.2 The Drift Flux Model.....	14
2.4 Friction Factor and Pressure Drop Correlations	15
2.4.1 Friction Factor for Single Phase Flow	15
2.4.2 Friction Factor for Two-phase flow	16
2.5 Classification of two-phase flow instabilities.....	16
3 Review of Density Wave Oscillations (DWO)	18
3.1 Fundamentals of DWO.....	18
3.2 Predicting stability	19
3.2.1 Stability maps.....	19
3.3 Review of density wave instability studies.....	21
3.3.1 Experimental investigations of DWO.....	22
3.3.2 Numerical investigations of DWO.....	35
3.4 Characterizing effects	39
3.4.1 Applied heat	39
3.4.2 Inlet subcooling.....	39
3.4.3 Pressure	40
3.4.4 Mass flux.....	40
3.4.5 Hypothesis.....	41

4 Simulated Density Wave Oscillations	42
4.1 Modeled System	42
4.2 Modeling procedure.....	44
4.3 Applied heat.....	45
4.4 Mass flux	53
4.5 Validation of the model and the effect of pressure and inlet subcooling	56
4.5.1 Lower points, low subcooling, high pressure	57
4.5.2 Mid points, low subcooling, low pressure	60
4.5.3 Upper points, high subcooling, low pressure.....	63
4.5.4 Numerically obtained stability map	65
4.6 Numerically obtained characterizing effects	66
5 Parametric Study of Experiments.....	68
5.1 Experimental system.....	68
5.1.1 Facility	68
5.2 Procedure and validation	70
5.3 Parameters affecting DWO characteristics	74
5.3.1 Applied heat	74
5.3.2 Inlet subcooling.....	78
5.3.3 Inlet pressure	80
5.3.4 Mass flux.....	82
5.4 Differences and similarities between numerical and experimental tests	84
6 Conclusion.....	86
6.1 Summary.....	86
6.2 Future work.....	87
References	88

List of figures

Figure 1: Flow regimes for forced convection boiling [Incropera et al., 2013].	11
Figure 2: Schematic of the system.	18
Figure 3: Stability map by Ishii and Zuber [1970].	20
Figure 4: Oscillatory behavior, showing convergent oscillations in a) and divergent oscillations in b) [Ruspini, 2013].	21
Figure 5: Relation between flow rate, amplitude and period [Akagawa et al., 1971].	23
Figure 6: Relation between pressure, amplitude and period for two different flow rates [Akagawa et al., 1971].	24
Figure 7: The relation between pressure drop and flow rate (characteristic curve) from Akagawa et al., [1971] as cited in Sørnum [2013].	25
Figure 8: Relation between mass flux and amplitude of DWO [Ding et al. 1995].	26
Figure 9: Relation between mass flux and period of DWO [Ding et al. 1995].	27
Figure 10: Relation between heat flux and amplitude of DWO [Ding et al. 1995].	27
Figure 11: Relation between heat flux and period of DWO [Ding et al. 1995].	28
Figure 12: Relation between inlet temperature and amplitude of DWO [Ding et al. 1995]. Be aware that increased inlet temperature implies decreased subcooling.	28
Figure 13: Relation between inlet temperature and period of DWO [Ding et al. 1995].	29
Figure 14: Comparison of the stability boundaries where “present study” refers to the experiments conducted in Comakli et al. [2002].	30
Figure 15: Relation between amplitude of DWO and heat flux for different mass fluxes for $P_{in}=7\text{bar}$ [Sørnum, 2013].	31
Figure 16: Relation between amplitude of DWO and heat flux for different mass fluxes for $P_{in}=7\text{bar}$, $\Delta T_{sub}=10\text{K}$ [Sørnum, 2013].	32
Figure 17: Relation between amplitude of DWO and inlet subcooling for different mass fluxes and power inputs for $P_{in}=7\text{bar}$ [Sørnum, 2013].	32
Figure 18: Relation between period of DWO and inlet subcooling for different mass fluxes and power inputs for $P_{in}=7\text{bar}$ [Sørnum, 2013].	33
Figure 19: Relation between the amplitude of DWO and the mass flux with three different power inputs and $\Delta T_{sub}=10\text{K}$, $P_{in}=7\text{bar}$ [Sørnum, 2013].	33
Figure 20: Relation between the period of DWO and the mass flux with three different power inputs and $\Delta T_{sub}=10\text{K}$, $P_{in}=7\text{bar}$ [Sørnum, 2013].	34
Figure 21: Relation between the amplitude of DWO and the inlet pressure with different power inputs, mass fluxes and $\Delta T_{sub}=10\text{K}$ [Sørnum, 2013].	34
Figure 22: Relation between the period of DWO and the inlet pressure with different power inputs, mass fluxes and $\Delta T_{sub}=10\text{K}$ [Sørnum, 2013].	35
Figure 23: Ratio of the fluid transit time to the period of oscillations evaluated by the linearized simplified HEM model. The red line is the predicted stability boundary [Ambrosini & Ferrer, 2006].	36

Figure 24: Stability thresholds obtained in parallel channels with different channel inclination [Colombo et al. 2012].	37
Figure 25: Amplitude of the oscillation in exit mixture velocity $u_{m,e}$ for marginally stable operating points at different levels of subcooling [Strømsvåg 2011].	38
Figure 26: Evolution of oscillation period t_p for marginally stable oscillations at different levels of subcooling [Strømsvåg 2011].	38
Figure 27: Schematic of the modeled system.	42
Figure 28: Mass flux curve with 200 Watt added to the horizontal channel.	46
Figure 29: The simulated mass flux in black and the diverging fitted sine curve in red for a power input of 200 W.	47
Figure 30: The simulated mass flux in black and the converging fitted sine curve in red for a power input of 180 W.	48
Figure 31: The simulated mass flux in black and the converging fitted sine curve in red for a power input of 190 W.	49
Figure 32: The simulated mass flux in black and the diverging fitted sine curve in red for a power input of 195 W.	50
Figure 33: The simulated mass flux in black and the fitted sine curve in red for a power input of 192 W.	51
Figure 34: Relationship between the α -values and the heat numbers N_{pch} .	52
Figure 35: Numerically obtained relation between power input and period/frequency.	53
Figure 36: The simulated mass flux in black and the fitted sine curve in red for a power input of 192 W.	54
Figure 37: The simulated mass flux in black and the fitted sine curve in red for a power input of 257 W.	55
Figure 38: Experimental results as shown in Sørum [2013].	56
Figure 39: The simulated mass flux in black and the converging fitted sine curve in red for a power input of 200 W.	57
Figure 40: The simulated mass flux in black and the diverging fitted sine curve in red for a power input of 250 W.	58
Figure 41: The simulated mass flux in black and the fitted sine curve in red for a power input of 247 W.	59
Figure 42: Mass flux curve in the inlet in red and in the outlet in blue for $q=247$ W.	60
Figure 43: The simulated mass flux in black and the converging fitted sine curve in red for a power input of 180 W.	61
Figure 44: The simulated mass flux in black and the fitted sine curve in red for a power input of 182 W.	62
Figure 45: The simulated mass flux in black and the diverging fitted sine curve in red for a power input of 255 W.	63
Figure 46: The simulated mass flux in black and the fitted sine curve in red for a power input of 240 W.	64

Figure 47: Numerically predicted stability threshold to the left and the experimentally obtained stability threshold from Sørnum [2013] to the right.	65
Figure 48: Simplified scheme of the facility.	69
Figure 49: Example of the LabVIEW interface.	70
Figure 50: Disturbed sine wave.	71
Figure 51: Samples for amplitude calculations in blue and the estimated outputted amplitude illustrated by the dashed black line.	72
Figure 52: Fast Fourier transform of the disturbed sine wave.	73
Figure 53: Illustrated data from experiment 20131127-E019.	75
Figure 54: Illustrated data from experiment 20131127-E001.	76
Figure 55: Illustrated data from experiment 20131127-E005.	77
Figure 56: Oscillations for the mass flux in a time interval of the experiment.	78
Figure 57: Oscillations for the mass flux in a time interval of the experiment.	79
Figure 58: Comparison between experiment E005 and E008, where E005 has a higher inlet temperature.	80
Figure 59: Comparison between experiment E005 (red) and E002 (blue), where E002 has a higher inlet pressure.	82
Figure 60: Comparison between experiment E006 and E023, where E023 has a higher mass flux.	83

List of tables

Table 1: Hypothesis on characterizing effects for DWO.	41
Table 2: Initial simulation data.	45
Table 3: Key values from a power input of 200 W.	47
Table 4: Key values from a power input of 180 W.	48
Table 5: Key values from a power input of 190 W.	49
Table 6: Key values from a power input of 195 W.	50
Table 7: Key values from a power input of 192 W.	51
Table 8: Relation between heat input, frequency and period.	52
Table 9: Initial simulation data.	53
Table 10: Key values from a power input of 257 W.	55
Table 11: Initial simulation data for validation of the “lower points” in figure 38.	57
Table 12: Key values from a power input of 200 W.	57
Table 13: Key values from a power input of 250 W.	58
Table 14: Key values from a power input of 247 W.	59
Table 15: Initial simulation data for validation of the “mid points” in figure 38.	60
Table 16: Key values from a power input of 180 W.	61
Table 17: Key values from a power input of 182 W.	62
Table 18: Initial simulation data for validation of the “upper points” in figure 38.	63

Table 19: Key values from a power input of 255 W	64
Table 20: Key values from a power input of 240 W	64
Table 21: The characterizing effects of DWO predicted by the model. Hypothesis based on the literature study for characterizing effects for DWO.....	66
Table 22: Estimated results from experiment 20131127-E019.....	75
Table 23: Estimated results from experiment 20131127-E001.....	76
Table 24: Estimated results from experiment 20131127-E005.....	77
Table 25: Estimated results from experiment 20130823-E005.....	78
Table 26: Estimated results from experiment 20130823-E008.....	79
Table 27: Estimated results from experiment 20131009-E005.....	81
Table 28: Estimated results from experiment 20131009-E002.....	81
Table 29: Estimated results from experiment 20131017-E006.....	83
Table 30: Estimated results from experiment 20131017-E023.....	83
Table 31: Comparison of characterizing effects from the literature study, the simulations and the studied experiments.....	84

Nomenclature

Abbreviations

DWO Density Wave Oscillations

PDO Pressure Drop Oscillations

PDE Partial Differential Equation

Non-dimensional parameters and variables

α Attenuation factor

α_v Void fraction

F Friction factor

K Restriction pressure drop coefficient

N_{sub} Subcooling number

N_{pch} Equilibrium phase change number

Re Reynolds number

x Vapor quality

Variables and parameters

ρ Density [kg/m^3]

μ Dynamic viscosity [kg/ms]

A Area [m^2]

A_G	Mean-to-peak mass flux amplitude [$\text{kg}/\text{m}^2\text{s}$]
B	Mean mass flux [$\text{kg}/\text{m}^2\text{s}$]
D_H	Hydraulic diameter [m]
f	frequency [Hz]
G	Mass flux [$\text{kg}/\text{m}^2\text{s}$]
h	Enthalpy [J/kg]
h_{fg}	Latent heat of vaporization [J/kg]
H	Heat transfer coefficient [$\text{W}/\text{m}^2\text{K}$]
j	Superficial velocity [m/s]
L	Length [m]
\dot{m}	Mass flow [kg/s]
p	Pressure [Pa]
P_H	Hydraulic perimeter [m]
q	Heat [W]
q'	Heat added per meter length [W/m]
q''	Heat flux [W/m^2]
Q	Volumetric flow rate [m^3/s]
t	Period [s] or time [s]
T	Temperature, both [$^{\circ}\text{C}$] and [K] used
ΔT_{sub}	Difference between current temperature and saturation temperature [$^{\circ}\text{C}$] or [K]
u	Velocity [m/s]
V	Drift velocity [m/s]
ϕ	Phase angle [$^{\circ}$]

Subscripts

l	liquid phase
g	gas phase
lo	liquid only
go	gas only
e	exit
i	inlet
m	mixture
sub	subcooling
in	inlet to channel
$inlet$	inlet at the reservoir
$trans$	transit time
osc	oscillations
sat	saturation
ext	externally imposed
pch	phase change

1 Introduction

1.1 Background and motivation

Boiling and condensation applications are used in many of today's industrial equipment such as nuclear reactors, two-phase flow heat exchangers, refrigeration systems, steam generators and tubular chemical reactors [Comakli et al., 2002]. These applications are desirable due to their high heat transfer coefficient that makes it possible to transfer high amounts of heat at lower heat differences [Wattelet et al., 1994]. However, the efficiency of two-phase flow systems can rapidly decrease under unstable conditions. In addition to lower the efficiency, the unstable conditions can cause failures such as premature burn-out, thermal fatigue, mechanical vibrations and system control problems [Ruspini, 2013]. Because of the importance of avoiding these downsides, the feature of predicting stability is paramount for a designer of two-phase flow systems. The designer's job is to predict the threshold of flow instability so that undesirable effects can be either compensated for, or to design the system in a different way [Bouré et al., 1973].

Studies of understanding the different flow instabilities that may arise have lasted more than sixty years, and in the recent years this have been a major research field especially within the nuclear energy industry. More than 90 % of the thermo-hydraulic research for nuclear reactors belongs to the field of nuclear safety [Ruspini, 2013], where the most relevant systems are vertically oriented. That has led to an exaggerated amount of focus on vertical systems. So even though horizontal systems are the most commonly encountered in industrial applications, models for predicting stability are mainly developed for vertical systems [Comakli et al., 2002]. Regarding other kind of industries where two-phase components are important, the understanding of two-phase flow instabilities is still lacking [Ruspini, 2013].

Density wave oscillations are the most studied of all the instabilities in boiling systems. The classical interpretation of the phenomenon ascribes to the origin of the instability to waves of "lighter" and "heavier" fluids that leads to density perturbations through the channel, so that the difference in fluid entering and exiting may lead to self-sustained oscillations [Papini et al., 2012]. The knowledge of how to control and stabilize systems is therefore of high importance. To know how to control an unstable system, the underlying mechanisms of the instability have to be investigated.

1.2 Objective

The main objective of this thesis is to perform numerical simulations of density wave oscillations and to study the wave characteristics due to changes in heat flux, pressure and inlet temperature. The results will then be compared both with experimental data already available from literature and from results obtained at the NTNU laboratory [Chiapero, 2013] [Ruspini, 2013] to validate

the model. In addition to the given assignment, the wave characteristics for changes in mass flux will also be considered.

1.3 Scope of work

Density wave oscillations will be studied in a single horizontal boiling channel through an already developed numerical model. The model assumes one-dimensional, thermodynamic equilibrium with constant inlet temperature. The pressure drop in the channel is assumed to be constant and the heat flux added to the system is assumed to be uniformly distributed. The comparing experimental data in is also gathered from a single boiling horizontal channel with a set up bypass valve large enough to impose a constant pressure drop over the investigated channel.

2 Review on two-phase flow

2.1 Flow regimes and heat transfer

Two-phase flow is a term referring to flow that consists of two phases, such as liquid-gas and solid-liquid processes. Liquid-gas processes can be boiling water reactors, condensers and many other industrial applications, while solid-liquid processes can be processes such as melting and solidification. Gas-solid mixtures are possible in some applications, like sublimation of carbon dioxide. In this paper it is always referred to two-phase flow as a mix of gas and liquid. Gas is further denoted by the subscript g and liquid as l .

The high heat transfer coefficient H for boiling and condensation is one of the reasons two-phase applications are so widely used. In figure 1 the development of the heat transfer coefficient is sketched along with the corresponding typical flow regimes. The substance enters the pipe in figure 1 as single phase liquid. It gets heated gradually by convective heat transfer, and subcooled boiling starts as bubbles appear close to the wall. When additional heat is added, bubbles start to spread to the core of the flow. This is called the bubbly flow regime. The heat transfer experiences a sudden increase when the boiling starts and continues to increase into the slug flow regime, where bubbles start to merge together. The highest heat transfer coefficient rises to its maximum in the annular flow regime, and is the reason for this flow regimes high use in today's industry. When the flow is close to single phase vapor at the end of the pipe and the wall is dry, the heat transfer coefficient reduces dramatically with equal increase in the temperature of the wall. This is called the critical heat flux or burnout [Wattelet et al., 1994], [Incropera et al., 2013].

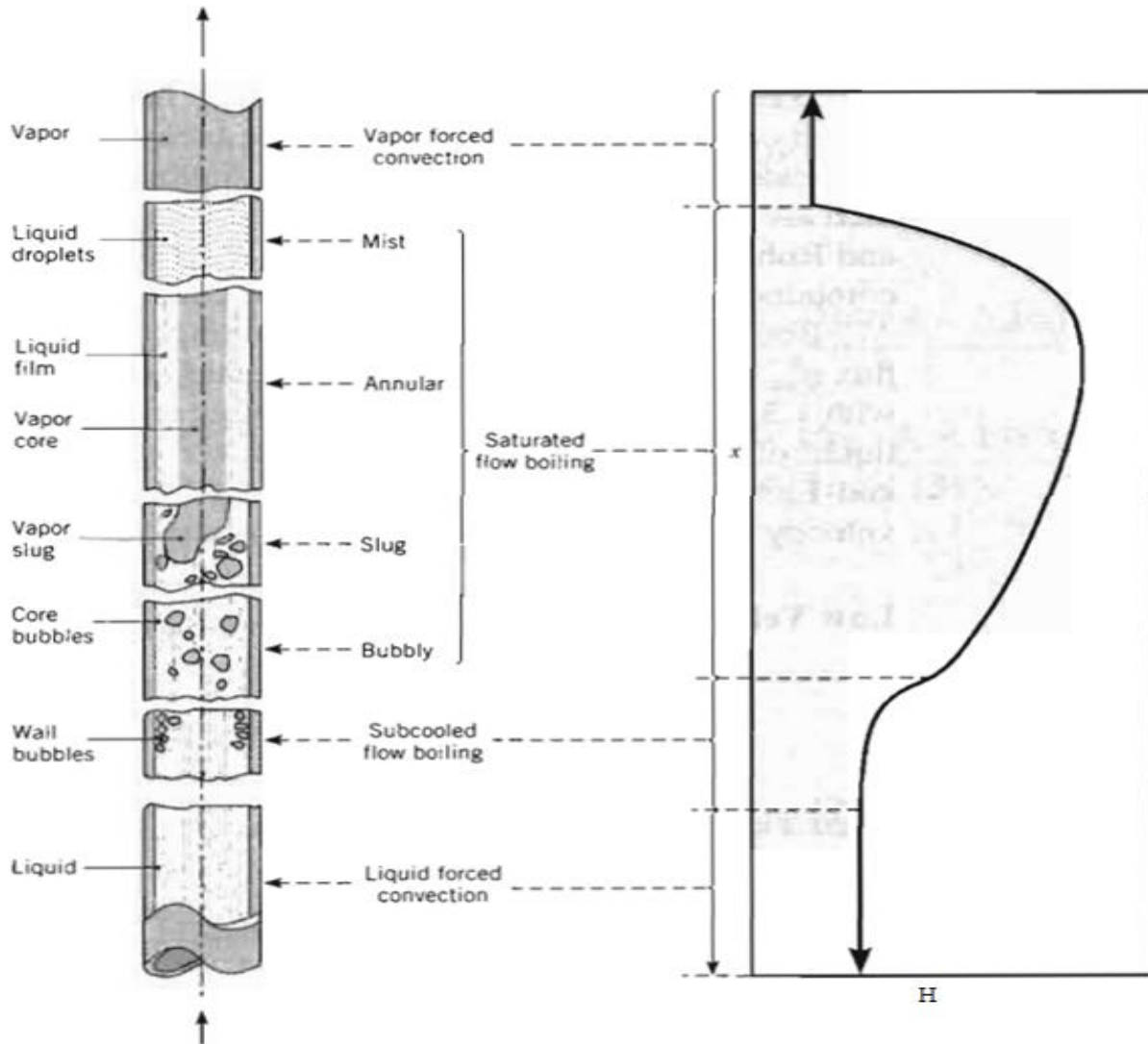


Figure 1: Flow regimes for forced convection boiling [Incropera et al., 2013].

2.2 Principles of two-phase flow

Density wave oscillations occur in two-phase flow systems and to describe and analyze density waves some fundamental parameters of two-phased flow is reviewed. The theory in the following section 2.2 is found in Ghiaasiaan [2008] with only small changes in notation. All the notations and eventual SI-units used in this thesis can be found in the nomenclature.

2.2.1 Vapor quality and void fraction

The vapor quality x is a measurement of how much of the mass flow rate that consist of vapor at a given cross section in the tube, and is here defined in equation 2.1 and 2.2:

$$x = \frac{\dot{m}_g}{\dot{m}_g + \dot{m}_l} = \frac{\dot{m}_g}{\dot{m}} \quad (2.1)$$

where \dot{m}_g is the mass flow rate of the gas phase, \dot{m}_l is the mass flow rate of the liquid phase and \dot{m} is the total mass flow rate. If thermodynamic equilibrium is assumed, the hydrodynamic quality can be considered equal to the thermodynamic quality:

$$x = \frac{h_m(z) - h_l}{h_{fg}} \quad (2.2)$$

where h_l is the saturated liquid enthalpy, h_{fg} is the latent heat of vaporization and $h_m(z)$ is the mixture enthalpy at the cross sectional located at z meters from the entrance. The latter is calculated as:

$$h_m(z) = h_i + \frac{1}{\dot{m}} \int_0^z q'(z) dz \quad (2.3)$$

where h_i is the enthalpy at the inlet and the integral of $q'(z)$ is the transferred heat per meter z to the boiling channel. **The void fraction** α_v is defined as the volumetric fraction of gas in the system and given as:

$$\alpha_v = \frac{A_g}{A_l + A_g} = \frac{A_g}{A} \quad (2.4)$$

where A_g is the cross sectional area occupied by gas (void) and A_l is the cross sectional area occupied by liquid. The total area A is given as the sum of A_l and A_g .

2.2.2 Velocities

The true average velocity refers to the actual average velocity for each of the two phases. The respective true average velocities for gas u_g and liquid u_l are shown below:

$$u_g = \frac{Q_g}{A_g} = \frac{Q_g}{\alpha A} \quad (2.5)$$

$$u_l = \frac{Q_l}{A_l} = \frac{Q_l}{(1 - \alpha)A} \quad (2.6)$$

Q_g and Q_l are the volumetric flow rates of gas and liquid.

The total mass flux G is found by dividing the total mass flow rate \dot{m} by the cross section of the flow A . It can also be expressed as a combination of mixture density ρ_m and velocity u that is

assumed to be the same for both the gas phase and liquid phase (as in HEM flow model explained in section 2.3.1):

$$G = \frac{\dot{m}}{A} = \rho_m u \quad (2.7)$$

The mixture density ρ_m is defined as:

$$\rho_m = \alpha \rho_g + (1 - \alpha) \rho_l \quad (2.8)$$

where ρ_g and ρ_l is the density of gas and liquid respectively. The mass flux of the gas phase is defined as:

$$G_g = Gx \quad (2.9)$$

while the mass flux of the liquid phase is:

$$G_l = G(1 - x) \quad (2.10)$$

The velocity that a phase would travel with if it was flowing alone in the whole cross section of the channel is the superficial velocity j . The respective superficial velocities for gas and liquid are shown below:

$$j_g = \frac{Gx}{\rho_g} = u_g \alpha \quad (2.11)$$

$$j_l = \frac{G(1 - x)}{\rho_l} = u_l (1 - \alpha) \quad (2.12)$$

The total superficial velocity is the sum of superficial velocities of gas and liquid:

$$j = j_g + j_l \quad (2.13)$$

The slip velocity u_s is defined as the difference between the true average velocity of the gas and liquid phase:

$$u_s = u_g - u_l \quad (2.14)$$

2.3 Flow models

2.3.1 Homogeneous Equilibrium Model (HEM)

The homogeneous equilibrium model is the simplest method for modeling and analysis of two-phase flow. The assumptions are:

- the two phases are well mixed everywhere – treats the mixture as a single fluid

- thermodynamic equilibrium
- both phases flows at the same velocity, giving the same true average velocities of the two phases, and they equal the total superficial velocity, $u_g = u_l = j$
- for a pure liquid or a pure gas mixture, HEM requires the mixture to be at saturation

These simplifications will give some deviations from the real flow behavior, but can still provide useful information in many cases [Ghiaasiaan, 2008].

The equations used in the model for mass, momentum and energy are [Ruspini, 2013]:

$$\text{Mass:} \quad \frac{\partial \rho_m}{\partial t} + \frac{\partial G}{\partial z} = 0 \quad (2.15)$$

$$\text{Momentum:} \quad \frac{\partial G}{\partial t} + \frac{\partial}{\partial z} \left(\frac{G^2}{\rho_m} \right) + \frac{\partial p}{\partial z} + \left(\frac{F}{D_H} + \sum_{j=1}^N K_j \delta(z - z_j) \right) \frac{G^2}{2\rho_m} = 0 \quad (2.16)$$

$$\text{Energy:} \quad \frac{\partial \rho_m h_m}{\partial t} + \frac{\partial G h_m}{\partial z} = q \frac{P_H}{A_x} \quad (2.17)$$

where p is the static pressure, h is the specific enthalpy, ρ is the density, q is the heat source, F is the Darcy friction factor, K_j is the constant value of concentrated local pressure drop for valves, D_H is the hydraulic diameter of the pipe, P_H is the hydraulic perimeter, A_x is the cross section area and z is the space coordinate. The subscript m is the mixture value. The pressure drop in the valves is calculated using a pressure drop concentrated value, K_j , for each valve. The relation can be expressed as:

$$K = \frac{\Delta p}{\frac{1}{2} \rho u^2} \quad (2.18)$$

where Δp is the pressure loss across the valve and u is the velocity. Friction losses are neglected in the energy equation. The assumption of equal velocities is most appropriate when there is little slip between the gas and liquid, such as in the bubbly flow regimes. The slip is especially large in annular flow, and the model then might fall short [Aldridge & Fowler, 1996].

2.3.2 The Drift Flux Model

The drift flux model takes into consideration that the velocities of gas and liquid can be different, called slip (eq. 2.14). The drift velocity express motion of the gas and liquid compared to a surface perpendicular to the direction of the flow, where this surface moves with the total superficial velocity j . The drift velocity of respectively gas and liquid is:

$$V_{gj} = u_g - j \quad (2.19)$$

$$V_{lj} = u_l - j \quad (2.20)$$

The drift flux is the volumetric flux relative to the perpendicular surface moving with the total superficial velocity j . The drift flux for the gas and liquid is then:

$$j_{gj} = \alpha V_{gj} \quad (2.21)$$

$$j_{lj} = (1 - \alpha)V_{lj} \quad (2.22)$$

The drift flux model adds conservation of mass for the gas to the three mixture equations used in the homogeneous model, with extra terms in the momentum and enthalpy equations due to slip. The equations for mass, momentum and energy for the drift flux model are not considered relevant for this text and the reader is referred to Aldridge & Fowler [1996] for additional information.

2.4 Friction Factor and Pressure Drop Correlations

The following section is based on theory from White [1991]. To determine the pressure drop in the boiling channel, the friction factor F and the Reynolds number, Re , must be found. The Reynolds number quantifies the relative importance of the inertial forces to the viscous forces and is in this text defined as:

$$Re = \frac{\text{Inertial forces}}{\text{Viscous forces}} = \frac{GD}{\mu} \quad (2.23)$$

where μ is the fluid dynamic viscosity. The flow is in a laminar state for low Reynolds numbers, where the fluid flows in parallel layers with no interaction between the layers. For the high Reynolds numbers the flow is fluctuating and agitated called turbulent flow. For the medium Reynolds numbers the flow is in a transitional flow regime in between the transition from laminar to turbulent flow.

2.4.1 Friction Factor for Single Phase Flow

Single phase flow occurs in the beginning of the boiling channel, and also if it transitions into pure vapor. To determine the friction factor in these regions the following correlations are used for respectively laminar flow in equation 2.24, transitional flow in equation 2.25, and turbulent flow for different Reynolds numbers in equation 2.26 and 2.27:

$$Re < 2000: \quad F = \frac{64}{Re} \quad (2.24)$$

$$2000 \leq Re < 4000: \quad F = (Re - 2000) \frac{0.316/Re^{0.25} - 64/Re}{2000} + \frac{64}{Re} \quad (2.25)$$

$$4000 \leq Re < 10^5: \quad F = \frac{0.316}{Re^{0.25}} \quad (2.26)$$

$$Re > 10^5: \quad F = \frac{1}{(1.8 \log(Re/6.9))^2} \quad (2.27)$$

2.4.2 Friction Factor for Two-phase flow

To find the friction factor for two-phased flow, F_m , there are several correlations available in the literature. The Muller-Steinhagen and Heck (1986) correlation is the correlation used in this paper [Thome, 2004]. The two-phase friction factor is correlated as:

$$F_m = F(1 - x)^{1/3} + Bx^3 \quad (2.28)$$

where the factors F and B is calculated as:

$$F = A + 2(B - A)x \quad (2.29)$$

$$A = f_{lo} \frac{\rho}{\rho_l} \quad (2.30)$$

$$B = f_{go} \frac{\rho}{\rho_g} \quad (2.31)$$

where the friction factors F_{lo} and F_{go} is the friction factor for respectively liquid only and gas only. These are calculated by the single-phase and Reynolds number equations from section 2.4.1.

2.5 Classification of two-phase flow instabilities

There are different types of instabilities that may occur inside a boiling channel. A flow is either steady or transient. The system parameters of steady flow is functions of space variables only, while the transient flow parameters are functions of both time and space variables. For a fixed set of boundary conditions, there are often multiple solutions for a steady-state operation of a two-phased flow system. Small perturbations may cause a system that has multiple solutions for the given boundary conditions to move from one set of operating conditions to a completely different set. It can also oscillate between two or more unstable operating conditions. The transient flow can be stable or unstable. The stable flow will return to its initial operating conditions when

disturbed, while the unstable flow is either subject to static and/or dynamic instabilities [Belblidia & Bratianu, 1979], [Ghiaasiaan, 2008].

Static instabilities occur when a steady-state system becomes unstable, and as a result of a perturbation it moves to a different steady-state condition as explained above. Examples include flow regime transitions (see section 2.1), Ledinegg instability (flow excursions) and burnout. The Ledinegg instability is an instability mode that results from the mass flux pressure drop characteristics of boiling channels.

Dynamic instabilities can be analyzed by transient dynamic and feedback characteristics of the system and will often lead to oscillations. Examples include density wave oscillations, pressure drop oscillations (PDO) and acoustic oscillations. Density wave oscillations are the most common and well examined phenomena of all the instabilities in boiling channels. The oscillations occur as a result of phase lag and feedback among flow rate, pressure drop, and phase-change processes [Ghiaasiaan, 2008]. While the DWO have a small amplitude and high frequency, the PDO have a much lower frequency and larger amplitude. As a result of the difference in their propagation, the interaction between them is small and it makes it possible to set apart density wave oscillations as a single phenomenon [Belblidia & Bratianu, 1979].

3 Review of Density Wave Oscillations (DWO)

3.1 Fundamentals of DWO

The exact physical mechanism of how self-sustained density waves occur has been explained in several ways. The classical description is based on an assumption of constant pressure drop over the channel presented in the schematic in figure 2 below. The schematic shown consists of a heated pipe, an inlet restriction and an outlet restriction with respective pressure drop coefficients K_{in} and K_{out} . The inlet reservoir pressure is denoted p_{inlet} and the outlet reservoir pressure p_{outlet} . T_{in} and p_{in} is the temperature and pressure going into the tube and q'' is the added heat flux. T_{out} and p_{out} is the temperature and pressure going out of the tube, respectively.

A positive instantaneous perturbation in inlet velocity is assumed to illustrate. This will cause the mass flow to increase in the inlet and also the density, and so it transforms into a wave from the inlet to the outlet. This causes the pressure drop in the outlet to instantaneously increase when the wave arrives and because the pressure drop over the whole channel is constant, the inlet velocity has to instantaneously decrease. The lower inlet velocity results in lower density, causing a new density wave that travels to the channel exit. The lower density wave reaches the outlet and causes the pressure drop at the channel exit to decrease and the inlet velocity to increase, resulting in a new cycle. Hence, the classical approach describes the oscillations as a result of enthalpy perturbations which travel with mixture flow velocity [Rizwan-Uddin, 1994].

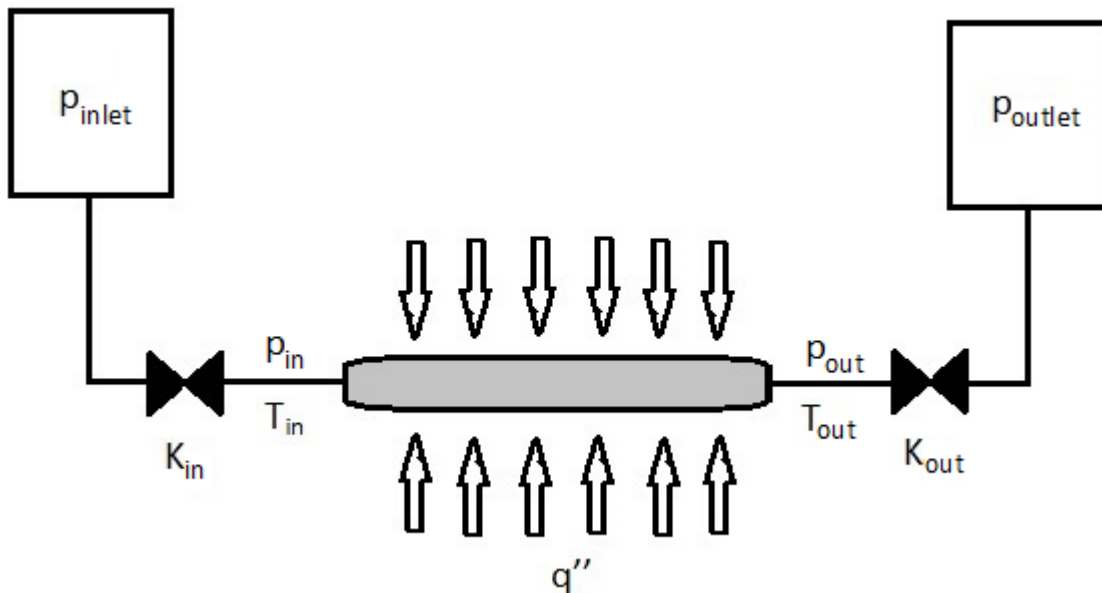


Figure 2: Schematic of the system.

It should be noted that the assumption of a constant pressure drop across the heated channel is not a realistic assumption with respect to typical experimental setup, where the mass flow rate is forced by an external feedwater pump instead of being freely driven according to the supplied power level. The constant pressure drop boundary condition can be assured by connecting a

bypass tube to the boiling channel. This is the case for the setup in the lab where the experimental data is gathered (for experimental setup, see section 5.1.1 or Chiapero [2013] and Ruspini [2013]). The presence of the bypass tube was studied experimentally by Collins and Gacesa [1969]. Their results implied that a sufficiently large bypass ratio, that is the ratio of bypass cross sectional area to the heated channel cross sectional area, is required to maintain the constant pressure drop boundary condition [Colombo et al., 2012].

3.2 Predicting stability

There are three main reasons why flow oscillations are undesirable: the oscillations affect heat transfer that may induce burnout, sustained flow oscillations may cause mechanical vibrations and they create system control problems [Belblidia & Bratianu, 1979]. As a result of these problems, DWO has been extensively studied and several methods have been developed for predicting the stability of the oscillations.

3.2.1 Stability maps

The main purpose of a stability map is to determine whether a system is stable or unstable. The variables of the axis are usually functions of dimensionless groups that reduce the number of independent variables [Aldridge & Fowler, 1996]. Ishii and Zuber [1970] used a drift-flux model to try to predict the stability in a flow system by plotting the stability threshold against the subcooling number N_{sub} and the equilibrium phase change number N_{pch} (figure 3). With these axes and a constant system pressure and inlet velocity gives a fixed Reynolds number, drift number and inlet and outlet restriction. The subcooling number and equilibrium phase change number are defined here as in Aldridge and Fowler [1996]:

Subcooling number:

$$N_{sub} = \frac{(\rho_l - \rho_g) \Delta h_l}{\rho_g h_{fg}} \quad (3.1)$$

where the inlet flow is subcooled by an enthalpy Δh_l below the saturation temperature, h_{fg} is the latent heat of vaporization, ρ is the density, and the subscripts l and g denotes liquid and gas, respectively.

Equilibrium phase change number:

$$N_{pch} = \frac{(\rho_l - \rho_g) q}{\rho_l A h_{fg} u_i} \quad (3.2)$$

where q is the constant uniform power added to the system, u_i the inlet velocity and A is the cross sectional area of the channel. N_{sub} scales the inlet subcooling and may be viewed as the dimensionless residence time of a fluid particle in the single-phase region, while the N_{pch} scales the rate of phase-change due to the addition of heat [Saha et. al., 1976]. The N_{pch} is later in the text also referred to as the heating number.

Ishii and Zuber stability map:

For a given system pressure, Ishii and Zuber recognized that the domain of operation is fixed where the axis consists of N_{sub} and N_{pch} [Ishii & Zuber, 1970] and the stability boundaries can be drawn as in figure 3 below:

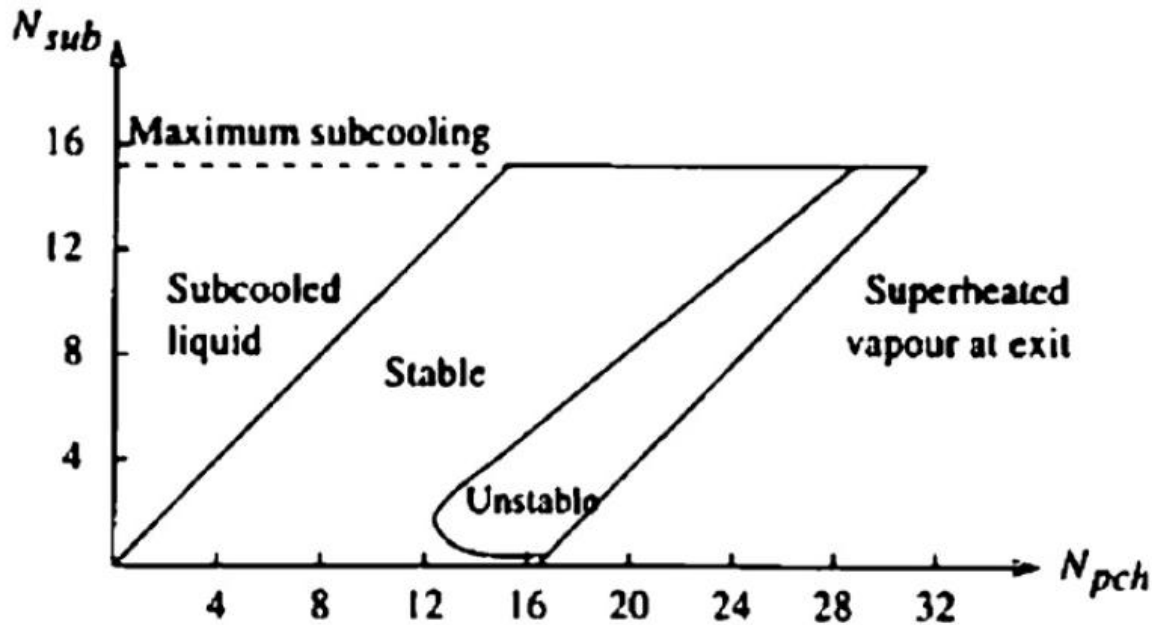
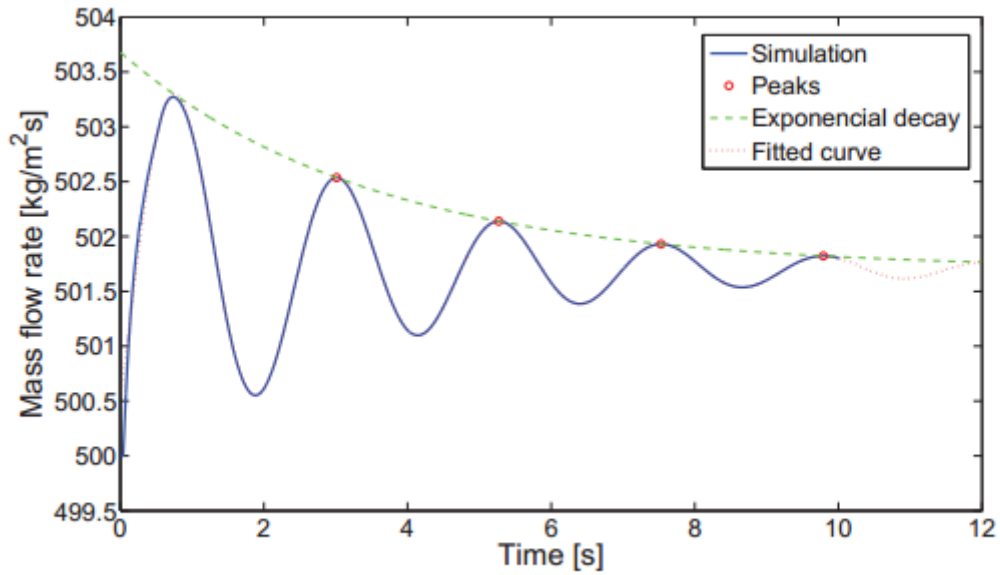
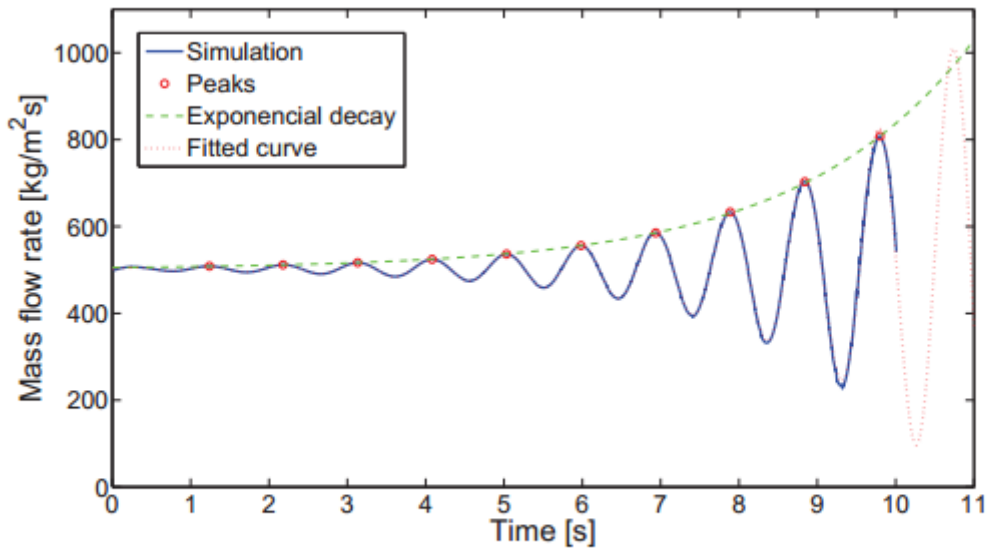


Figure 3: Stability map by Ishii and Zuber [1970].

The straight line to the left shows the boundary between single phase liquid and two-phase flow. That means that the vapor quality x , explained in section 2.2.1, is zero along this line ($x=0$). The area to the left of this line is considered stable. As the equilibrium phase change number is increased, the as system goes into a two-phase flow and continuous from a stable to an unstable system. The line furthest to the right is the line that differs between two-phase flow and pure vapor ($x=1$). The pure vapor area is considered stable. For the lowest subcooling numbers, the stable area will last all the way to the pure vapor area. As the subcooling number increases the unstable area will first experience a growth, then for medium to high subcooling numbers the stable area again increases. The stable flow will return to its initial operating conditions when disturbed (convergent oscillatory behavior, figure 4a), while the unstable area will experience a diverging oscillatory behavior when perturbations occur in the system. This type of behavior is shown in figure 4 b) below from Ruspini [2013]. Operating on the stability threshold will in theory give marginally stable oscillations, so they are self-sustained. That means periodic oscillations with constant amplitude [Belblidia & Bratianu, 1979]. Several other stability maps have been proposed and a summary can be found in Aldridge and Fowler [1996].



(a) Stable case



(b) Unstable case

Figure 4: Oscillatory behavior, showing convergent oscillations in a) and divergent oscillations in b) [Ruspini, 2013].

3.3 Review of density wave instability studies

Density wave oscillation is the most studied type of oscillation in two-phase flow instability problems, and especially the amount of published experimental work is vast [Kakac & Bon, 2008]. Literature reviews of both experimental and theoretical investigations have been collected

in for example Bouré et al., [1973], Belblidia & Bratianu [1979] and in Kakac & Bon [2008]. The reason for having to include a large number of studies in this literature review is due to the encountered opposing results found on parametric effects with regards to changes in amplitude and period. The goal of the review is to establish a qualified hypothesis for the DWO's characterizing effects of applied heat, inlet subcooling, pressure and mass flux before producing self-made results in chapter 4 and 5.

The so called classical description of density waves described in 3.1 relates the mixture density as the governing mechanism to determine the channel pressure drop characteristics. The oscillation period based on this description is commonly reported [Ambrosini & Ferreri, 2006] to be approximately twice the channel transit time resulting in the expression below:

Classical description:
$$\frac{t_{trans}}{t_{osc}} = 0.5 \quad (3.3)$$

Bouré et al., [1973] reviewed several parametric effects and stated that an increase of pressure will reduce the void fraction and causes the two-phase flow friction and momentum pressure to drop. That is because the friction forces acting on the steam are much less than the frictional forces acting on the liquid. The increase of pressure decreases the amplitude of the void response to disturbances and stabilizes the flow. The frequency of oscillation was not significantly affected.

3.3.1 Experimental investigations of DWO

Even though there has been performed numerous experimental studies of DWO, there are not a vast amount performed for horizontal systems focusing on wave characteristics such as amplitude and period. Most studies are concerned with the possibility of avoiding instabilities and not to investigate the underlying mechanisms of the density waves and as mentioned earlier, the majority of studies are investigating vertical systems [Comakli et al., 2002]. This section will chronologically present findings mainly on characterizing effects from experimental studies conducted in different horizontal systems. Because of the lack of found experimental studies for pressure variations in horizontal systems, three vertically oriented experimental studies are mentioned for the sake of being able to compare pressure experiments with theory. These studies must be used with caution since axial gravity has to be included for vertical systems and can cause unexpected behavior of the flow. It is important to recognize that even though most of these results originate from horizontal systems, the operating conditions can be very different and therefore might produce contradicting results.

Dolgov & Sudnitsyn [1965] used water in a vertical multitubed system and found that an increase of system pressure reduced the density wave oscillation amplitude. The effects of inlet

subcooling and inlet pressure drop were also examined, but for this report it is preferable to find these effects from studies performed in horizontal systems.

Mathisen [1967] used water in a single heated vertical channel and among the findings were that the increase of system pressure stabilized the system, and that the density wave oscillation period did not depend on system pressure.

Akagawa et al. [1971] used refrigerant R-113 as working fluid in a very long, horizontally coiled, heated section consisting of three parallel channels and studied the relation between flow rate, amplitude and period. Figure 5 indicates that the period of the density wave oscillations is increasing with increasing flow rate, while the amplitude is decreasing with increasing flow rate.

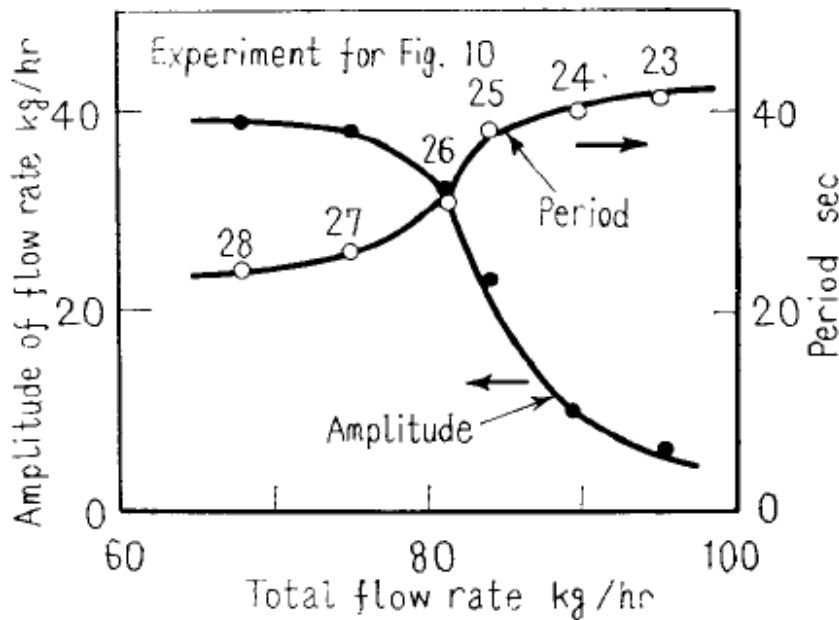


Figure 5: Relation between flow rate, amplitude and period [Akagawa et al., 1971].

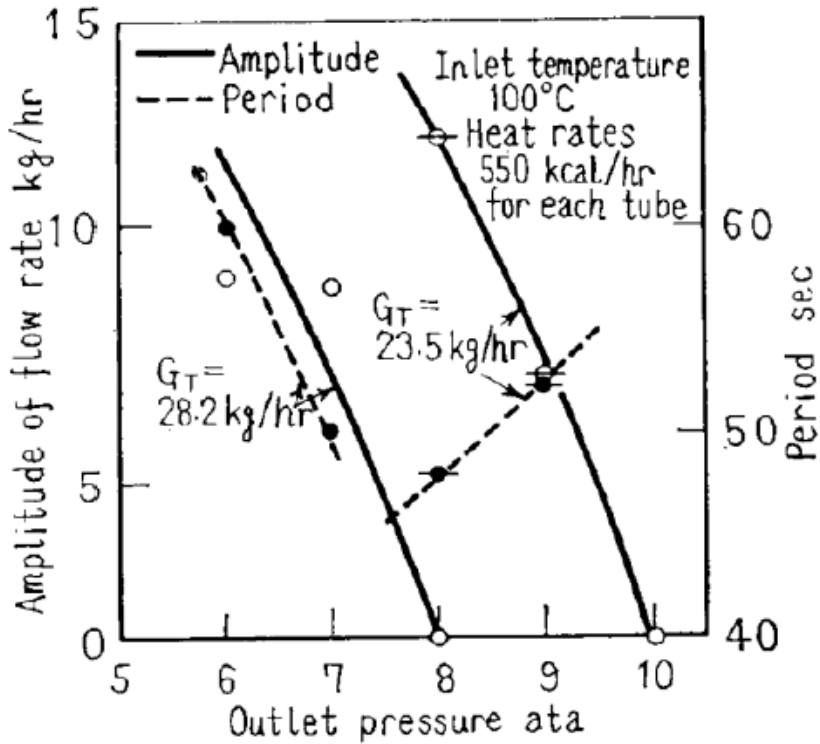


Figure 6: Relation between pressure, amplitude and period for two different flow rates [Akagawa et al., 1971].

The relation between outlet pressure and amplitude and period for two different flow rates is also examined, shown in figure 6. For both flow rates, an increase of outlet pressure leads to a decrease in amplitude. An increase in the outlet pressure for the largest flow rate results in a lower period, while an increase in outlet pressure for the smaller flow rate results in a higher flow rate. This cannot be directly compared to the inlet pressure, because the pressure drop in the channel varies with flow rate as shown in figure 7. The inlet pressure equals the outlet pressure added to the pressure drop.

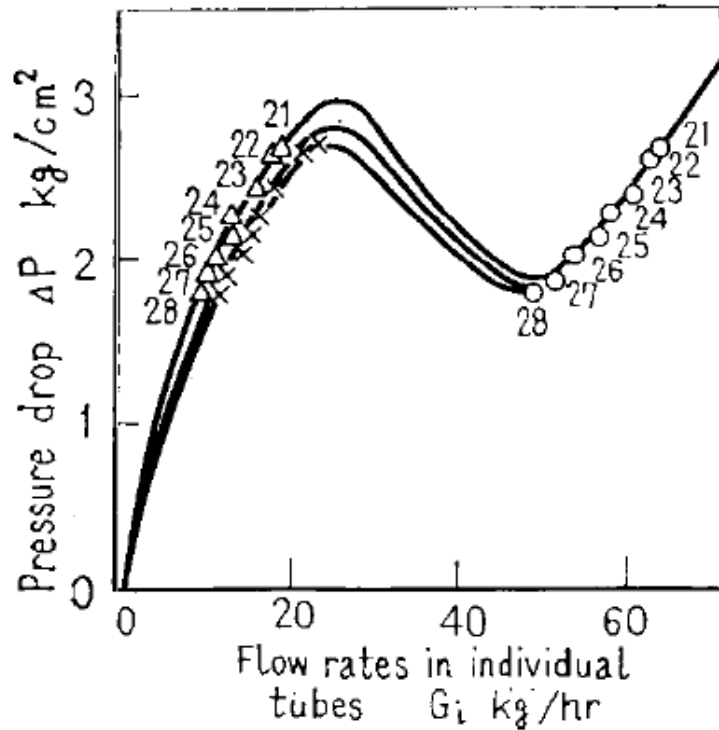


Figure 7: The relation between pressure drop and flow rate (characteristic curve) from Akagawa et al., [1971] as cited in Sørum [2013].

Saha et al. [1976] used refrigerant R-113 in a single heated horizontal channel and imposed a constant pressure drop by using a large bypass channel. It was found that for low values of subcooling, an increase of subcooling would have destabilizing effect. For medium to high subcooling, an increase in subcooling would stabilize the flow. This trend occurs due to the competing effects of momentum pressure drop (destabilizing) and single-phase friction (stabilizing). An increase of the subcooling number N_{sub} resulted in a reduced period and the inlet pressure had no influence on system stability. Increased inlet pressure drop coefficient stabilized the system, while increased exit pressure drop coefficient destabilized the system at low subcooling numbers. When increasing the added power input to the channel, the oscillations were found to increase in amplitude. The term destabilize implies that the stability boundary from figure 3 is pushed to the left, and thus increasing the unstable area so that DWO will occur at a larger number of operating conditions.

Osawa et al. [1979] used refrigerant R-113 in a single, heated, horizontal channel and found that an increased inlet subcooling (lower inlet temperature) lead to an increase in oscillation period.

Yuncu [1990] used refrigerant R-11 as working fluid in a single heated horizontal channel and the main finding were that the amplitude of the mass flux oscillations increased by increasing the heat flux and by increasing the mass flux. Yuncu et al. [1991] used the same system to find that as the amplitude increased with increasing heat flux, so does the frequency of oscillations. The

outlet pressure drop coefficient was increased by decreasing the exit orifice diameter and the amplitude, period and system stability then increased.

Wang et al. [1994] used water in a single vertical heated channel and found that as the system pressure increased, the oscillation periods and that the system stability increased.

Ding et al. [1995] used R-11 in a single heated horizontal channel and examined the effects of adjusting heat input, mass flux and inlet temperature under different working conditions. These dependencies are shown in the figures below. From figure 8 and 9 it is found that the amplitude and period is almost independent of mass flux at low heat input (54.6 kW/m^2). At the two higher heat inputs, both the amplitude and the period increase with increased mass flux. The results from figure 10 and 11 imply that increased heat flux results in reduced amplitude and period for all three inlet temperatures with slightly different gradients. Figure 12 and 13 shows that both the amplitude and the period decrease with increased inlet temperature (reduced subcooling) for three different mass flux levels. The oscillations of pressure and mass flux were found to be in phase.

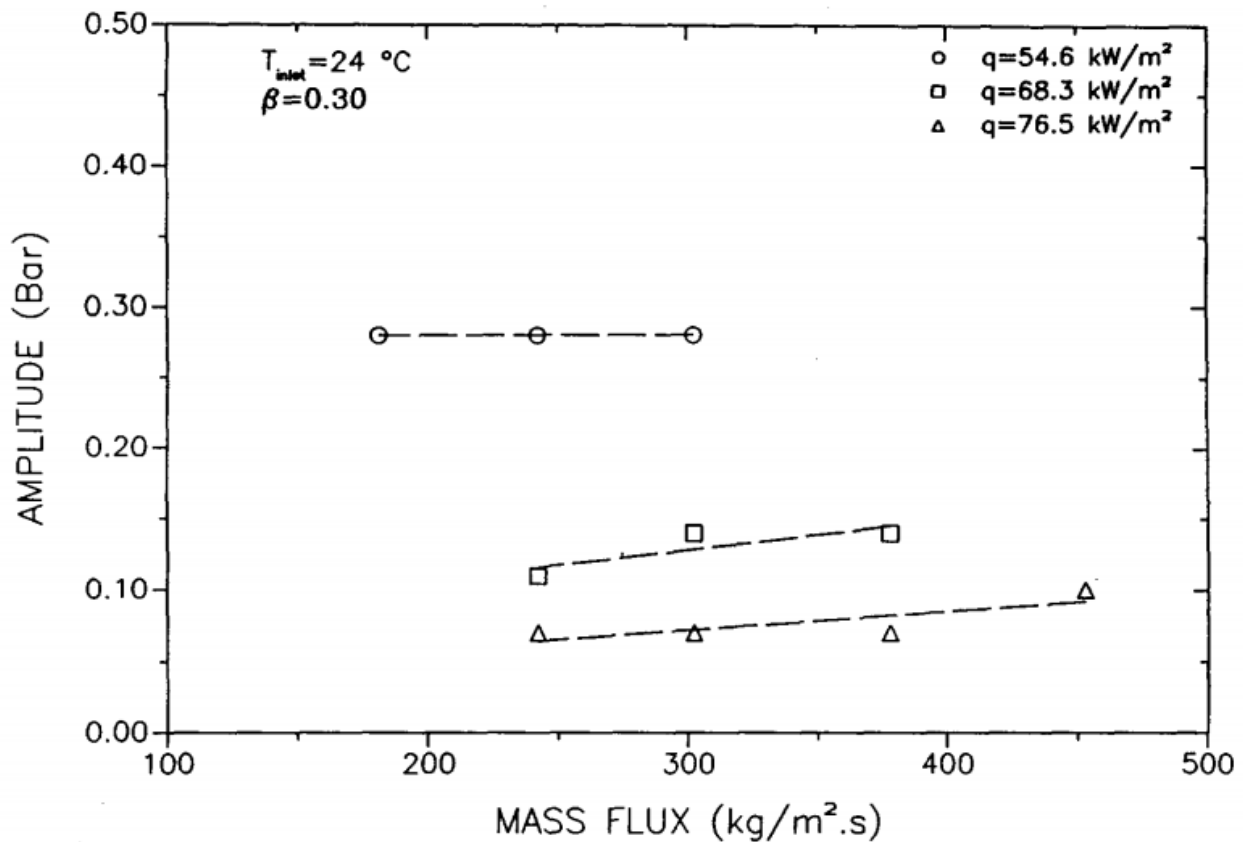


Figure 8: Relation between mass flux and amplitude of DWO [Ding et al. 1995].

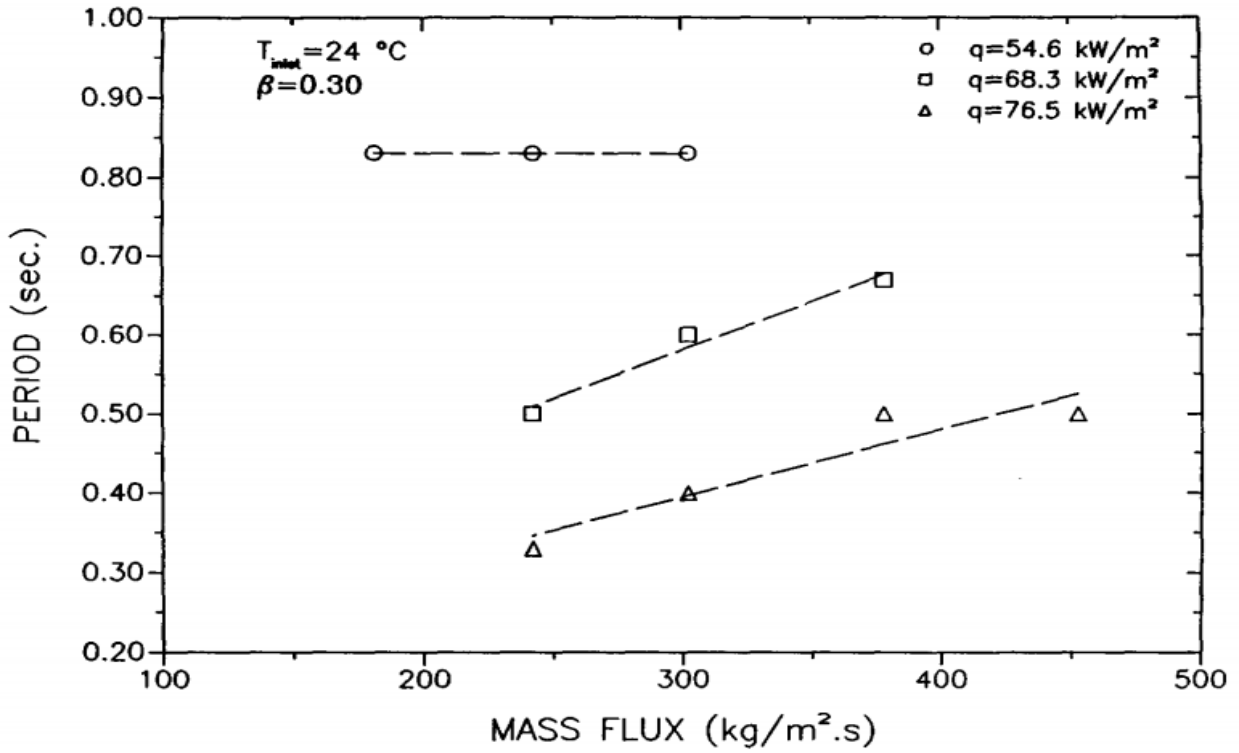


Figure 9: Relation between mass flux and period of DWO [Ding et al. 1995]

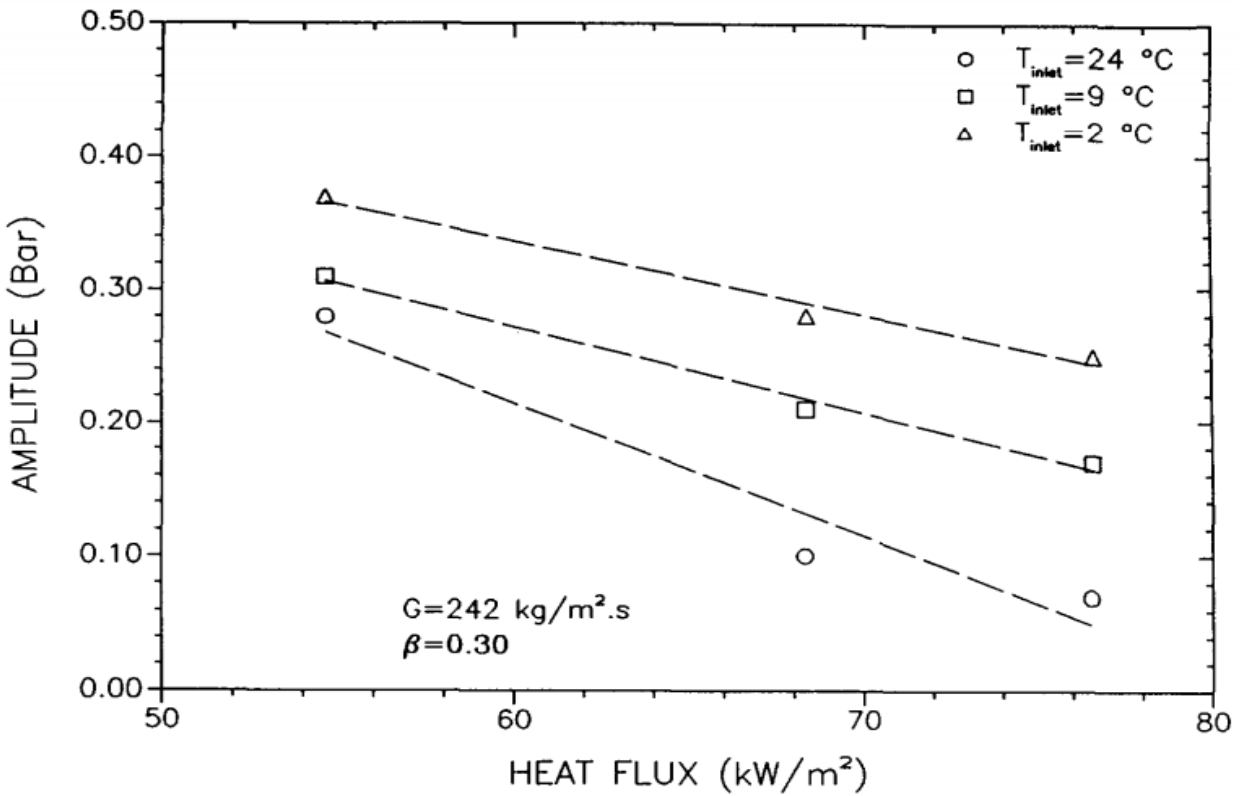


Figure 10: Relation between heat flux and amplitude of DWO [Ding et al. 1995]

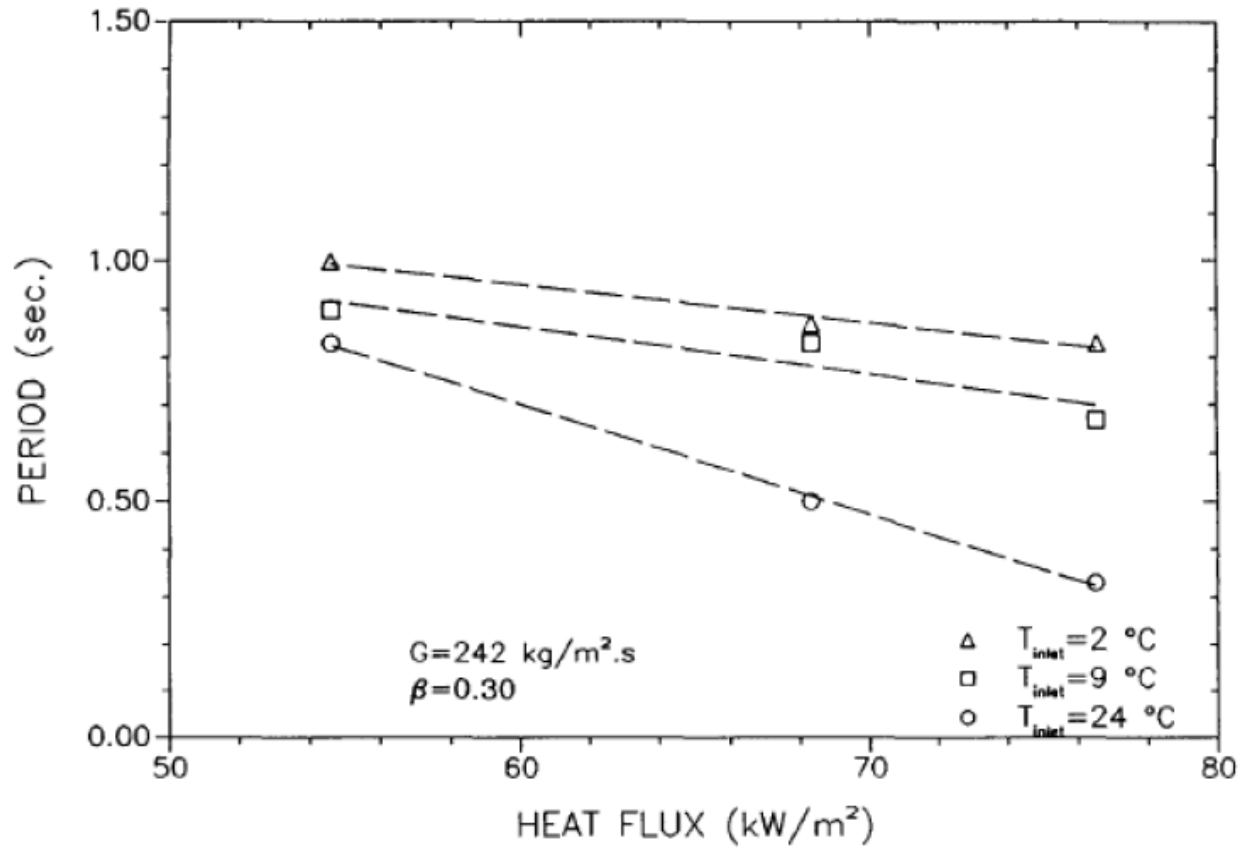


Figure 11: Relation between heat flux and period of DWO [Ding et al. 1995].

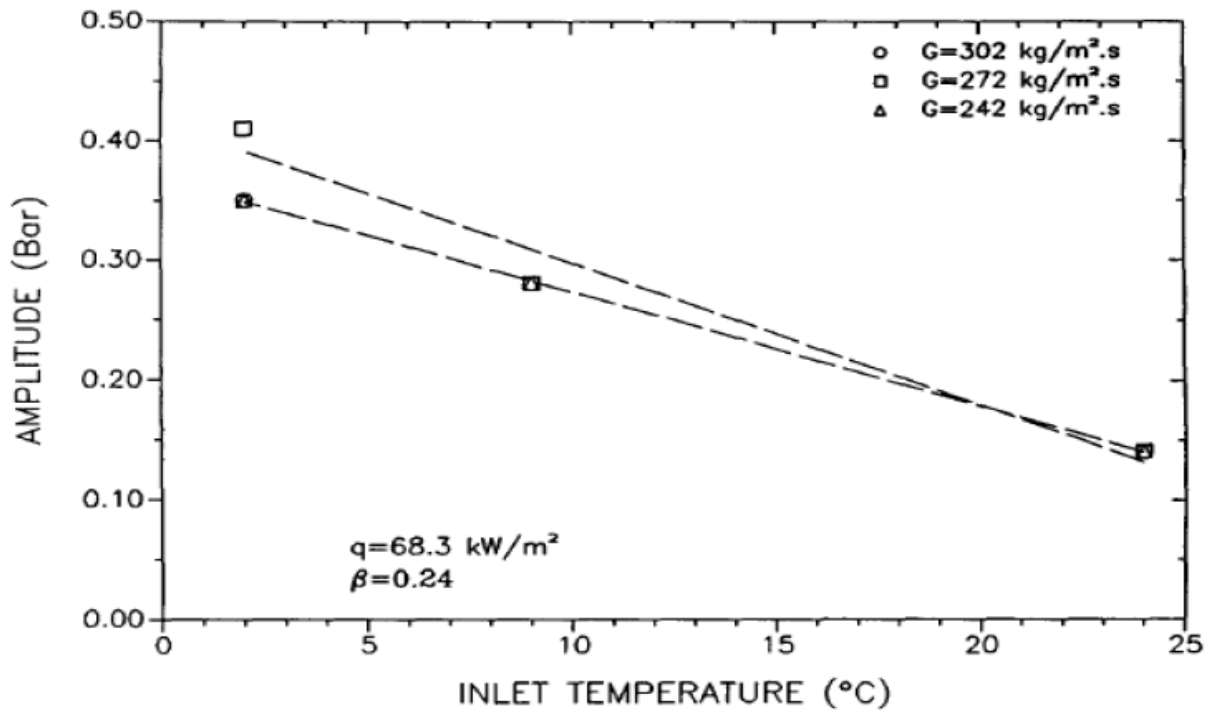


Figure 12: Relation between inlet temperature and amplitude of DWO [Ding et al. 1995]. Be aware that increased inlet temperature implies decreased subcooling.

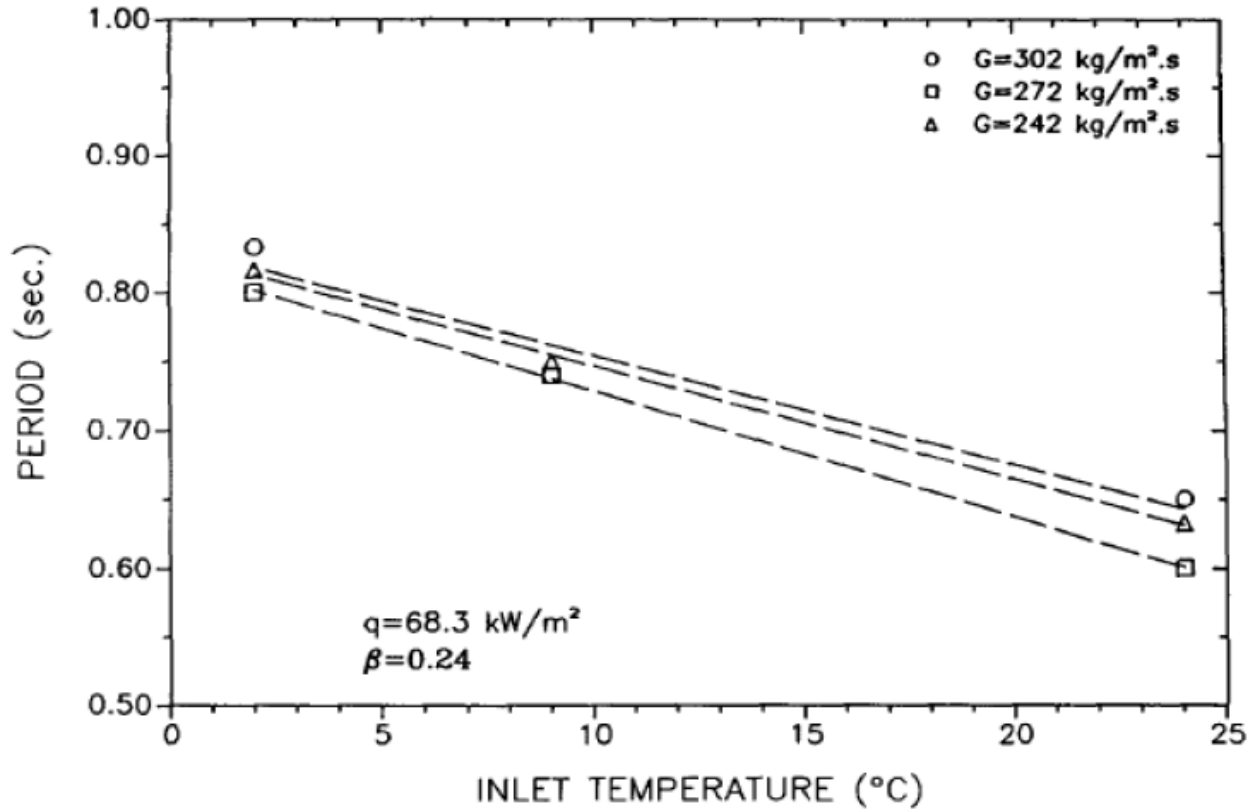


Figure 13: Relation between inlet temperature and period of DWO [Ding et al. 1995].

Comakli et al. [2002] used R-11 in a single heated horizontal channel and studied the effects of adjusting inlet subcooling and mass flow while the applied heat, system pressure and exit restriction were held constant. The period and amplitude of density wave type oscillation were found to decrease with decreasing mass flow rate and increasing with decreasing inlet temperature. It is also mentioned that the stability boundary obtained from the experiments do not coincide with Ding (1993) or Widmann (1994) as cited in Comakli et al. [2002] shown in figure 14. The differences may be attributed to experimental setup such as length, diameter of the tube and exit restriction or it may be caused by different operational conditions. These differences may also be the reason why some of the previously mentioned studies do not coincide on certain characterizing effects.

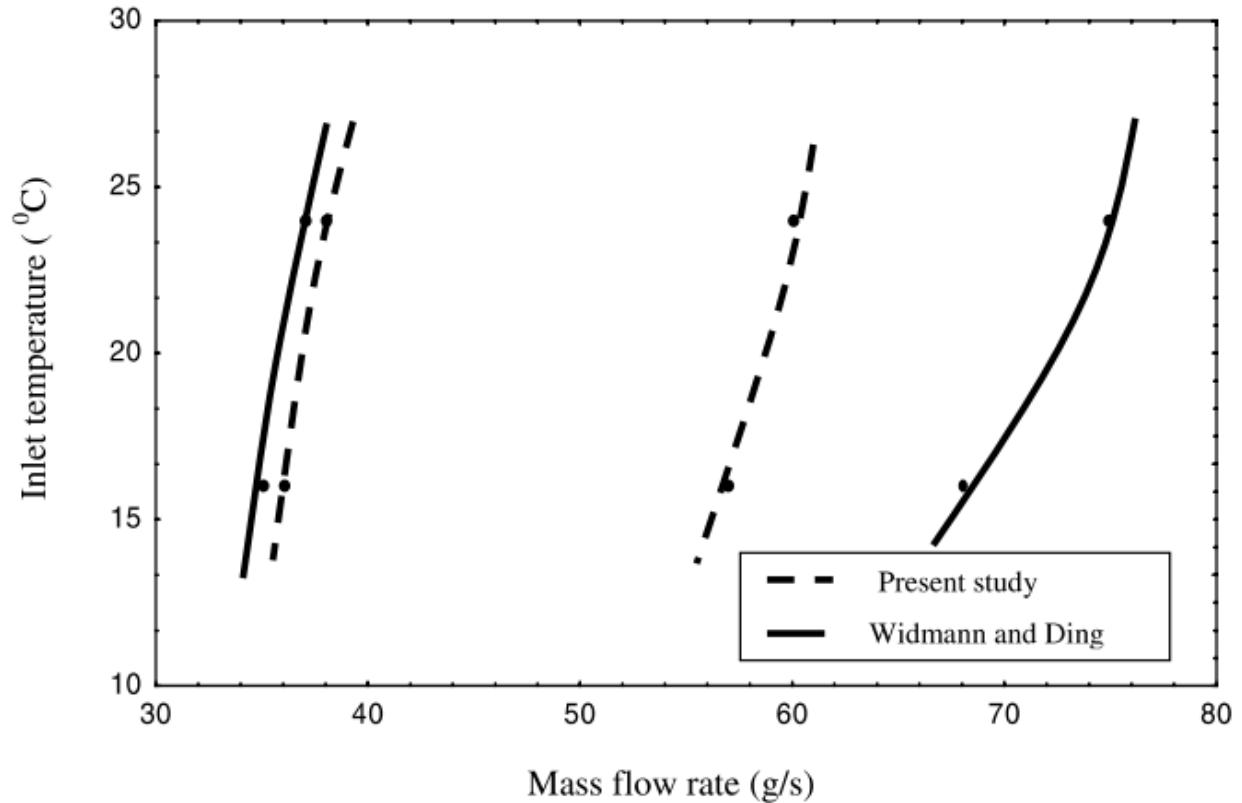


Figure 14: Comparison of the stability boundaries where “present study” refers to the experiments conducted in Comakli et al. [2002].

From the facility at NTNU [Ruspini, 2013] [Chiapero, 2013] experimental investigations are done on a single heated horizontal channel using R-134a as working fluid by for example Ugueto [2013] and Sørnum [2013]. Ugueto found that the oscillation amplitude and frequency increased with increasing heat flux and that the Ishii-Zuber stability map (see section 3.2.1) was appropriate to represent system stability. Sørnum studied the characterizing effects of heat flux, inlet subcooling, mass flux and pressure. The effect of increased heat flux correlated with Ugueto’s research and is illustrated in figure 15 and 16. It is commented that the heat seems to reach a limit of how much it can increase the amplitude, but further investigation are limited by max temperatures in the lab setup. The x-axis ΔT_{sub} from figure 17 is the difference between the saturation temperature and the inlet temperature ($\Delta T_{\text{sub}} = T_{\text{sat}} - T_{\text{in}}$) and the y-axis is given as the amplitude of mass flux divided average mass flux ($\Delta G/G$), and implies that the amplitude increases with increased subcooling for all the different mass fluxes and power inputs investigated, and the period was also found to increase with increased subcooling (figure 18). Even though increased inlet subcooling gave increased amplitudes, the system was shown to be stabilized by raising the threshold value of heat. The threshold value of heat refers to the applied heat needed to provoke DWO. Increased mass flux gave reduced amplitude (figure 19) and varying effects for the period (figure 20) depending on the heat inputs. The increased inlet pressure in figure 21 led to an increase in amplitude at the lower mass flux, and a decrease in

amplitude for higher mass flux, while the period was found to increase with increased inlet pressure for all mass fluxes (figure 22).

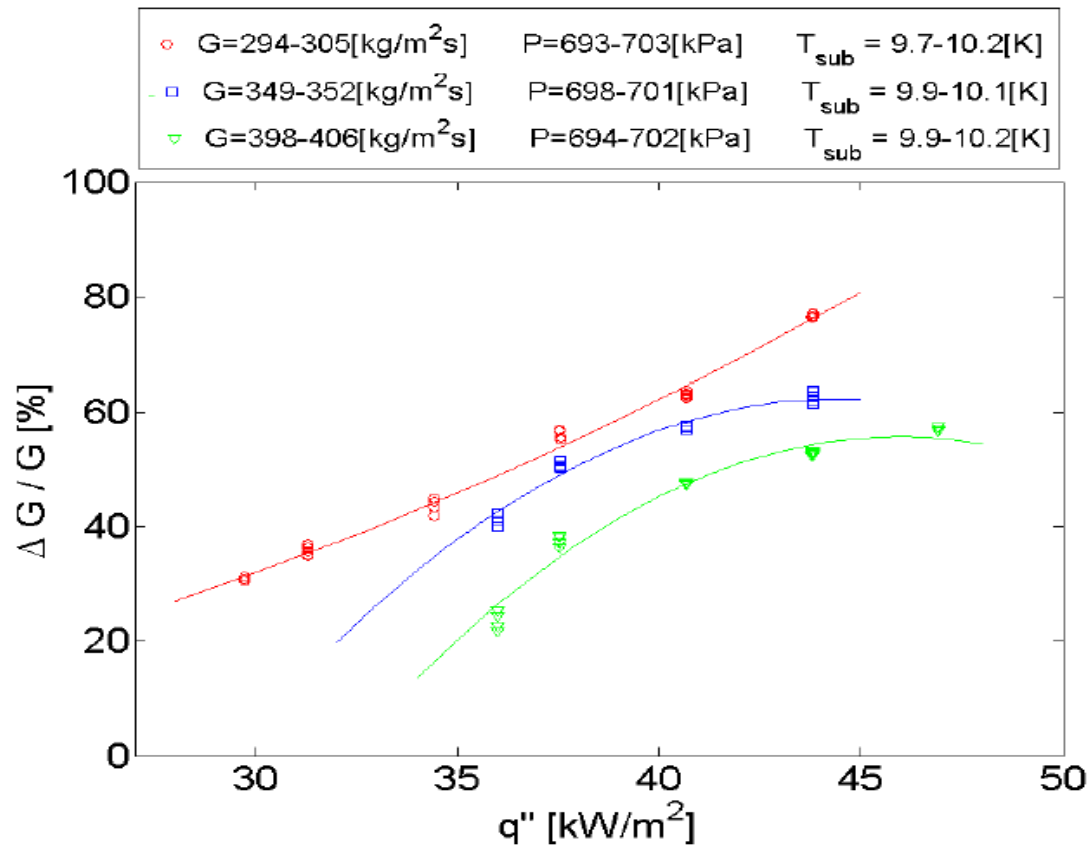


Figure 15: Relation between amplitude of DWO and heat flux for different mass fluxes for $P_{\text{in}}=7\text{bar}$ [Sørum, 2013].

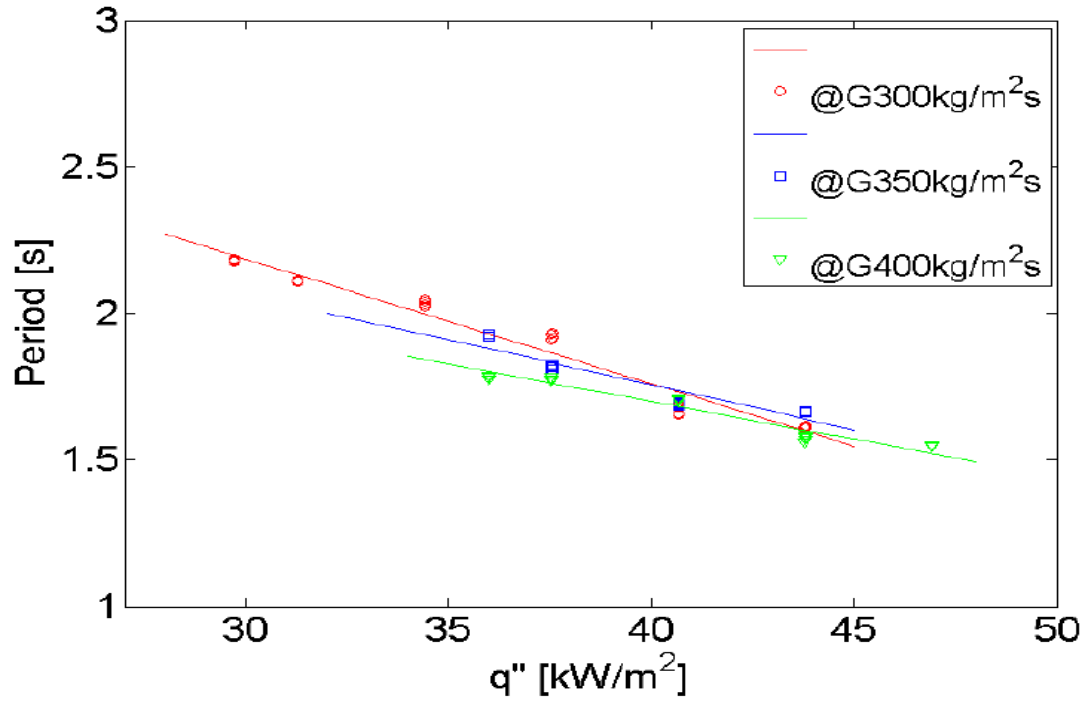


Figure 16: Relation between amplitude of DWO and heat flux for different mass fluxes for $P_{in}=7\text{bar}$, $\Delta T_{sub}=10\text{K}$ [Sørum, 2013].

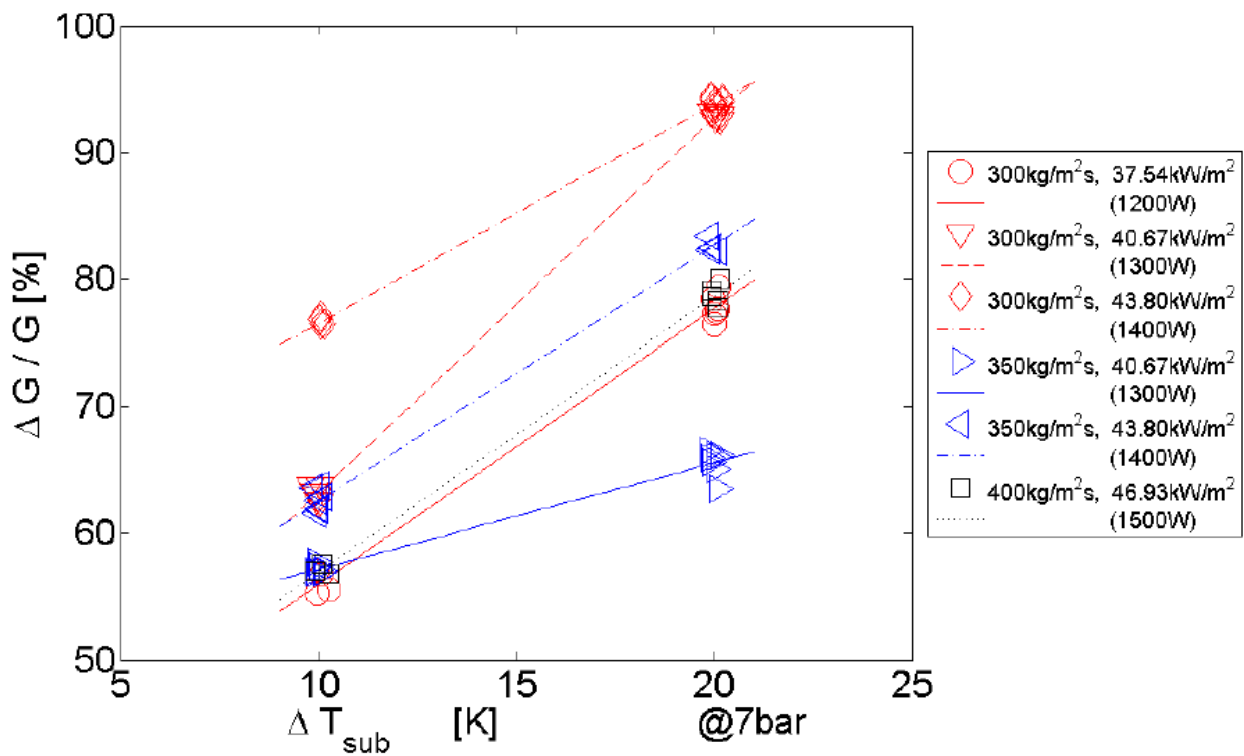


Figure 17: Relation between amplitude of DWO and inlet subcooling for different mass fluxes and power inputs for $P_{in}=7\text{bar}$ [Sørum, 2013].

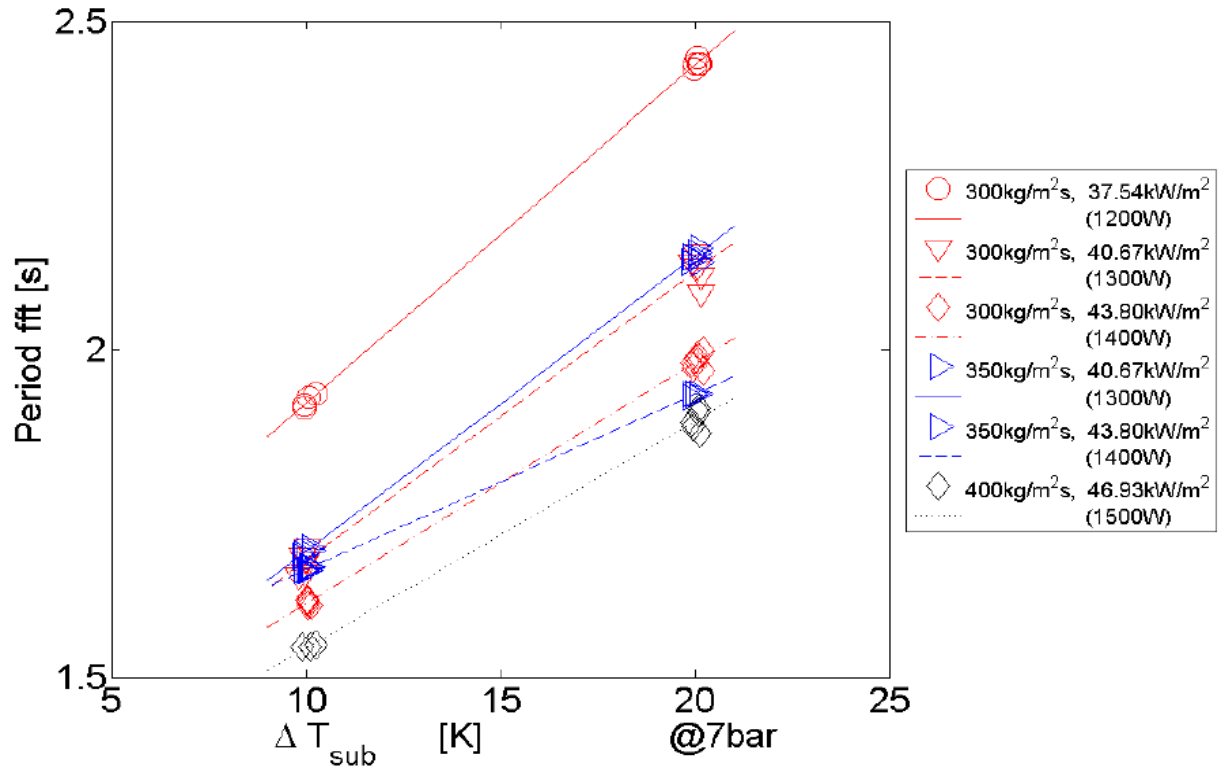


Figure 18: Relation between period of DWO and inlet subcooling for different mass fluxes and power inputs for $P_{in}=7\text{bar}$ [Sørum, 2013].

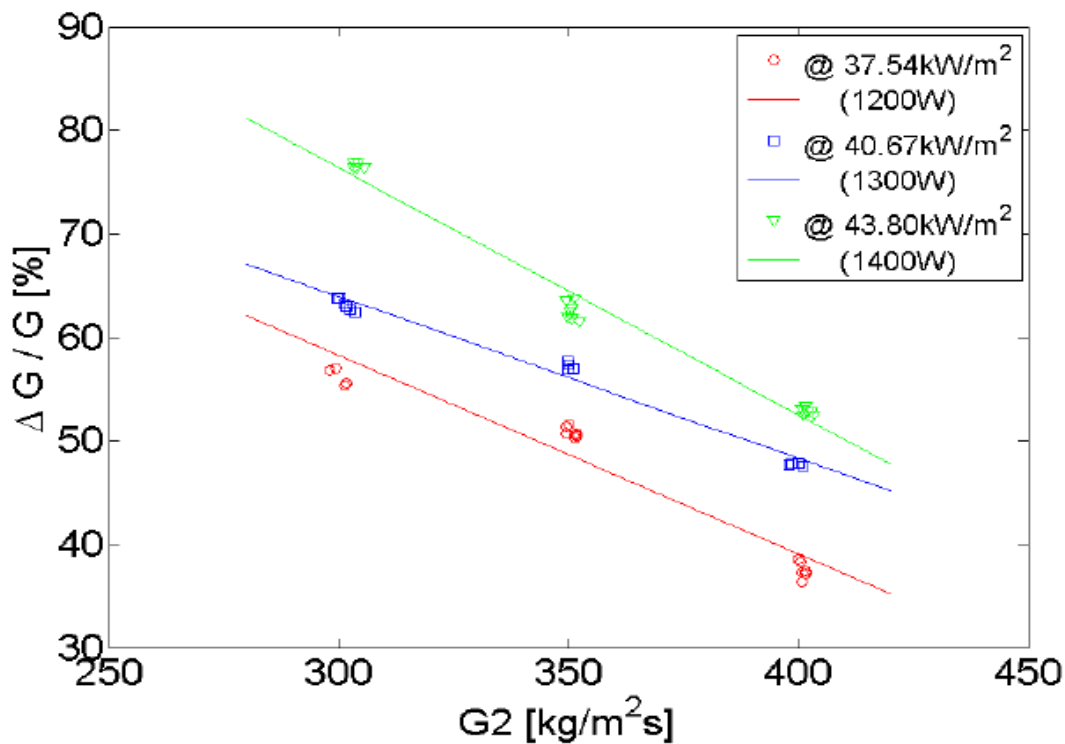


Figure 19: Relation between the amplitude of DWO and the mass flux with three different power inputs and $\Delta T_{sub}=10\text{K}$, $P_{in}=7\text{bar}$ [Sørum, 2013].

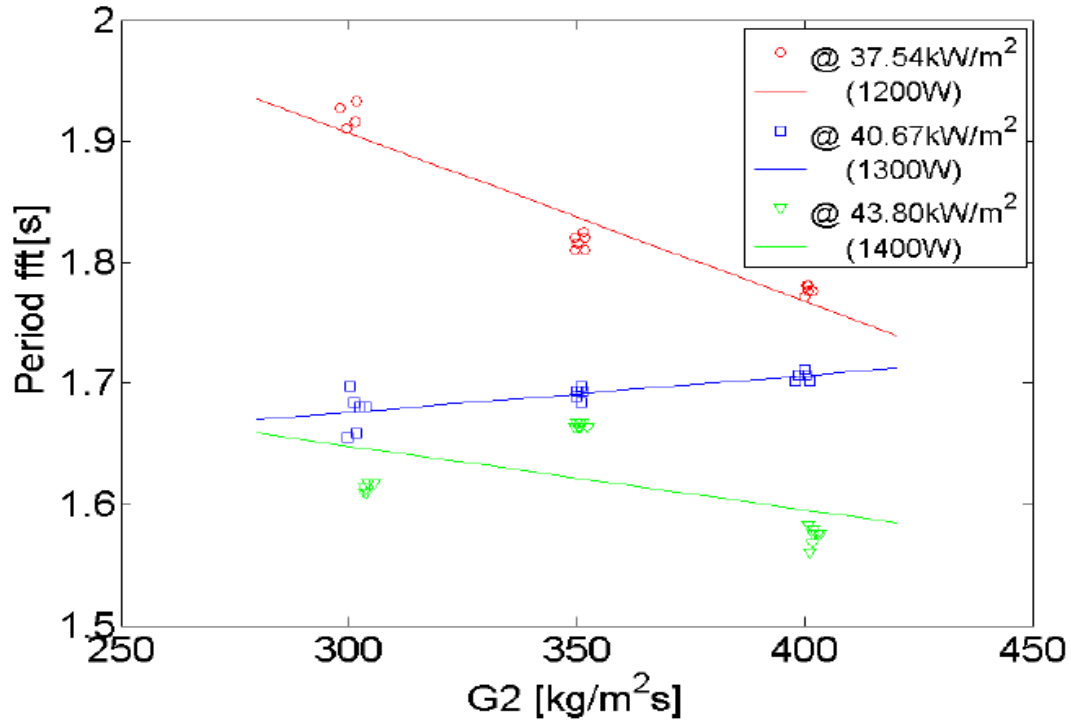


Figure 20: Relation between the period of DWO and the mass flux with three different power inputs and $\Delta T_{\text{sub}}=10\text{K}$, $P_{\text{in}}=7\text{bar}$ [Sørum, 2013].

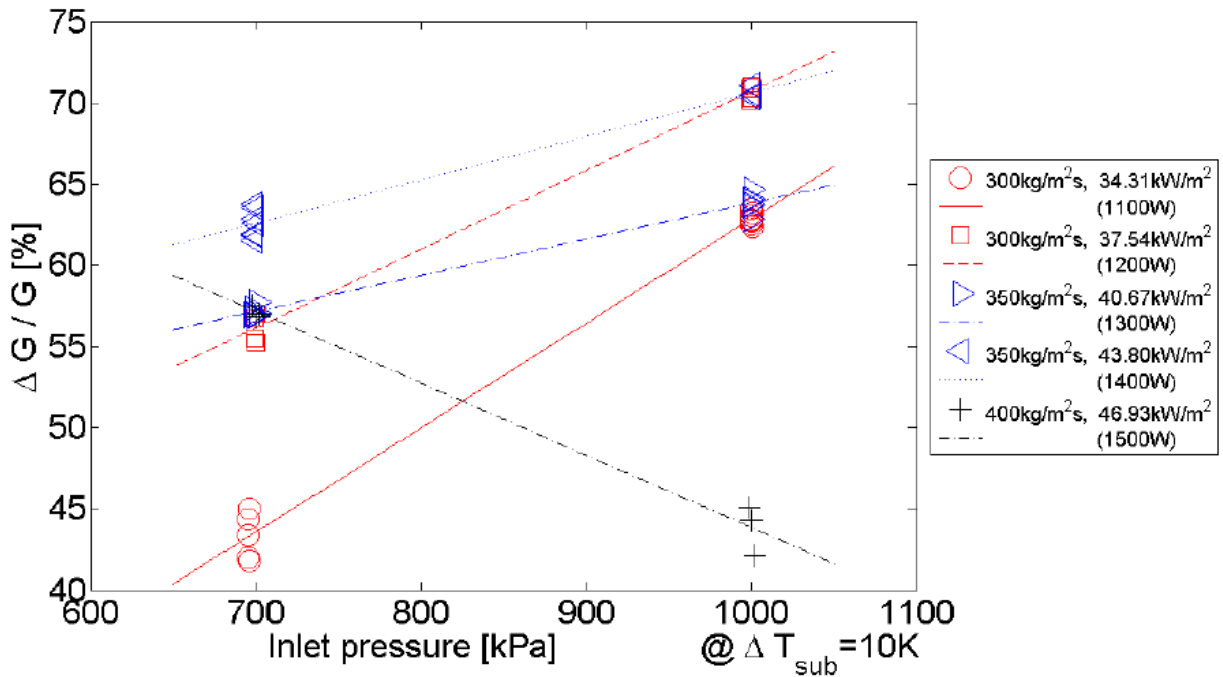


Figure 21: Relation between the amplitude of DWO and the inlet pressure with different power inputs, mass fluxes and $\Delta T_{\text{sub}}=10\text{K}$ [Sørum, 2013].

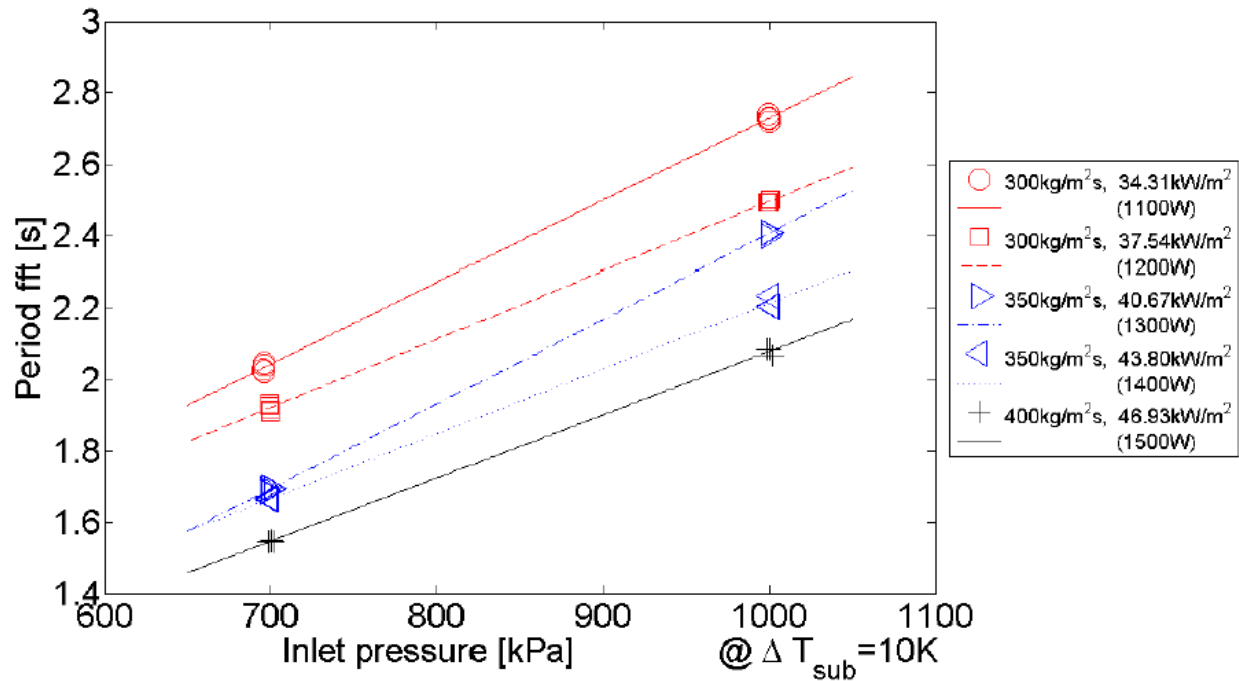


Figure 22: Relation between the period of DWO and the inlet pressure with different power inputs, mass fluxes and $\Delta T_{sub}=10K$ [Sørum, 2013].

3.3.2 Numerical investigations of DWO

Qualified numerical simulation tools can be applied to the study of boiling channel instabilities in order to get quantitative predictions of flow behavior and numerous numerical studies of density waves have been conducted in the recent years [Papini et al., 2011]. In a broad way numerical methods can be viewed as discrete approximation operator and when they are applied to the set of two-phase flow equations these operators yield numerical models suitable for computer implementation [Belblidia & Bratianu, 1979]. Most of the numerical studies are concerned with predicting stability boundaries and not with characterizing effects, but some of them are still mentioned for the sake of insight in the theoretical research field. Some numerical codes encountered in literature are discussed, in order to see what the code used in chapter 4 is capable of compared to other DWO simulation-codes.

Riswan-Uddin [1994] studied two-phase flow boiling systems numerically using a model based on two non-linear, integro-differential equations and reported that the mixture velocity was the main governing mechanism instead of the mixture density as reported in classical description. The oscillation period was found to be between three and four times the channel transit time, so that equation 3.3 would get values roughly between 0.25 to 0.33 and not 0.5 as commonly reported.

Ambrosini [2000] and Ambrosini & Ferrer [2006] used both a six equations non-homogeneous non-equilibrium model and a HEM model to study density waves implemented by the so-called

RELAP5 code (U.S. NRC Nuclear Safety Analysis Division, 2001), and united the two opposing views of Riswan-Uddin [1994] and the classical description by stating that the reason for the difference in the ratio of channel transit time to the oscillation period was different levels of subcooling. The classical description was stated to rely on a lower subcooling than Riswan-Uddin [1994]. Ambrosini displayed the relation between subcooling and the ratio between channel transit time and the oscillation period in a stability map as in figure 23:

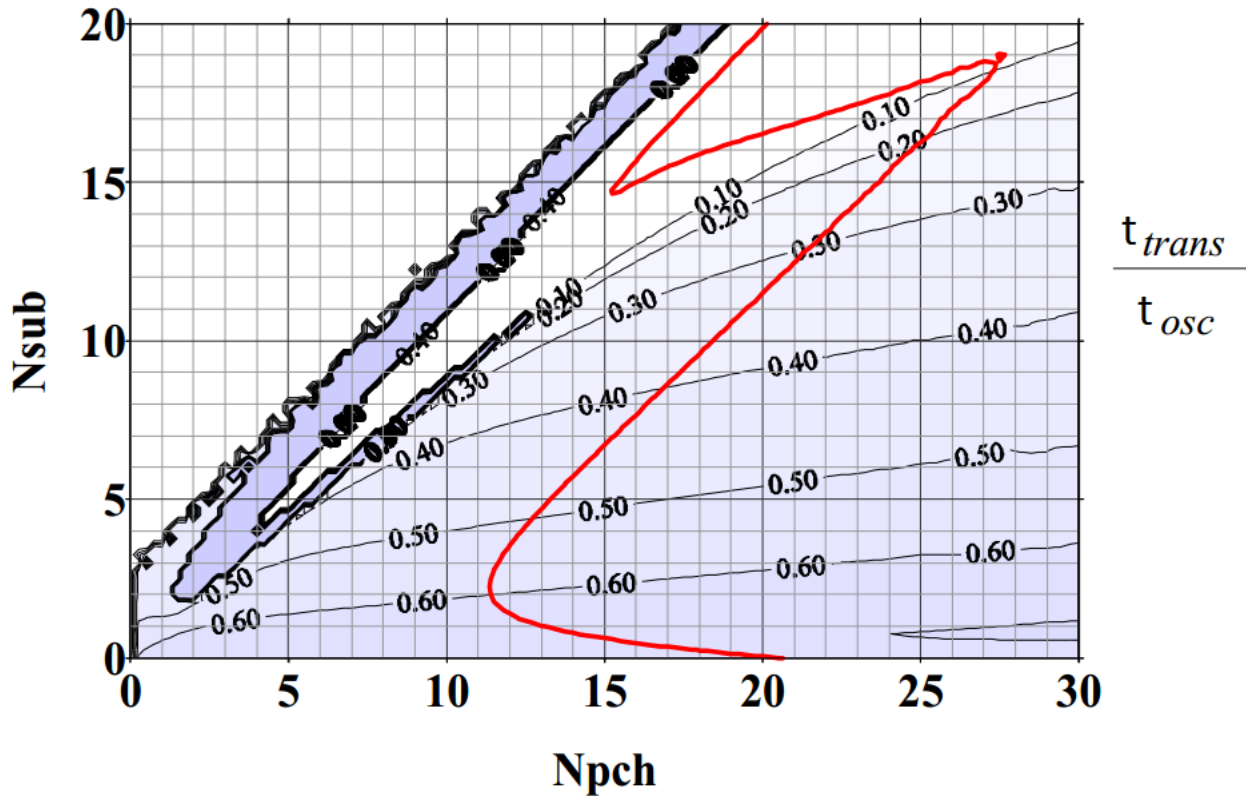


Figure 23: Ratio of the fluid transit time to the period of oscillations evaluated by the linearized simplified HEM model. The red line is the predicted stability boundary [Ambrosini & Ferrer, 2006].

Figure 23 implies that channel transit time divided by the oscillation period decreases with the increasing subcooling number.

Colombo et al. [2012] also used the RELAP5 code to contribute to the assessment of the code's capability to detect the onset of DWO. The study tried to reproduce results conducted in an experimental facility including a single channel and two helically coiled parallel channels. For the different configurations the code predicted threshold of instability close to the experimentally found threshold. The effect of a large bypass valve to impose a constant pressure drop over the channel where also investigated numerically and the code reproduced values close to the experimentally attained results. By increasing the inclination from a horizontal to a vertical duct, stabilizing effects were found due to a higher gravitational pressure drop term shown in figure 24.

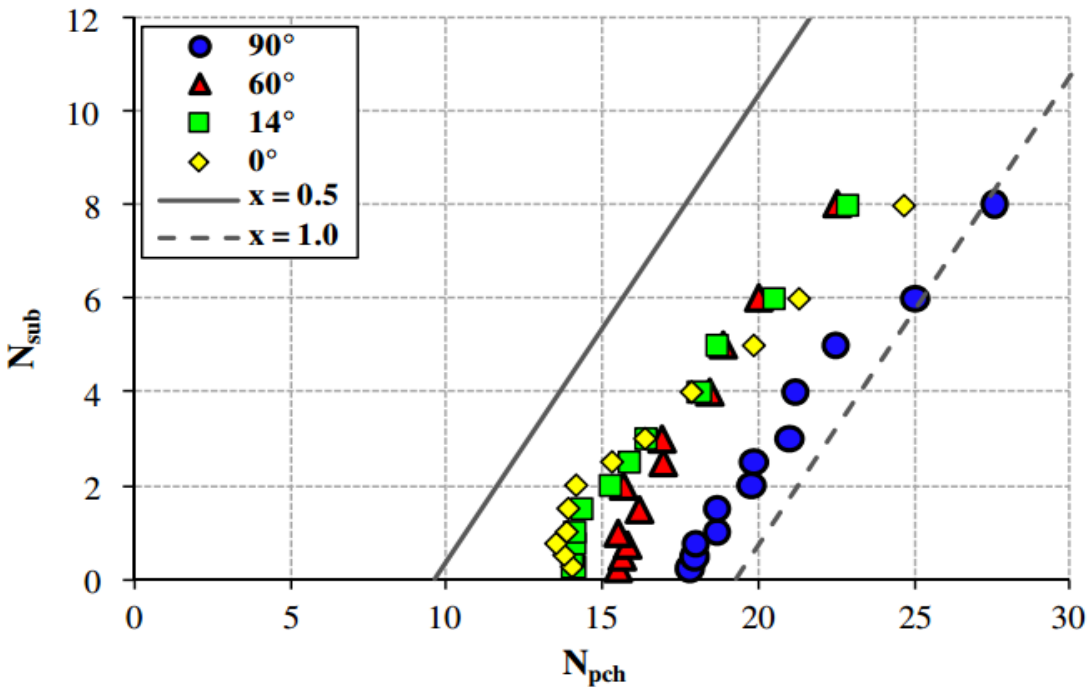


Figure 24: Stability thresholds obtained in parallel channels with different channel inclination [Colombo et al. 2012].

Papini et al. [2011] and Papini et al. [2012] used RELAP5 and another code called COMSOL, a multiphysics code, to study DWO for both time-domain linear and non-linear conditions. The COMSOL Multiphysics® (COMSOL, Inc, 2008) is a numerical code gaining importance in recent years, based on its possibility to solve different numerical problems by implementing directly the system of equations in PDE-form (partial differential equation) by means of finite element techniques, which is different from RELAP5 that considers finite volume discretization of the governing equations. In Papini et al. [2011] a parametric discussion for thermal power, flow rate, inlet subcooling, system pressure and inlet/exit throttling are given, focusing on stability boundaries. In Papini et al. [2012] the theoretical steps were explained in more detail. First the steady-state conditions are calculated by solving the set of governing equations. The steady-state solutions are then used as initial conditions for the integration of the equations in order to obtain the time evolution of each computed state variable. The systems transient response will then expose the instability threshold by passing through damping out oscillations, limit cycle oscillations (referred to as marginally stable in chapter 4 and 5) and divergent oscillations. This is similar to the code used in chapter 4. The code is not able to produce limit cycle oscillations within the unstable area, which are evidently occurring as seen from the study of the experimental results in chapter 5.

The effect of inlet subcooling has been investigated numerically by Strømsvåg [2011], using water as working fluid in a horizontal single heated channel. Among the findings was that an increased subcooling lead to an increase in amplitude of the exit mixture velocity variation shown in figure 25 and an increase in oscillation period shown in figure 26. However, between point 1

and 2 in figure 25 and point 6 and 7, the amplitude appears to decrease with increasing amplitude. This indicates that even though the overall tendency of the amplitude seems to increase with increased subcooling, there are some deviations present for some of the operating conditions.

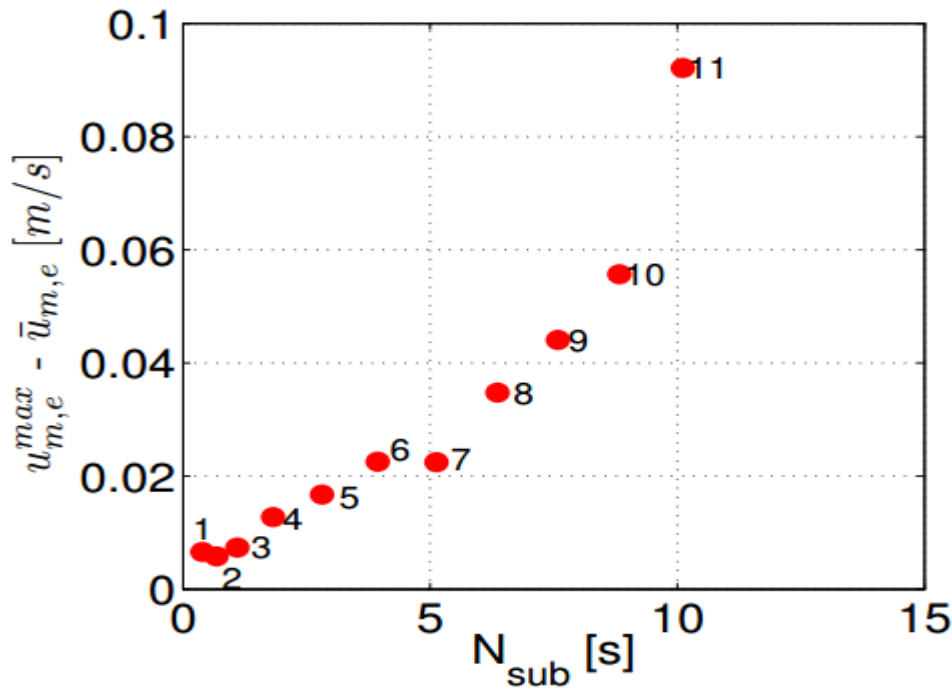


Figure 25: Amplitude of the oscillation in exit mixture velocity $u_{m,e}$ for marginally stable operating points at different levels of subcooling [Strømsvåg 2011].

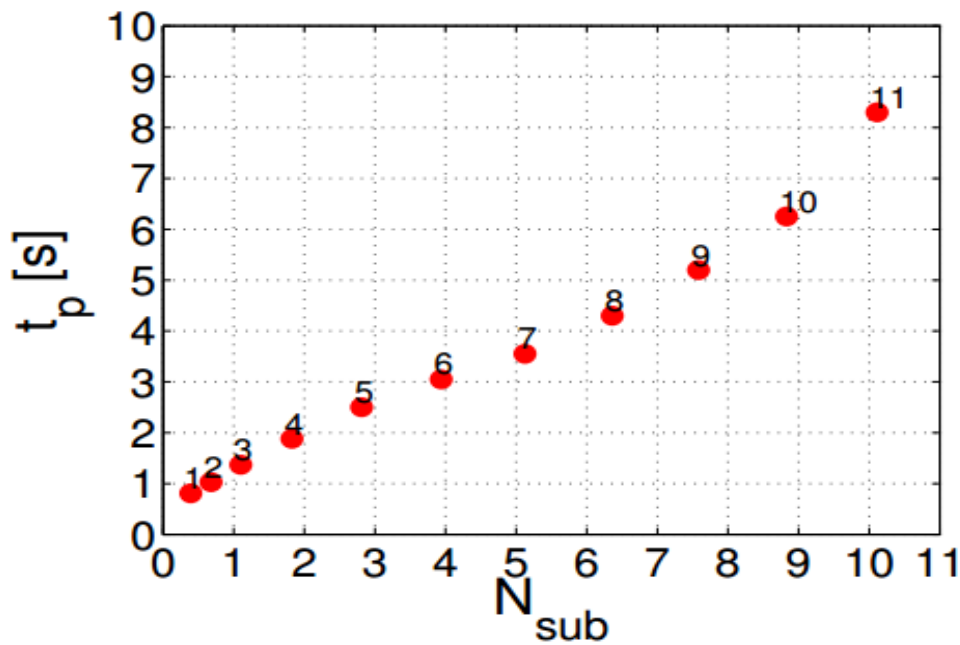


Figure 26: Evolution of oscillation period t_p for marginally stable oscillations at different levels of subcooling [Strømsvåg 2011].

3.4 Characterizing effects

From the literature study it is seen that some opposing effects are stated, so a hypothesis for characterizing effects of DWO would be helpful for comparing theory with results later in this thesis. Here the characterizing effects are summed up:

3.4.1 Applied heat

Amplitude

Studies that mentions an *increase* in amplitude by increasing the applied heat:

- Saha et al. [1976],
- Yuncu [1990]
- Ugueto [2013]
- Sørnum [2013]

Study that mentions a *decrease* in amplitude by increasing the applied heat:

- Ding et al. [1995]

Period

Studies that mentions a *decrease* in period by increasing the applied heat:

- Yuncu [1990]
- Ding et al. [1995]
- Ugueto [2013]
- Sørnum [2013]

No opposing views found regarding the period of increasing the applied heat.

3.4.2 Inlet subcooling

Amplitude

Studies that mentions an *increase* in amplitude by increasing the inlet subcooling ΔT_{sub} :

- Ding et al. [1995]
- Comakli et al. [2002]
- Strømsvåg [2011]
- Sørnum [2013]

The results of Strømsvåg showed that the amplitude was not strictly increasing with increased subcooling, as some deviations occurred.

Period

Studies that mentions an *increase* in period by increasing the inlet subcooling ΔT_{sub} :

- Osawa et al. [1979]
- Ding et al. [1995]
- Comakli et al. [2002]

- Strømsvåg [2011]

Study that mentions a *decrease* in period by increasing the inlet subcooling ΔT_{sub} :

- Saha et al. [1976]

3.4.3 Pressure

Amplitude

The system pressure is in this thesis defined as the mean value of the absolute pressure measured in the entrance of the test section. Studies that mentions a *decrease* in amplitude by increasing the pressure:

- Dolgov & Sudnitsyn [1965] (vertical channel)
- Bouré et al., [1973] (literature review)
- Mathisen [1967] (vertical channel)

Study that mentions both a *decrease and an increase* in amplitude by increasing the pressure depending on the level of mass flux:

- Sørnum [2013]

Period

Studies that mentions an *increase* in period by increasing the pressure:

- Wang et al. [1994] (vertical channel)
- Sørnum [2013]

Studies that mentions *no effect* of pressure variations on the period:

- Bouré et al., [1973] (literature review)
- Mathisen [1967] (vertical channel)

3.4.4 Mass flux

Amplitude

Studies that mentions an *increase* in amplitude by increasing the mass flux:

- Yuncu [1990]
- Ding et al. [1995]

Studies that mentions a *decrease* in amplitude by increasing the mass flux:

- Akagawa et al., [1971]
- Comakli et al. [2002]
- Sørnum [2013]

Period

Studies that mentions an *increase* in period by increasing the mass flux:

- Akagawa et al., [1971]
- Ding et al. [1995]

- Comakli et al. [2002]

Study that mentions both a *decrease and an increase* in period by increasing the mass flux depending on the level of applied heat:

- Sørnum [2013]

3.4.5 Hypothesis

On the basis of the literature study, the following hypothesis is made on the parametric effects regarding amplitude and period of the DWO oscillations:

	Increased heat	Inc. subcooling	Inc. pressure	Inc. mass flux
Amplitude	Positive	Positive	Negative	Negative
Period	Negative*	Positive	No effect	Positive

Table 1: Hypothesis on characterizing effects for DWO.

*no opposing effects found in literature

With the exception of the period for increased heat, there are different effects mentioned for all the parameters. This might be caused by different operating conditions, so opposing effects can arise as seen from example in figure 20 and 21.

4 Simulated Density Wave Oscillations

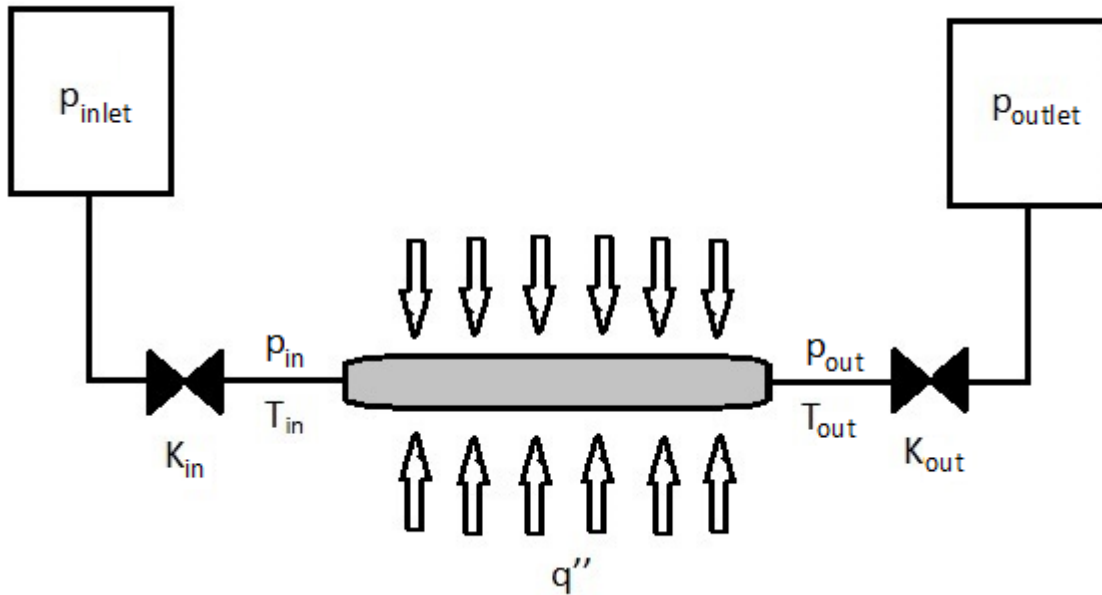


Figure 27: Schematic of the modeled system.

4.1 Modeled System

Figure 27 shows a schematic of the modeled system. The model consists of a heated pipe, an inlet restriction and an outlet restriction with respective pressure drop coefficients K_{in} and K_{out} . The inner diameter of the pipe is set to 5 mm for all simulations. The inlet reservoir pressure is denoted p_{inlet} and the outlet reservoir pressure p_{outlet} . T_{in} and p_{in} is the temperature and pressure going into the tube and q'' is the added heat flux. T_{out} and p_{out} is the temperature and pressure going out of the tube, respectively. The model will be used to study density wave oscillations and to characterize the effect of applied heat, inlet subcooling and pressure with regards to period and amplitude of the mass flux. Increase in power input leads to an increase in the applied heat to the pipe so the terms “power input”, “heat flux” and “applied heat” are used interchangeably. As discussed in section 3.2.1 the marginally stable flow with constant period and amplitude is attained when operating on the stability boundary. Operating to the right of the stability threshold in figure 3 gives diverging flow behavior where the driving forces of acceleration is predominant [Belblidia & Bratianu, 1979]. The mass flux curve will over time then in theory resemble figure 4 b) and oscillate out of proportions. Operating to the left of the stability boundary will in theory produce convergent mass flux oscillations, shown in figure 4a), due to the damping effect caused by frictional forces [Belblidia & Bratianu, 1979].

The explanation of density waves in section 3.1 suggests that both the velocity and density will show oscillating behavior in the boiling channel. The mass flux is a function of both of these

parameters (see equation 2.7), so the mass flux oscillations over time will be investigated in order to study density waves. As figure 4 in section 3.2.1 suggested, an unstable diverging behavior is characterized by an increase of amplitudes while the frequency expresses how often the density waves occur. To determine the characterizing effects of the affecting parameters, the changes in amplitude and period needs to be extracted and studied. The affecting parameters studied are heat applied to the system, inlet subcooling, pressure and mass flux.

The model is implemented by an already existing code. The following assumptions are made concerning the system flow in the model:

- One-dimensional
- Horizontal channel
- Homogeneous flow
- Thermodynamic equilibrium
- Constant externally imposed pressure drop
- Constant inlet temperature
- Constant uniform heating

It is important to note that the only instability produced by the model is DWO, so there is no possibility of mistaking the DWO for other instabilities as PDO, acoustic oscillations etc. (see section 2.5). The model solves the conservation equations for mass, momentum and energy as discussed in section 2.3.1:

$$\text{Mass:} \quad \frac{\partial \rho_m}{\partial t} + \frac{\partial G}{\partial z} = 0 \quad (4.1)$$

$$\text{Momentum:} \quad \frac{\partial G}{\partial t} + \frac{\partial}{\partial z} \left(\frac{G^2}{\rho_m} \right) + \frac{\partial p}{\partial z} + \left(\frac{F}{D_H} + \sum_{j=1}^N K_j \delta(z - z_j) \right) \frac{G^2}{2\rho_m} = 0 \quad (4.2)$$

$$\text{Energy:} \quad \frac{\partial \rho_m h_m}{\partial t} + \frac{\partial G h_m}{\partial z} = q \frac{P_H}{A_x} \quad (4.3)$$

One benefit of performing horizontal simulations is that gravitational effects can be neglected in the axial direction. The pressure drop in the valves is calculated using a pressure drop concentrated value, K_j , for each valve. The relation can be expressed as:

$$K = \frac{\Delta p}{\frac{1}{2} \rho u^2} \quad (4.4)$$

where Δp is the pressure loss across the valve and u is the velocity. Friction losses are neglected in the energy equation. To solve the governing equations, the Space-Time Least-Square Spectral

Element Method is utilized. For more information about the used numerical scheme used in the model, the reader is referred to Maerschallck [2003] for more information.

The program REFPROP8 (REference Fluid PROPERTIES v. 8.0) developed by the National Institute of Standards and Technology (NIST) is used to acquire fluid properties. The mixture density ρ_m is regarded as a function of the mixture enthalpy h_m and the steady state inlet pressure p_{in} throughout the boiling channel [Strømsvåg, 2011].

The working fluid used in all simulations is 1,1,1,2-tetrafluorethane, referred to as refrigerant R-134a. At atmospheric pressure R-134a has a boiling point of -26.3°C , and a latent heat of vaporization of $2.17 \cdot 10^5$ J/kg. That is significantly below the boiling point and the latent heat of vaporization of water (100°C and $2.26 \cdot 10^6$ J/kg), which makes it ideal to use.

4.2 Modeling procedure

The model simulates the system's transient response to the initial conditions set by the steady state solution. The steady state system is simulated first to validate that the initial conditions are indeed a steady state solution by assuming input values for the mass flux G and exit pressure p_{out} . That gives the necessary inlet reservoir pressure p_{in} . Then it goes on to solve the transient (time dependent) system with the inlet and exit reservoir pressures, p_{inlet} and p_{outlet} , as boundary conditions, giving a constant externally imposed pressure drop $\Delta p_{ext} (=p_{inlet}-p_{outlet})$.

To characterize the effects of applied heat, input data are assumed. The mass flux curve over time will then be convergent, divergent or marginally stable if the heat is sufficient to produce oscillations. As a hypothesis in accordance with the literature study, it is assumed that increased heat will lead to an increase in amplitude. To extract one single amplitude there is a need to find the marginally stable solution, as it is not possible to find one single amplitude for converging or diverging flow. The oscillations can be expressed as an approximate sine function, either damped (convergent) or amplified (divergent) on the form:

$$\text{Fitted damped/amplified sine wave: } y = A_G * \sin(2\pi ft + \phi)e^{(-\alpha t)} + B \quad (4.5)$$

where y is the axis for mass flux, A_G denotes the mean-to-peak amplitude (for an undamped operating condition), f is the frequency, t is the time coordinate, ϕ is the phase angle, α is the attenuation factor and B is the mean mass flux. Note that the α -value is defined with a minus sign in equation 4.5 so a negative α means increasing (diverging) oscillations. Each simulation has to compile for about four days to finish so it is essential to minimize the numbers of simulations needed to find the marginally stable operating parameters. If the first simulation results in diverging mass flux oscillations, the heat have to be decreased to find the marginally stable sine wave according to the hypothesis that an increase in applied heat results in an increase of amplitude, but for how much can be difficult to estimate and it may take a lot of simulations

using the “try-and-fail”-method. To make a qualified guess for the parameters in equation 4.5, the function “nlinfit” (or the “lsqcurvefit”-function) in matlab is used to fit an amplified sine wave to the diverging oscillations. The marginally stable sine wave will be on the form:

$$\text{Fitted marginally stable sine wave:} \quad y = A_G * \sin(2\pi ft + \varphi) + B \quad (4.6)$$

implying that the attenuation factor α is zero ($\epsilon=1$). Then it is assumed to be a linear relationship between the α -values and N_{pch} . When a couple of simulations are compiled for different heat numbers, a line can be drawn (shown later in figure 34) to guess the heat number that gives an attenuation factor of zero. The constant uniform power can for the estimated heat number then be extracted through the relation of equation 3.2, repeated in equation 4.7 below:

$$\text{Equilibrium phase change number:} \quad N_{pch} = \frac{(\rho_l - \rho_g)}{\rho_g} \frac{q}{\rho_l A h_{fg} u_i} \quad (4.7)$$

By following this procedure a value for heat input closer to the marginally stable case is found and the number of simulations can be diminished. To validate the model, experimental results from the lab are studied and compared to the results from the simulations (see section 4.5 and chapter 5). All the mass flux curves displayed is measured in the outlet of the channel in the simulated system. The simulation time is 100 seconds if the simulation is not interrupted.

4.3 Applied heat

To illustrate the procedure of finding the marginally stable oscillations the initial input data for the model is:

P_{in}	5.5 bar
P_{inlet}	6.05 bar
P_{out}	5 bar
ΔT_{sub}	15 K
K_{in}	7
K_{out}	3
G	300 kg/m ² s

Table 2: Initial simulation data.

The objective is to find the marginal stable case by adjusting the power applied to the system, denoted q below. The rest of the input data is held constant. The respective heat and cooling number N_{pch} and N_{sub} found below are time-averaged values. The calculation of the N_{pch} ignores the first part where the flow starts up and causes disturbances (see mass flux curves below). One of the reasons to not go directly to set input data that match experiments from the literature and rather set up a “self-made” case is to avoid any unconscious (or conscious) bias of the results. The y-axis is adjusted for every simulation so that a potential marginally stable case can be better visualized.

Heat simulation nr 1) $q = 200$ W, diverging

The given input data and a power input of 200 Watt gives the following flow curve in the outlet of the tube:

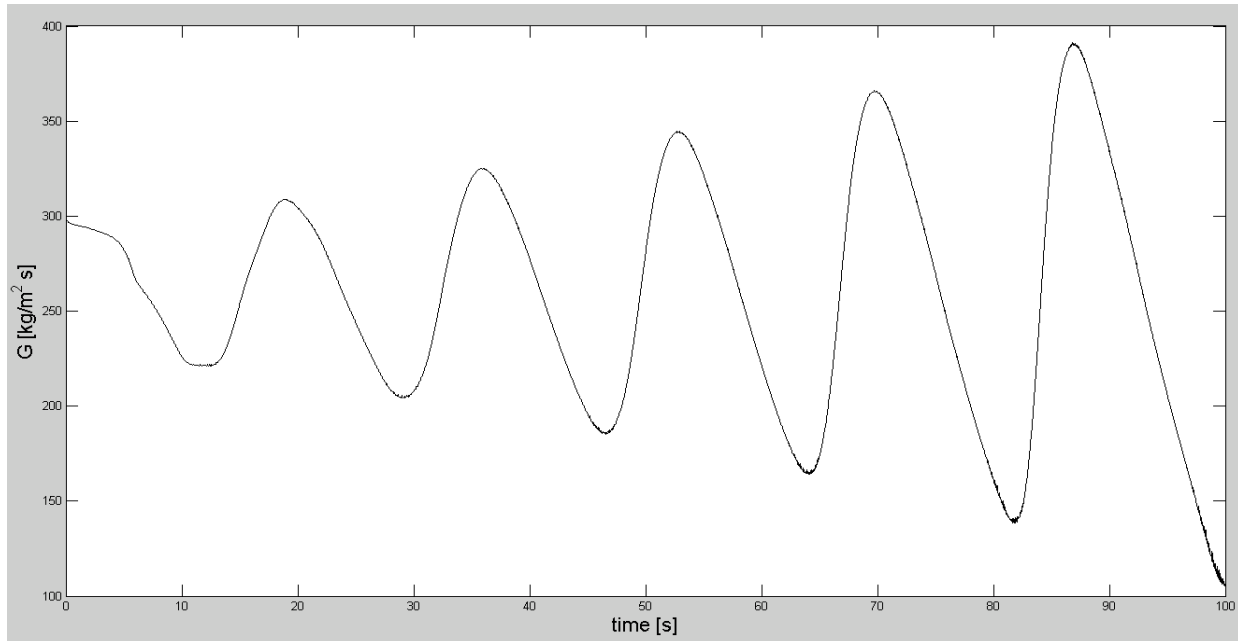


Figure 28: Mass flux curve with 200 Watt added to the horizontal channel.

The mass flux curve in figure 28 gives a diverging curve with increasing amplitudes. The disturbances during the approximately first 10 seconds are caused by the startup of the flow. The respective extracted average values for the heat and subcooling numbers are $N_{pch}=12.07$ and $N_{sub}=4.45$. The fitted sine curve is then found by using the “nlinfit”-function as explained in section 4.2 and becomes:

$$\text{Fitted amplified sine wave: } y = 39.32 * \sin(2\pi * 0.0578t + 0.8349)e^{(0.0123t)} + 260.78$$

The simulated mass flux is plotted along with the fitted sine curve for visualization purposes in figure 29 below. It is seen that the fitted curve is relatively close to the simulated mass flux curve, and it is wanted to be as close as possible to get a good estimate. The function for the sine wave will not be showed for every simulation to come, but the frequency and the α -value will be given. The fitted sine curve will be graphed for every simulation to get an idea of how good of a fit the estimated numbers will be, seeing that the results for frequency, the α -value and the amplitude for the marginally stable oscillations are based on this fit. The heat and subcooling numbers are based on the original curve marked as “simulated mass flux” in the graphs to come.

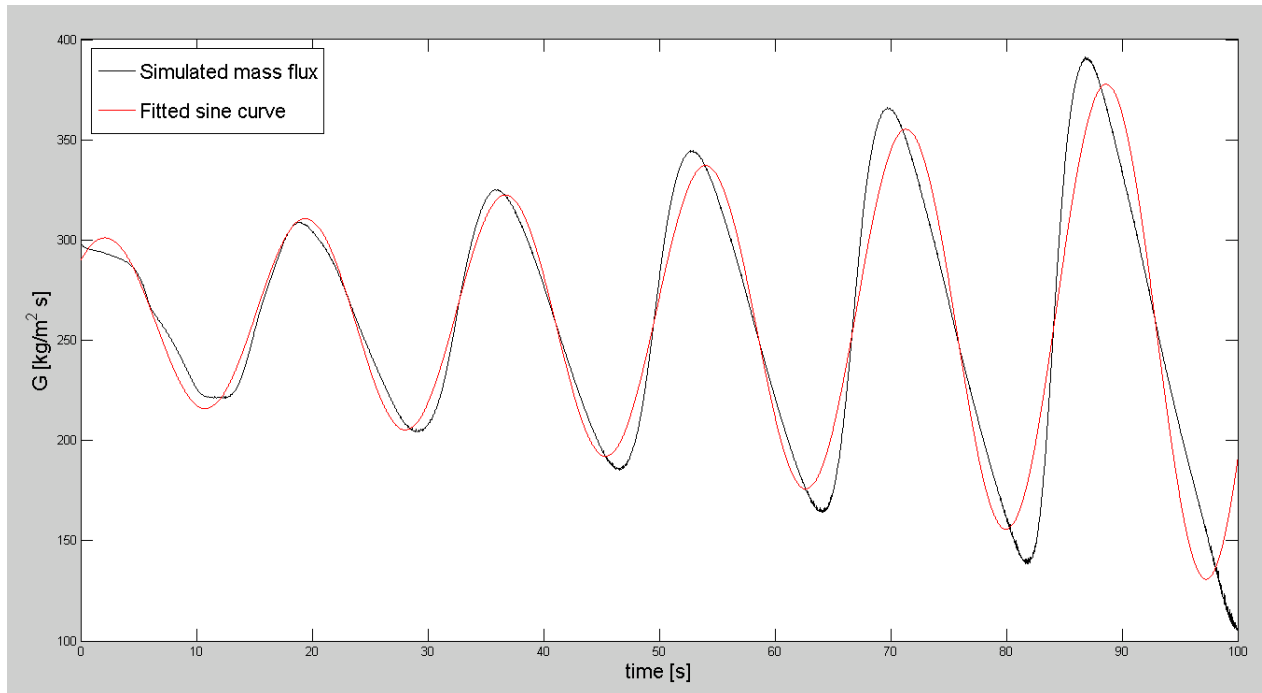


Figure 29: The simulated mass flux in black and the diverging fitted sine curve in red for a power input of 200 W.

Key values summed up from the simulation:

<i>Oscillation type</i>	Diverging
N_{pch}	12.07
N_{sub}	4.45
<i>Attenuation factor, α</i>	-0.0123
<i>Frequency and period</i>	0.0578 Hz giving a period of 17.3 seconds

Table 3: Key values from a power input of 200 W.

Heat simulation nr 2) $q = 180$ W, converging:

According to the hypothesis in section 3.4.5 it is seen that a decrease in heat input will supposedly give diminished amplitudes, so to find the marginally stable operating condition the power input is lowered to 180 W. That gives the following mass flux curve:

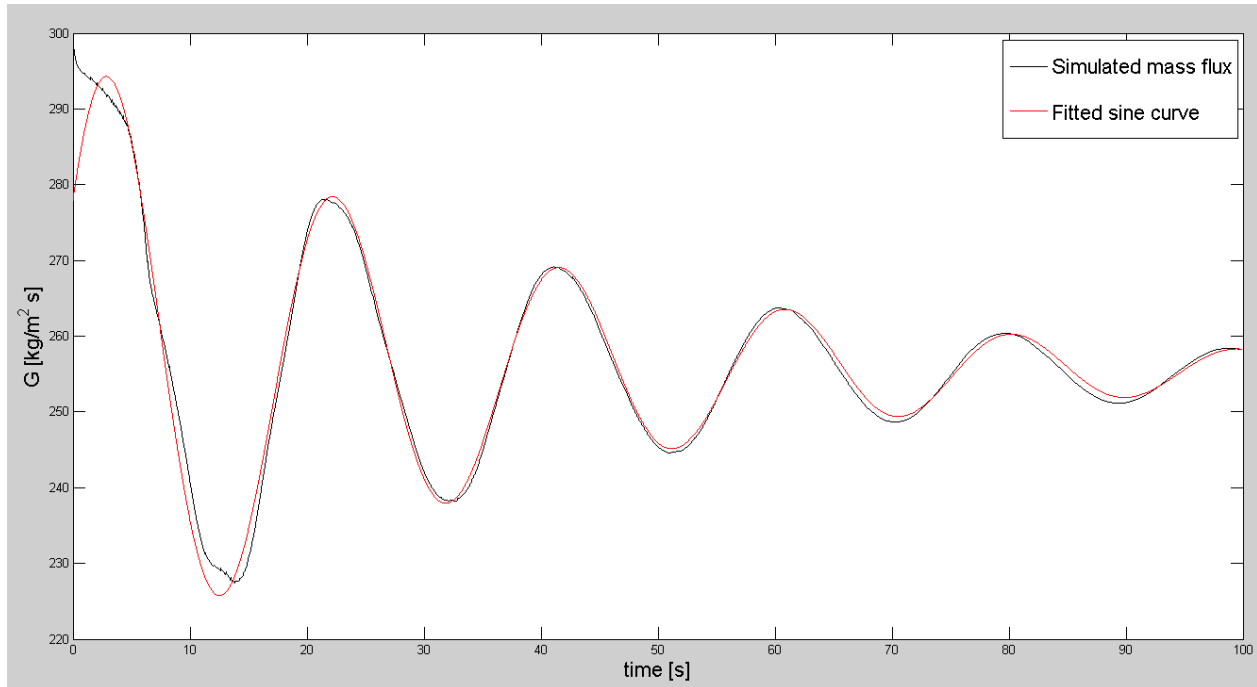


Figure 30: The simulated mass flux in black and the converging fitted sine curve in red for a power input of 180 W.

The decreased heat input made the oscillations converge instead of the previous diverging behavior. This supports the hypothesis of decreasing amplitude as a result of decreasing applied heat. Summed up:

<i>Oscillation type</i>	Converging
N_{pch}	9.66
N_{sub}	4.45
<i>Attenuation factor, α</i>	0.0272
<i>Frequency and period</i>	0.0517 Hz giving a period of 19.3 seconds

Table 4: Key values from a power input of 180 W.

Heat simulation nr 3) $q = 190$ W, slowly converging

To continue the search for the marginally stable case that operates on the stability boundary, the assumption is now that it lies in between the power input of 180 Watt and 200 Watt. The power input is then adjusted to be 190 Watt:

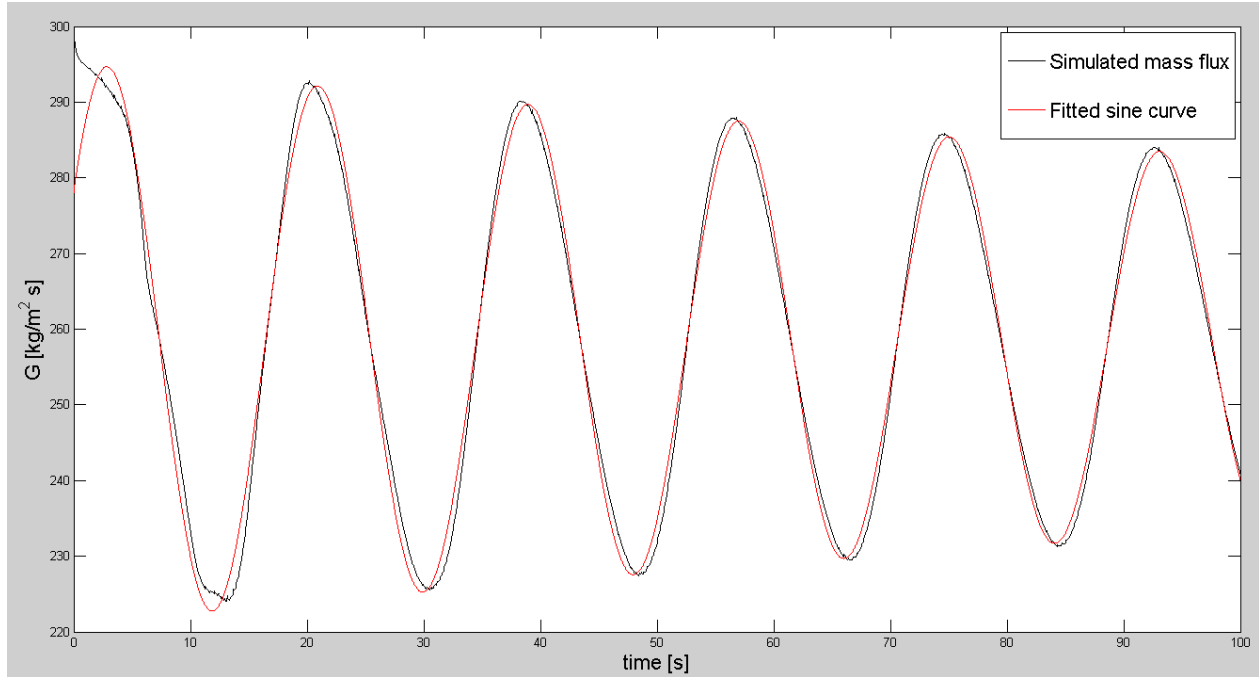


Figure 31: The simulated mass flux in black and the converging fitted sine curve in red for a power input of 190 W.

The mass flux curve has slowly diminishing amplitudes, and the key numbers becomes:

<i>Oscillation type</i>	Converging
N_{pch}	10.21
N_{sub}	4.45
<i>Attenuation factor, α</i>	0.0040
<i>Frequency and period</i>	0.0554 Hz giving a period of 18.1 seconds

Table 5: Key values from a power input of 190 W.

This is seen to be close to give limit cycle oscillations, and the threshold now has to occur between 190 and 180 W.

Heat simulation nr 4) $q = 195 \text{ W}$, interrupted halfway and assumed to be slowly diverging
 The power input is then set to 195 Watt. To save time the simulation is interrupted after 50 seconds after seeing a tendency towards a diverging behavior.

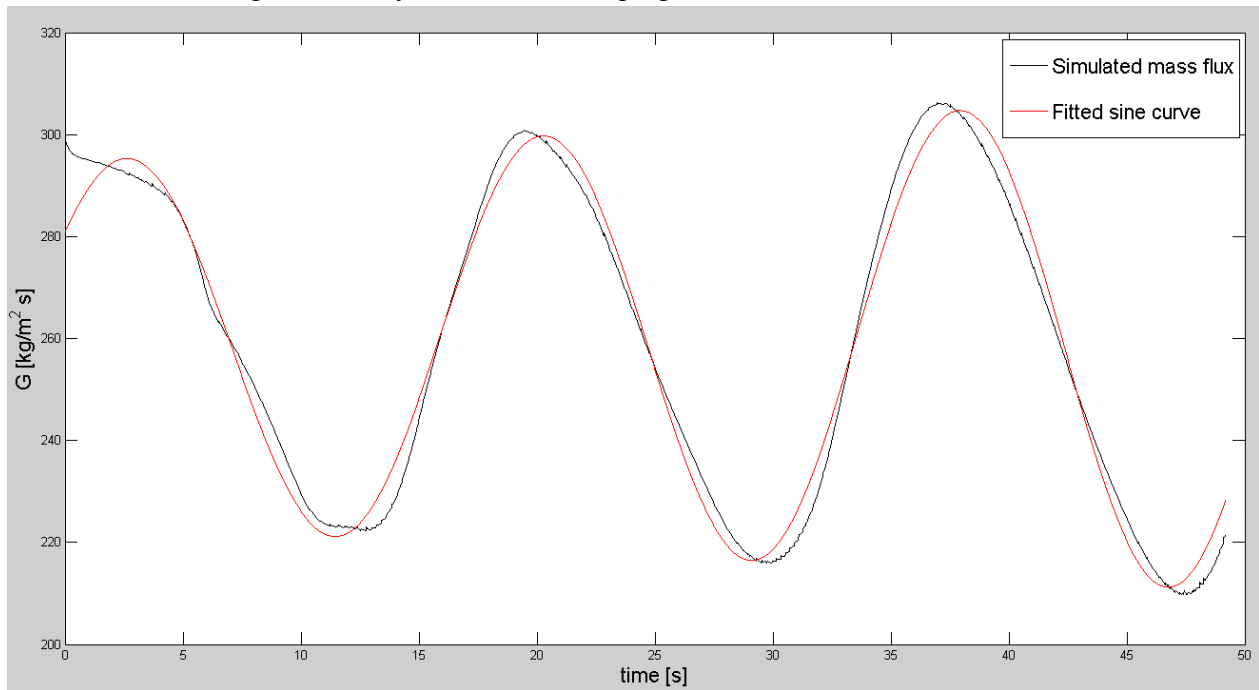


Figure 32: The simulated mass flux in black and the diverging fitted sine curve in red for a power input of 195 W.

Summed up:

<i>Oscillation type</i>	Diverging
N_{pch}	10.62
N_{sub}	4.45
<i>Attenuation factor, α</i>	-0.0066
<i>Frequency and period</i>	0.0566 Hz giving a period of 17.7 seconds

Table 6: Key values from a power input of 195 W.

Heat simulation nr 5) $q = 192 \text{ W}$, approximated to be marginally stable

The power input is then set to 192 Watt, giving the following mass flux curve:

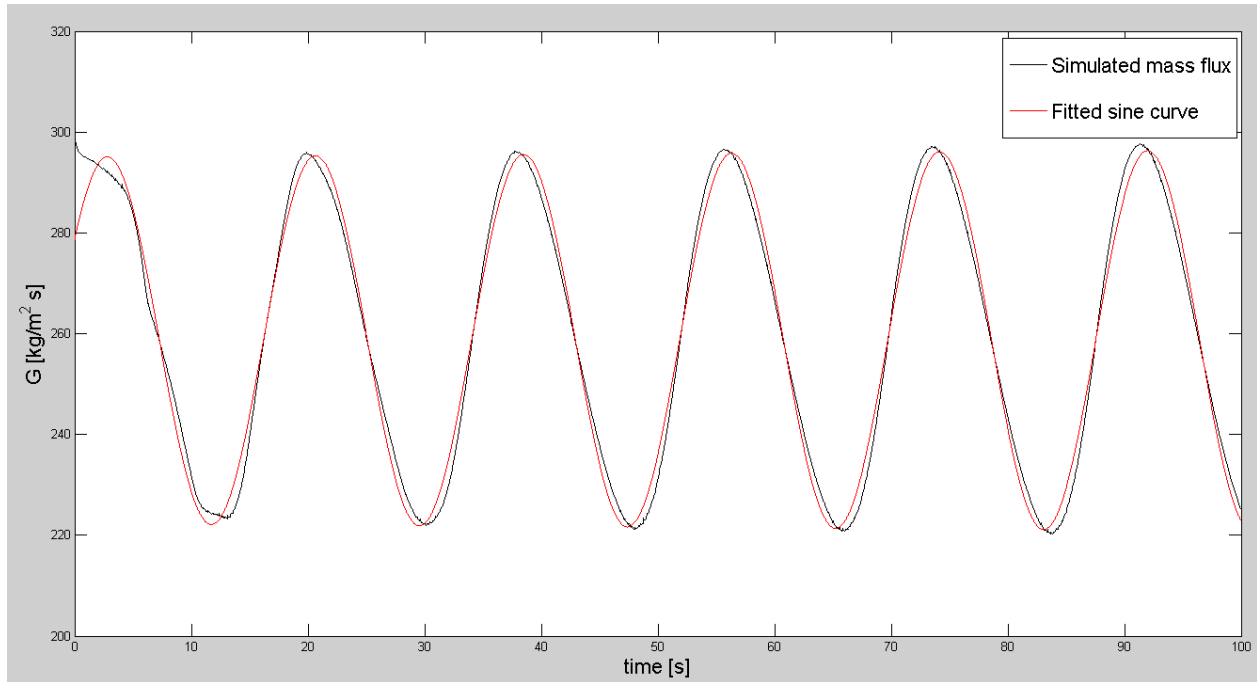


Figure 33: The simulated mass flux in black and the fitted sine curve in red for a power input of 192 W.

<i>Oscillation type</i>	Marginally stable
N_{pch}	10.39
N_{sub}	4.45
<i>Attenuation factor, α</i>	$-3.8 \times 10^{-4} \approx 0$
<i>Frequency and period</i>	0.0561 Hz giving a period of 17.8 seconds
<i>Peak-to-peak amplitude</i>	74.2 kg/sm^2

Table 7: Key values from a power flux input of 192 W.

The attenuation factor α is so small that it is approximated to be zero. From the discussion in section 4.2 this must be operating on the stability boundary and reveals that the threshold value for the stability map is given by the heat and subcooling numbers above for the given operating conditions.

Here the marginally stable case is found by the “try-and-fail” method. As explained in section 4.2, the number of simulations can be reduced to find the marginally stable operating point if a linear relationship between the α -values and the heat number N_{pch} is assumed. To see if this is reasonable the five previous simulations are plotted below:

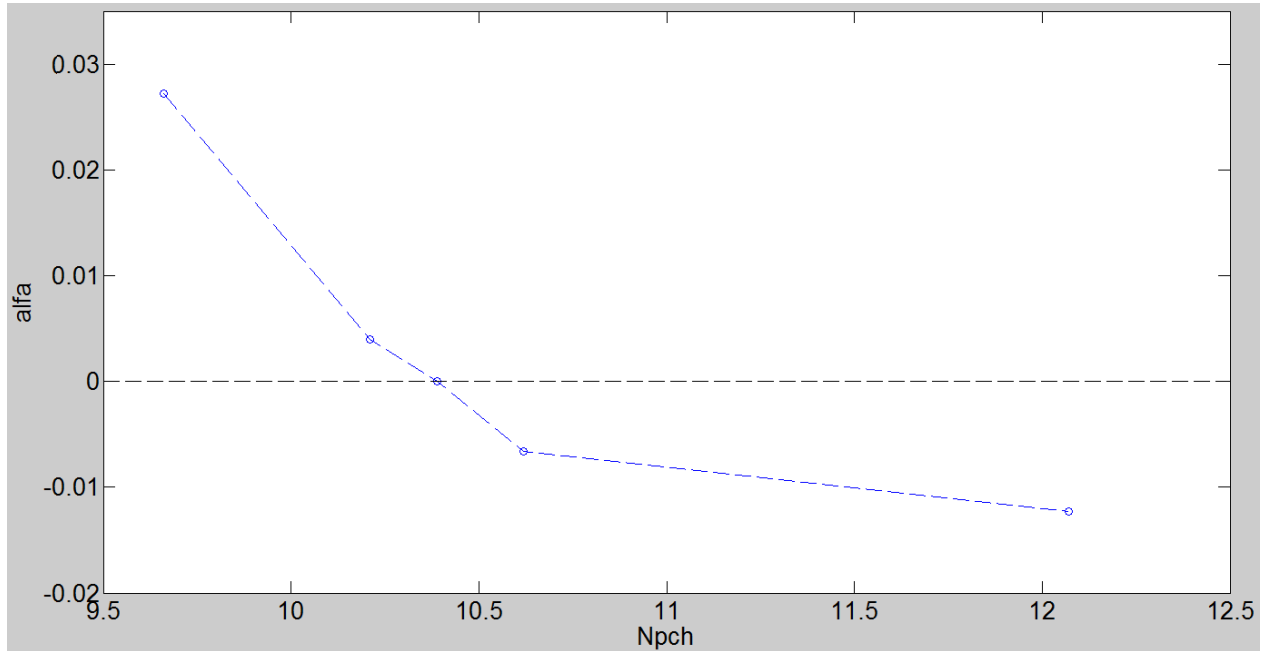


Figure 34: Relationship between the α -values and the heat numbers N_{pch} .

From figure 34 it is seen that a linear relationship is almost true for the points closest to the marginally stable condition ($\alpha=0$). This is utilized in order to pick reasonable input data for some of the coming simulations if the flow curve seems to be close to the stability threshold, with the intention of saving time. In the following sections, the search for a marginally stable condition will only be shown by a couple of simulations to shorten the read.

The results show the tendency that an increase in the applied heat gives increasing amplitudes in the form of diverging behavior. A single amplitude can only be extracted at the stability threshold, but as the increased heat also increases the diverging behavior and causes faster increase of amplitude it is assumed to support the hypothesis from section 3.4.5 of increased amplitudes resulting from increased heat. The table below shows the relation between the applied heat and the frequencies of the mass flux curves from the previous simulations:

Power input	Frequency	Period
180 W	0.0517 Hz	19.3 s
190 W	0.0554 Hz	18.1 s
192 W	0.0561 Hz	17.8 s
195 W	0.0566 Hz	17.7 s
200 W	0.0578 Hz	17.3 s

Table 8: Relation between heat input, frequency and period.

This gives the following graph for the power input, frequency and period:

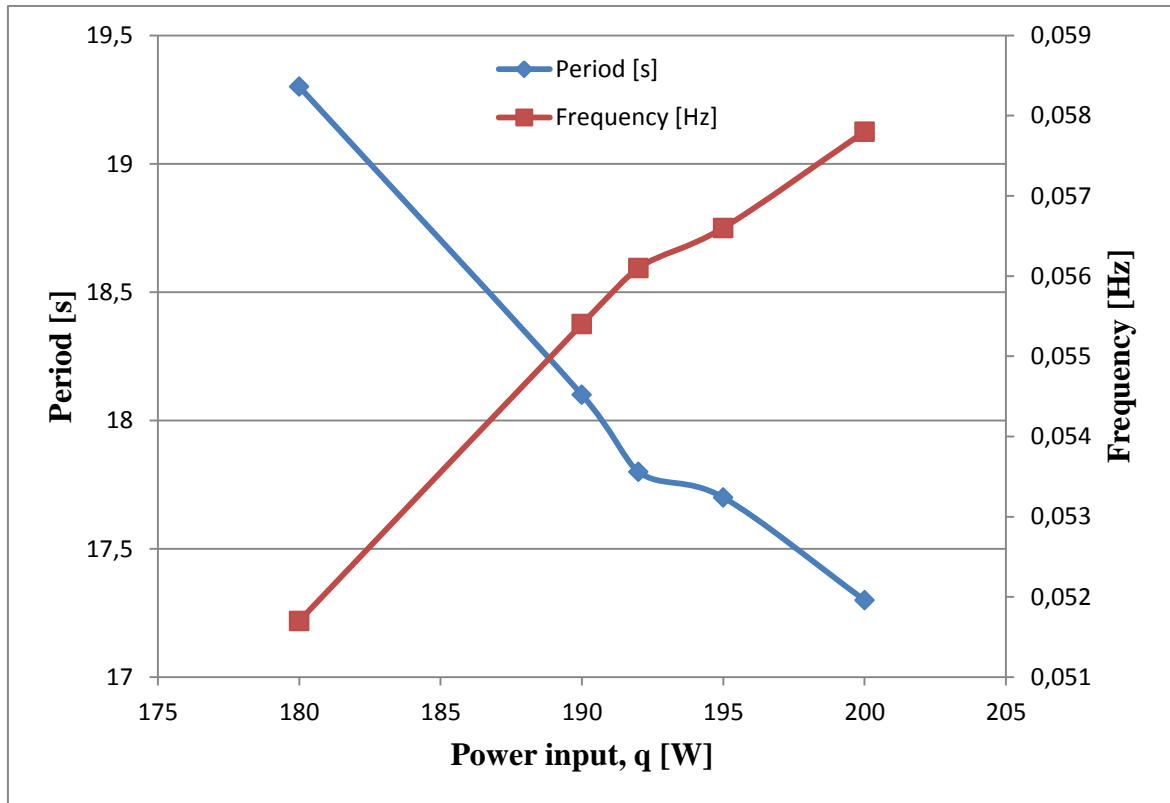


Figure 35: Numerically obtained relation between power input and period/frequency.

Table 8 and figure 35 implies that an increase in applied heat leads to an increase in frequency and thereby a decrease in period for the operating conditions examined. This correlates with the hypothesis established in section 3.4.5.

For the following tested parameters many simulations are omitted in order to not get repetitive as long as it is clear how the marginally stable cases are obtained.

4.4 Mass flux

The mass flux is then increased from $300 \text{ kg/m}^2\text{s}$ to $400 \text{ kg/m}^2\text{s}$. The rest of the initial simulation data is held constant.

P_{in}	5.5 bar
P_{inlet}	6.05 bar
P_{out}	5 bar
ΔT_{sub}	15 K
K_{in}	7
K_{out}	3
G	$400 \text{ kg/m}^2\text{s}$

Table 9: Initial simulation data.

Mass flux simulation nr 1) $q = 192\text{ W}$, no oscillations

For the same heat input of the previous marginally stable case in section 4.3 of 192 Watt the flow becomes stable after a short amount of time after the flow starts. This is shown in figure 36:

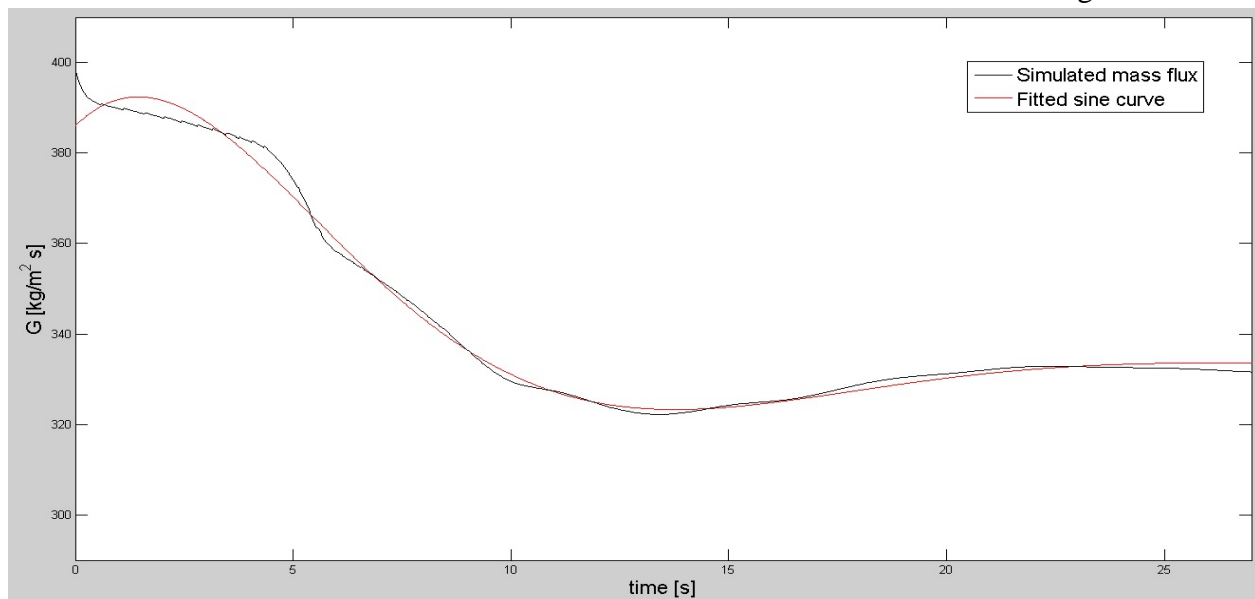


Figure 36: The simulated mass flux in black and the fitted sine curve in red for a power input of 192 W.

No data is rendered here because it is clear that no density wave oscillations takes place. That also means that no conclusions will be made based on this change.

Mass flux simulation nr 2) $q = 257 \text{ W}$, marginally stable

To find the marginally stable case several simulations are performed before it is found to occur at 257 Watt:

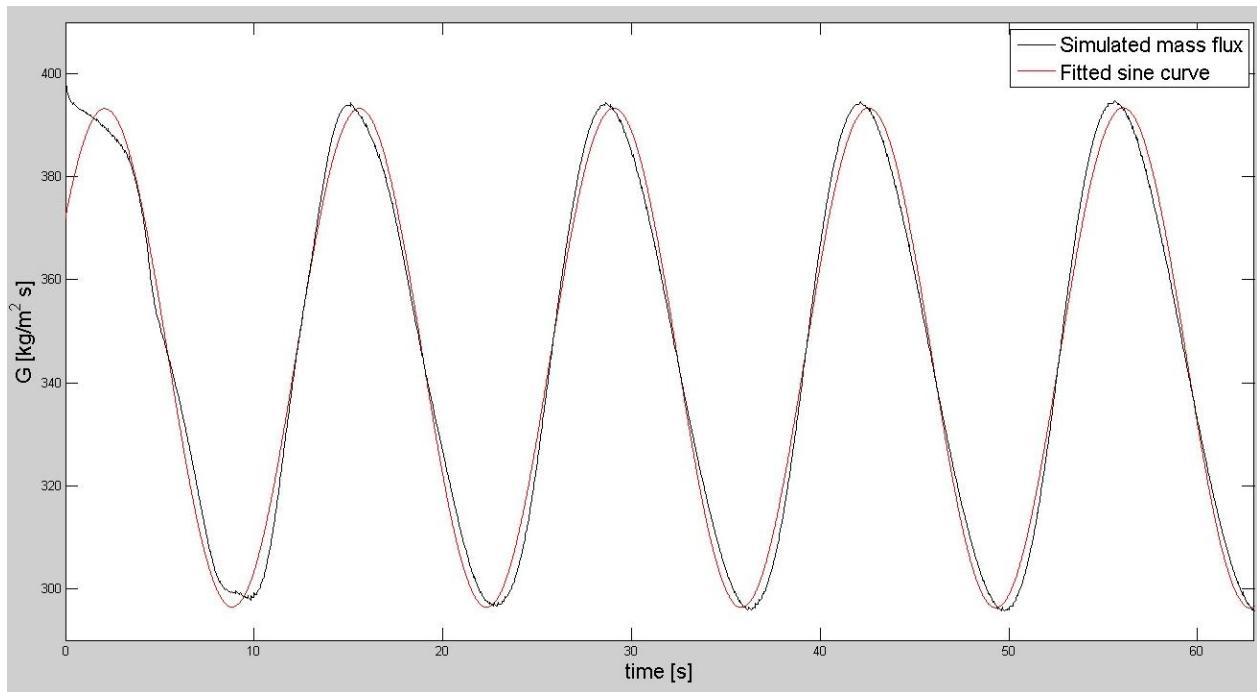


Figure 37: The simulated mass flux in black and the fitted sine curve in red for a power input of 257 W.

<i>Oscillation type</i>	Marginally stable
N_{pch}	10.36
N_{sub}	4.48
<i>Attenuation factor, α</i>	$-6.9 \times 10^{-5} \approx 0$
<i>Frequency and period</i>	0.0741 Hz giving a period of 13.5 seconds
<i>Peak-to-peak amplitude</i>	96.8 kg/sm ²

Table 10: Key values from a power input of 257 W.

The stability boundary is approximately the same for both the mass flux of 400 kg/m²s as for 300 kg/m²s seen from comparing the heat and subcooling numbers from table 7 and 10. The heat input for the present case is larger than for heat simulation nr 3. From the hypothesis in section 3.4.5 and section 4.3 the heat is shown to increase amplitude and decrease the period. The amplitude is larger and the period is lower for this case and can be caused both by the heat or the mass flux increase, so no conclusion can be made from this case regarding the characterizing effects of mass flux.

4.5 Validation of the model and the effect of pressure and inlet subcooling

To validate the numerically obtained data, the results are compared to experimentally obtained data gathered in the lab from Sørnum [2013]. Study of characterizing effects of changing inlet subcooling and inlet pressure is done simultaneously as the validation.

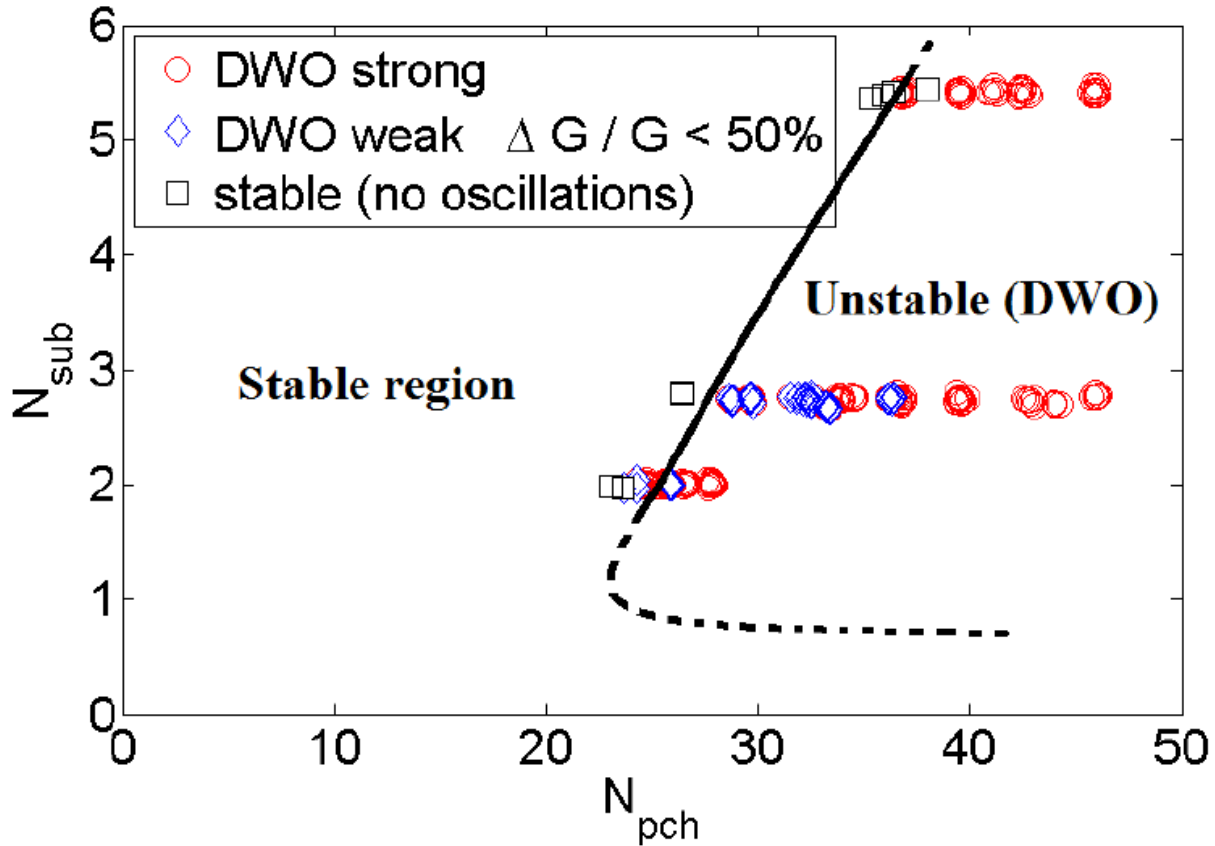


Figure 38: Experimental results as shown in Sørnum [2013].

The experiments from figure 38 are divided into three different groups: The upper points have an inlet subcooling (ΔT_{sub}) of 20 Kelvin and an inlet pressure (P_{in}) of 7 bar. The points in the middle have a subcooling of 10 Kelvin and a pressure of 7 bar. The lowest points are conducted with a subcooling of 10 Kelvin and an elevated pressure of 10 bar. This figure will be used to validate the model, by setting up the same input data as in the lab facility they were conducted in. The inlet and outlet pressure drop coefficients are constant for all experiments, where $K_{in}=2.63$ and $K_{out}=2.70$. It is important recognize that in principle, any result from the lab facility is correct (neglecting measurement errors etc.) so if the experiments and the model do not coincide, the model is assumed to be inaccurate.

$\Delta T_{sub}=20$ K is in the coming section referred to as high subcooling and $\Delta T_{sub}=10$ K as low subcooling. $P_{in}=7$ bar is referred to as low pressure and $P_{in}=10$ bar as high pressure. The dashed line at the lower subcooling numbers is assumed upon experience from former studies and is not found experimentally by Sørnum [2013].

4.5.1 Lower points, low subcooling, high pressure

The lower points are studied first. The initial input data for the numerical simulations are:

P_{in}	10 bar
P_{inlet}	11 bar
P_{out}	9.5 bar
ΔT_{sub}	10 K
K_{in}	2.63
K_{out}	2.70
G	300 kg/m ² s

Table 11: Initial simulation data for validation of the “lower points” in figure 38.

Low subcooling, high pressure, simulation nr 1) $q = 200$ W, converging

The procedure is similar to the simulations in section 4.3 and 4.4. A power input of 200 W for the given initial conditions gives the following mass flux curve:

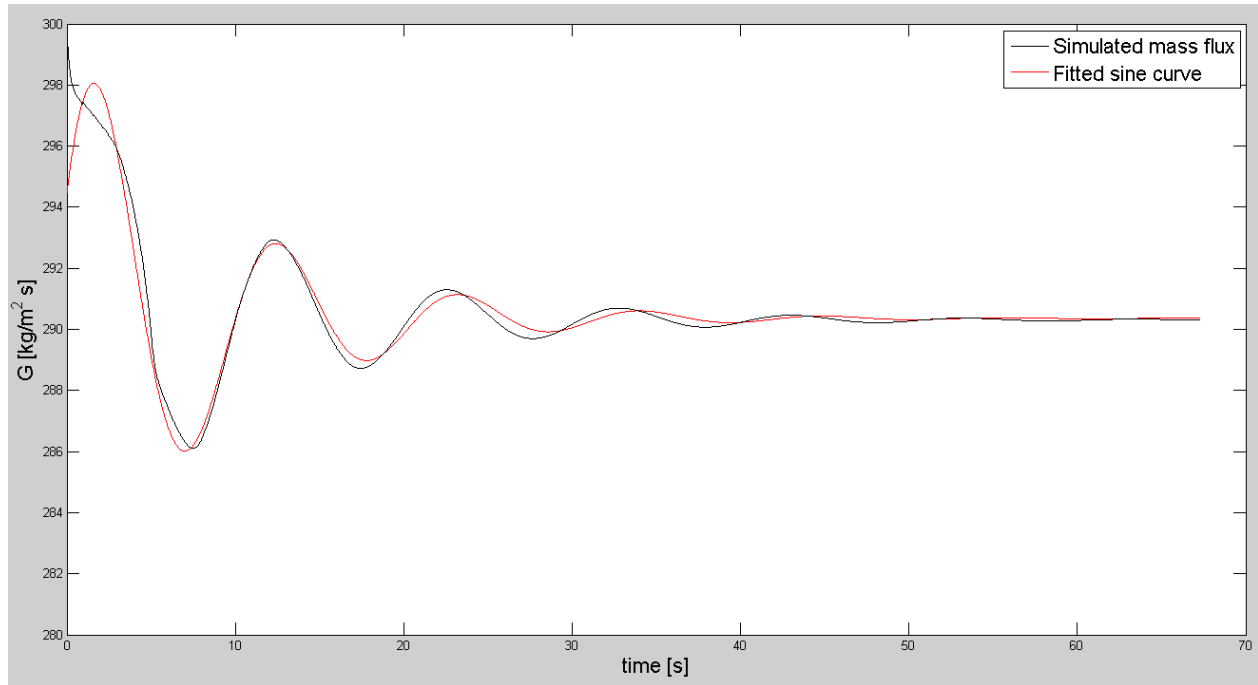


Figure 39: The simulated mass flux in black and the converging fitted sine curve in red for a power input of 200 W.

<i>Oscillation type</i>	Converging
N_{pch}	5.03
N_{sub}	1.72
<i>Attenuation factor, α</i>	0.106
<i>Frequency and period</i>	0.0925 Hz giving a period of 10.8 seconds

Table 12: Key values from a power input of 200 W.

Looking at the heat and subcooling number this is well into the stable region of figure 38 and should be converging, and the model predicts so as well.

Low subcooling, high pressure, simulation nr 2) $q = 250$ W, slowly diverging

By increasing the heat input to 250 Watt gives:

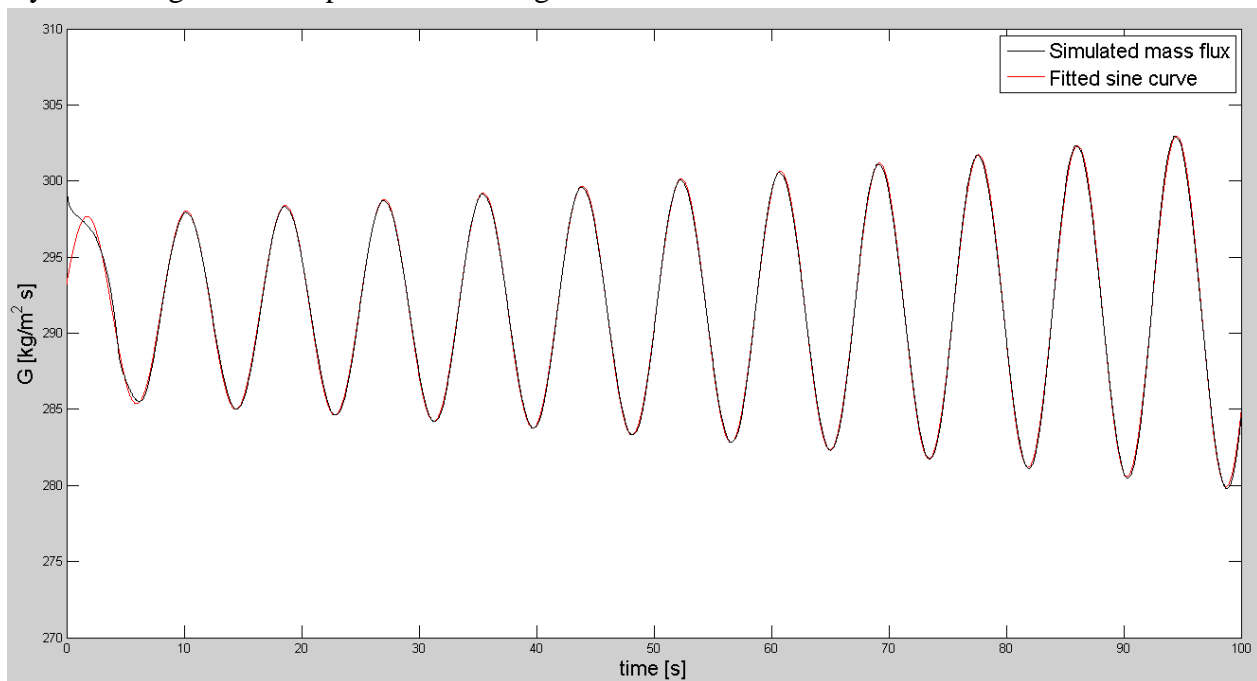


Figure 40: The simulated mass flux in black and the diverging fitted sine curve in red for a power input of 250 W.

<i>Oscillation type</i>	Diverging
N_{pch}	6.27
N_{sub}	1.72
<i>Attenuation factor, α</i>	-0.0068
<i>Frequency and period</i>	0.1186 Hz giving a period of 8.4 seconds

Table 13: Key values from a power input of 250 W.

According to the attained heat and subcooling numbers this should still be well into the stable area of figure 38, but the model predicts it to be into the unstable area. Hence, the code does not predict the same threshold value in the stability map for these operational conditions with elevated pressure and high subcooling. To find the marginally stable case and thereby the predicted stability boundary by the model, the applied heat is lowered.

Low subcooling, high pressure, simulation nr 3) $q = 247$ W, marginally stable

Two simulations are run in between this case and the previously shown simulation before this case of approximated marginally stable case is found. As mentioned earlier, be aware that the y-axis is adjusted with each simulation to better visualize that this is approximate to stability threshold operating condition.

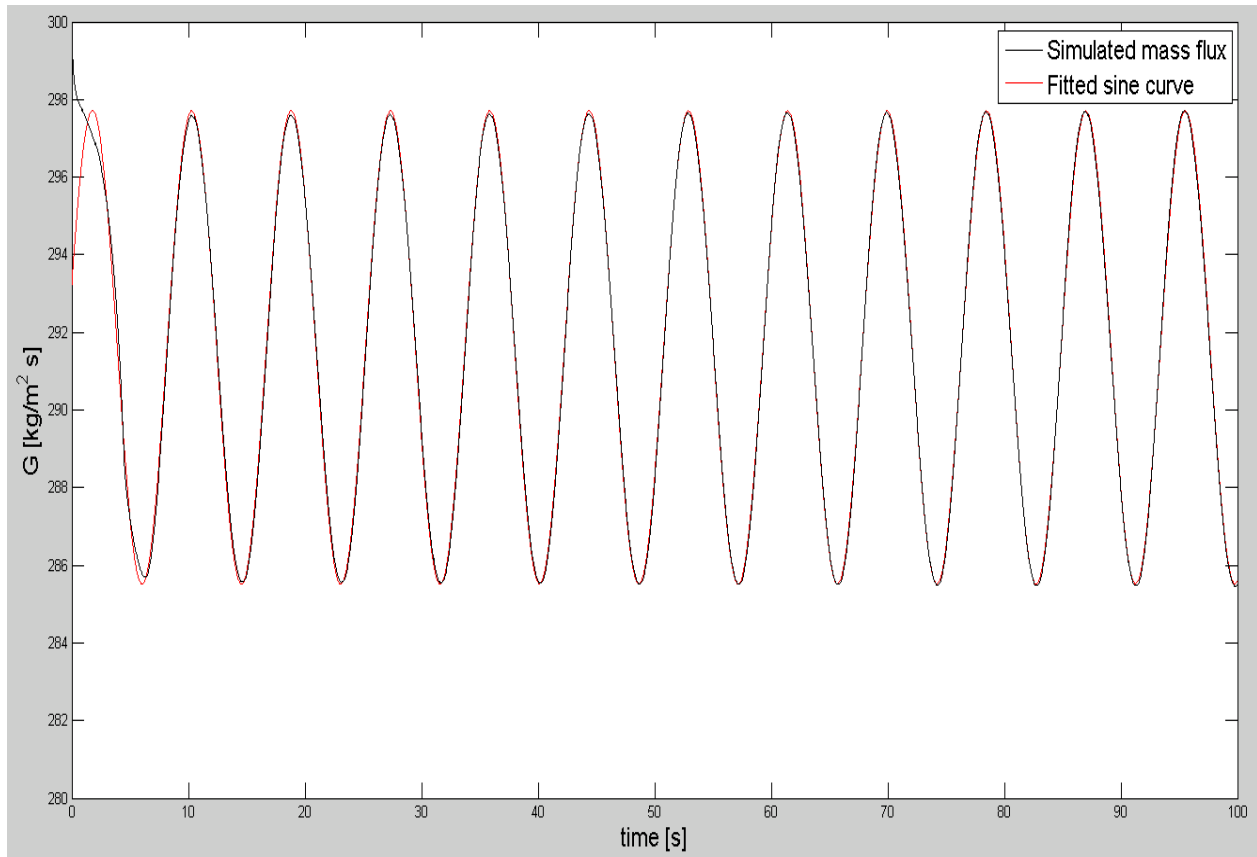


Figure 41: The simulated mass flux in black and the fitted sine curve in red for a power input of 247 W.

<i>Oscillation type</i>	Marginally stable
N_{pch}	6.19
N_{sub}	1.72
<i>Attenuation factor, α</i>	$1.2 \times 10^{-5} \approx 0$
<i>Frequency and period</i>	0.1173 Hz giving a period of 8.5 seconds
<i>Peak-to-peak amplitude</i>	12.2 kg/sm ²

Table 14: Key values from a power input of 247 W.

The stability threshold is revealed to be at the heat and subcooling numbers given in table 14, which is significantly different from the boundary predicted in figure 38. This is illustrated further in section 4.5.4.

4.5.2 Mid points, low subcooling, low pressure

The initial input data is for the mid points are:

P_{in}	7 bar
P_{inlet}	7.7 bar
P_{out}	6.5 bar
ΔT_{sub}	10 K
K_{in}	2.63
K_{out}	2.70
G	300 kg/m ² s

Table 15: Initial simulation data for validation of the “mid points” in figure 38.

It is important to notice that the difference between the mid points and the lower points is the lowered pressure while the rest is held constant, with the exception for the varied heat input.

Low subcooling, low pressure, simulation nr 1) $q = 247$ W, strongly diverging

First, by using a power input equal to the previous marginally stable case, the following mass flux curve appears in the inlet and outlet. The inlet mass flux is shown here to reveal why the simulation stops after 18 seconds.

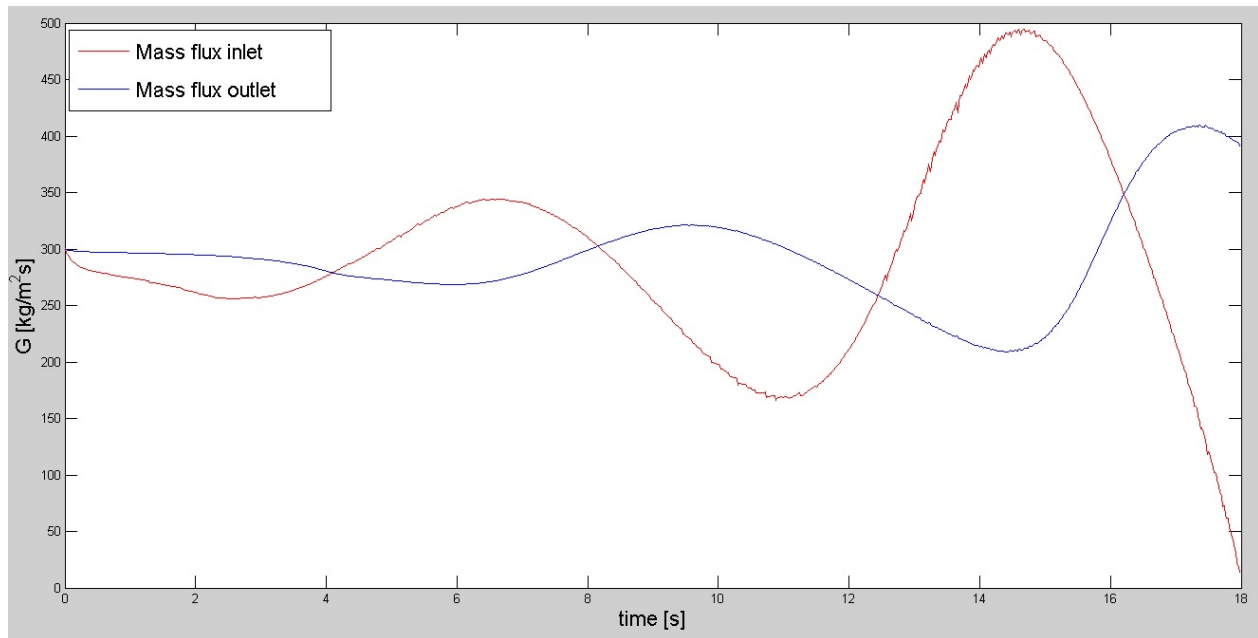


Figure 42: Mass flux curve in the inlet in red and in the outlet in blue for $q=247$ W.

This is a strongly diverging curve so it is evident from the studied effects of heat earlier that the stability threshold will be at a significantly lower heat input. The subcooling number is $N_{sub}=2.24$. No other data is given for this simulation due to the short simulation time. The simulation stops because the mass flux in the inlet reached zero. This shows a tendency that the decreased pressure destabilizes the flow by moving the inception of the stability boundary to the left in the stability map. This resulting curve also illustrates the difficulties of simulating experimental results with a high heat number as most of the experimental results in chapter 5, as the mass flux oscillations will be so large that the physical limits are exceeded.

Low subcooling, low pressure, simulation nr 2) $q = 180$ W, slowly converging

The power input is decreased to 180 W:

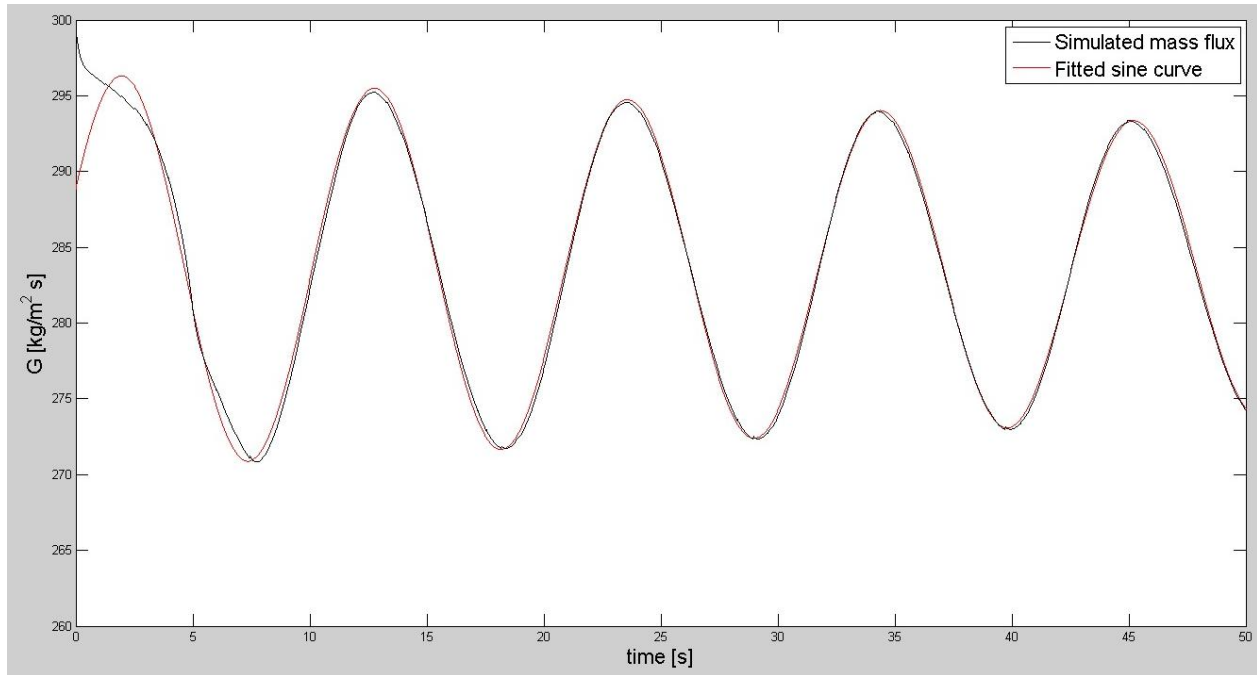


Figure 43: The simulated mass flux in black and the converging fitted sine curve in red for a power input of 180 W.

<i>Oscillation type</i>	Converging
N_{pch}	6.75
N_{sub}	2.24
<i>Attenuation factor, α</i>	0.0060
<i>Frequency and period</i>	0.0925 Hz giving a period of 10.8 seconds

Table 16: Key values from a power input of 180 W.

This is seen to be close to the stability threshold by the slowly converging curve and low attenuation factor. When the tendency of converging behavior is confirmed, this simulation is interrupted so the simulation time is only 50 seconds.

Low subcooling, low pressure, simulation nr 3) $q = 182 \text{ W}$, marginally stable

The power input is increased by 2 Watt from the previous case to obtain the marginally stable mass flux curve:

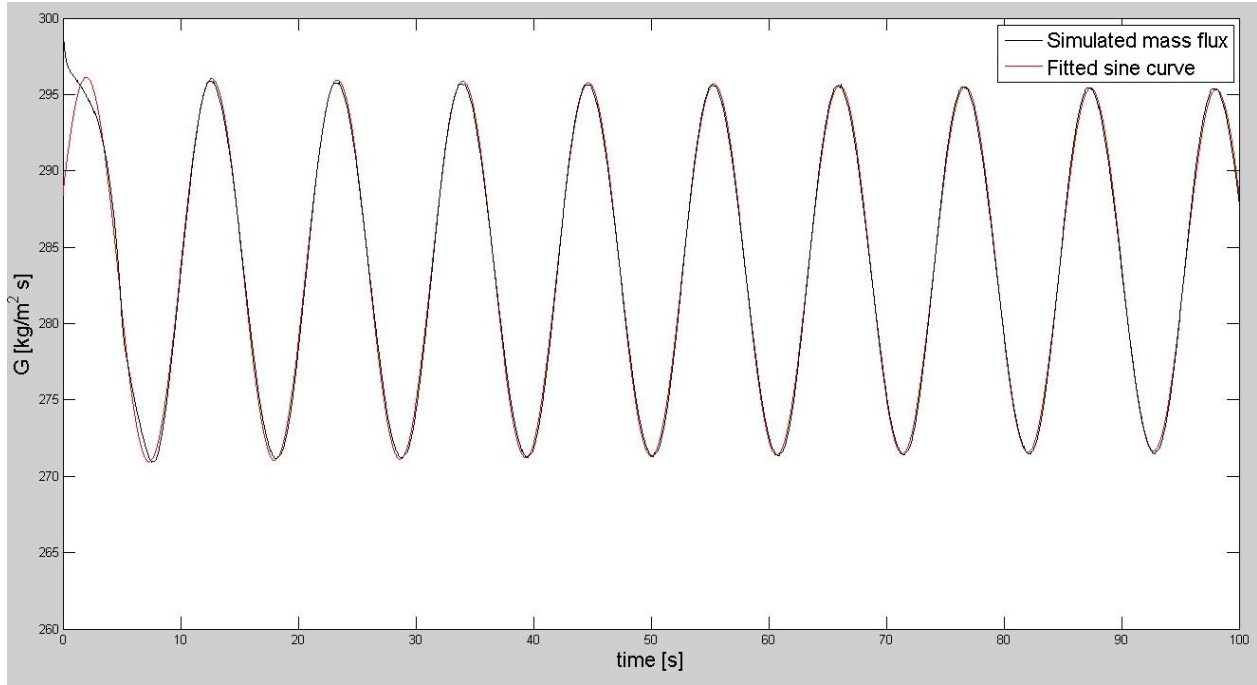


Figure 44: The simulated mass flux in black and the fitted sine curve in red for a power input of 182 W.

<i>Oscillation type</i>	Marginally stable
N_{pch}	6.83
N_{sub}	2.24
<i>Attenuation factor, α</i>	$6.8 \times 10^{-4} \approx 0$
<i>Frequency and period</i>	0.0937 Hz giving a period of 10.7 seconds
<i>Peak-to-peak amplitude</i>	12.6 kg/sm ²

Table 17: Key values from a power input of 182 W.

The numerically obtained stability threshold of is given by the heat and subcooling number above. This is far to the left of the experimentally obtained stability boundary in figure 38 and implies that the threshold value of heat for DWO to occur is less for the simulations than the experiments, both for the case of high and low pressure. This is further illustrated in section 4.5.4.

From the literature study and section 4.3, the effects of increasing applied heat is decreasing periods and increasing amplitudes. When comparing the cases of the two marginally stable cases from the previous section (lower points, elevated pressure) and the current section (mid points, lower pressure), it is seen that the amplitudes of the current case with lower pressure and lower heat input gives larger peak-to peak amplitude. This occurs even though the heat input is significantly lower ($247 \text{ W} - 182 \text{ W} = 65 \text{ W}$). The effect of decreasing the pressure is by this observation assumed to be increasing the amplitude. The period of 8.5 seconds from the

marginally stable case of the lower points with higher heat input has then increased to 10.7 seconds for the present case with lower heat input. This can be caused both by the pressure change or the heat change so no conclusion can be made regarding the period (because decreasing the heat input increases the period). The first simulated case of the mid points could not be used for the purpose of extracting the period either because the large amplitudes in the inlet forced the simulation to stop.

4.5.3 Upper points, high subcooling, low pressure

The initial input data is for the upper points are:

P_{in}	7 bar
P_{inlet}	7.7 bar
P_{out}	6.5 bar
ΔT_{sub}	20 K
K_{in}	2.63
K_{out}	2.70
G	300 kg/m ² s

Table 18: Initial simulation data for validation of the “upper points” in figure 38.

High subcooling, low pressure, simulation nr 1) $q = 255$ W, diverging

Because of the high subcooling more power is needed to reach the simulated stability threshold compared to the previous operating conditions. The power input of 255 W and the given initial input data gives:

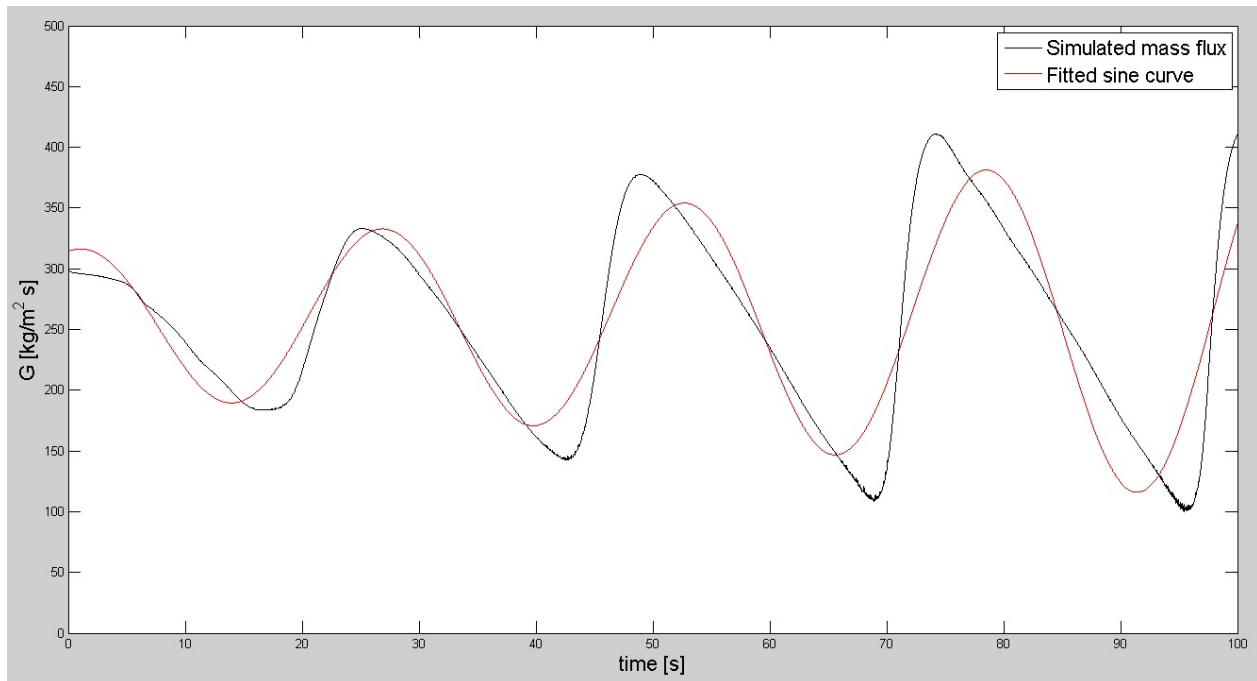


Figure 45: The simulated mass flux in black and the diverging fitted sine curve in red for a power input of 255 W.

The fitted sine curve is shown to not fit as well as the former simulations because of the “angled” oscillations. The frequency and the α -value extracted from the fitted curve are still assumed to give reasonable estimates.

<i>Oscillation type</i>	Diverging
N_{pch}	12.82
N_{sub}	5.09
<i>Attenuation factor, α</i>	-0.0095
<i>Frequency and period</i>	0.0387 Hz giving a period of 25.8 seconds

Table 19: Key values from a power input of 255 W.

It is seen that the heat has to be decreased in order to obtain limit cycle oscillations.

High subcooling, low pressure, simulation nr 2) $q = 240$ W, marginally stable

The power input is decreased to 240 W:

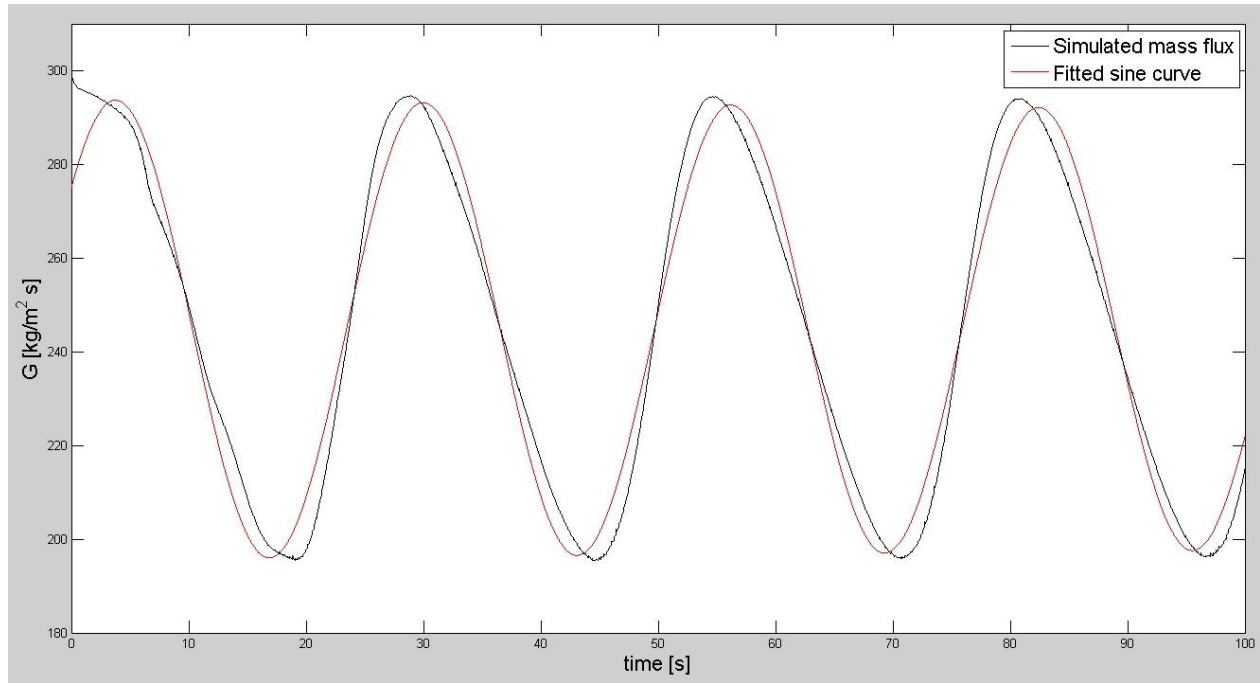


Figure 46: The simulated mass flux in black and the fitted sine curve in red for a power input of 240 W.

<i>Oscillation type</i>	Marginally stable
N_{pch}	10.79
N_{sub}	5.09
<i>Attenuation factor, α</i>	$4.1 \times 10^{-4} \approx 0$
<i>Frequency and period</i>	0.0381 Hz giving a period of 26.2 seconds
<i>Peak-to-peak amplitude</i>	98.1 kg/sm ²

Table 20: Key values from a power input of 240 W.

The amplitude of the mass flux oscillations has increased by a large amount compared to both of the previous validation cases, and even though the heat input is lower than the marginally stable case for lower points, the amplitude is more than 8 times as large for this case of higher

subcooling. The lower case has a higher pressure than the current case and from the discussion in 4.5.2 this should lead to a lower amplitude effect for the lower case. The fact that the current case, at lower pressure and lower heat, still displays an amplitude much larger than the previous cases leads to the indication of increasing amplitudes by increasing the subcooling. The period of 26.2 seconds is higher than the marginally stable case at low subcooling and the same pressure (mid points). Because the investigated effect of increasing heat is shown to decrease the period and because the current case with the higher subcooling still displays larger periods, a tendency of increased period caused by increased subcooling is present.

4.5.4 Numerically obtained stability map

By the using the obtained results the numerically obtained stability threshold is then compared to the experimental data from figure 38:

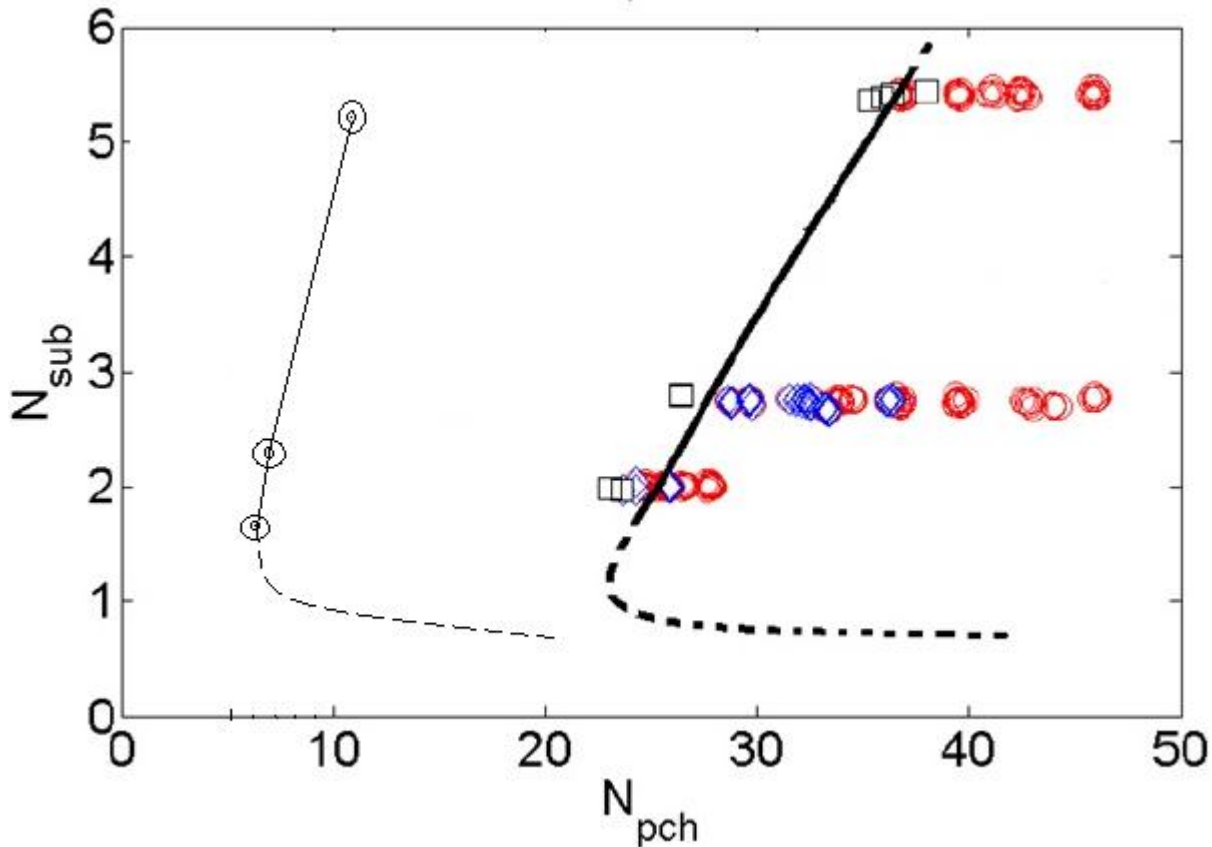


Figure 47: Numerically predicted stability threshold to the left and the experimentally obtained stability threshold from Sørum [2013] to the right.

The predicted subcooling numbers for the simulations are consequently slightly lower than the experimental and might occur due to rounding of numbers or different ways of calculating the average gas and liquid density. The numerically obtained stability threshold is predicted to be far to the left of the experimentally obtained threshold, making the unstable area to the right of the stability boundaries larger. It is important to recognize that the experimental results from the lab

per definition is assumed to be correct and represents the real stability threshold. All the possible reasons for this error are too many to mention, but it might be due to backflow through the channel as the oscillations increase, inertial effects, user made errors in the simulation code or physical limitations such as the confinement walls. This is left as an assignment for further investigation. The code's inability to predict the correct stability boundary is assumed to not influence its ability to predict the characterizing effects because the preliminary tests in section 4.3 shows expected tendencies for the mass flux curve. The dashed lines at the lower subcooling numbers are both assumed lines based on experience from other developed stability maps and are only drawn to show that a minimum subcooling has to be exceeded in order to produce DWO. The model is here just a pipe between two tanks and it may be that having a pump instead to drive the flow as the experiments in chapter 5 would improve the model, but this is beyond the scope of this report.

4.6 Numerically obtained characterizing effects

What makes the study of effects of parameter changes difficult is the code's inability to produce marginally stable oscillations within the unstable area (as opposed to the experimental results shown later in chapter 5). Still, by assuming that the effect of applied heat obtained from the literature study and in section 4.3 is true, the characterizing effects of changes in pressure and subcooling are justified by comparing three different cases in section 4.4 with the exception of the period of oscillations for pressure variations.

It is important to understand that the literature study was not unambiguous. With the exception of the period for increased heat, other characterizing effects based on the literature study could have been made. The characterizing effects from the literature study are here repeated along with the numerically obtained parametric characterizing effects. Be aware that the effects from the model prediction for subcooling, pressure and mass flux are based on the condition that the effect for increased heat is valid for all the operating conditions simulated. This is supported both by the literature study and the simulations, and the only opposing effect found by the writer is the results of Ding et al. [1995] that suggested decreasing amplitudes with increasing heat flux (rendered in figure 10).

<i>Hypothesis</i>	Increased heat	Inc. subcooling	Inc. pressure	Inc. mass flux
Amplitude	Positive	Positive	Negative	Negative
Period	Negative*	Positive	No effect	Positive
<i>Model prediction</i>	Increased heat	Inc. subcooling	Inc. pressure	Inc. mass flux
Amplitude	Positive	Positive	Negative	Inconclusive
Period	Negative	Positive	Inconclusive	Inconclusive

Table 21: The characterizing effects of DWO predicted by the model. Hypothesis based on the literature study for characterizing effects for DWO.

*no opposing effects found in the literature study

Apart from the inconclusive period effect for increased pressure and the inconclusive mass flux, the same characterizing effects are predicted from the numerical results as the hypothesis suggested. Another factor that has to be considered is the possible changing parameter effects for different operating conditions, as illustrated by the results from Sørum [2013] in for example figure 20 and 21 in chapter 3.3.1. Whether or not the code predicts the same behavior for other operating conditions is left as an assignment for future studies.

5 Parametric Study of Experiments

The following is a parametric study based on results obtained from the laboratory at NTNU [Ruspini, 2013] [Chiapero, 2013]. The lab experiments are not performed by the writer, only the study of the data. The facility where the experiments have been executed is described in chapter 5.1.1. As explained in chapter 4 the description of density waves in section 3.1 suggests that both the velocity and density will show oscillating behavior in the boiling channel. The mass flux is a function of both of these parameters (see equation 2.7), so the mass flux oscillations over time will be investigated in order to study density waves. As figure 4 in section 3.2.1 suggested, an unstable diverging behavior is characterized by an increase of amplitude, while the frequency expresses how often the density waves occur. To determine the characterizing effects of the affecting parameters, the changes in amplitude and period needs to be extracted and studied. The affecting parameters studied are heat applied on the channel, inlet subcooling, pressure and mass flux.

5.1 Experimental system

The data from the studied experiments are gathered in the laboratory at NTNU and were not conducted by the writer. The experimental setup for the experiments is presented in this section, with the purpose of better understanding of the results. REFPROP8 (REference Fluid PROPERTIES v. 8.0) developed by the National Institute of Standards and Technology (NIST) is used to acquire fluid properties. The density is throughout the boiling channel regarded as a function of enthalpy only, assuming a constant channel inlet pressure p_{in} found from the time-averaged measured inlet pressures obtained in the experiments.

5.1.1 Facility

A simplified scheme of the experimental facility is shown in figure 48 and is designed in such a way that density waves can be generated. The working fluid used in all experiments is 1,1,1,2-tetrafluoroethane, referred to as refrigerant R-134a. At atmospheric pressure R-134a has a boiling point of -26.3°C and a latent heat of vaporization of $2.17 \cdot 10^5 \text{ J/kg}$. That is significantly below the boiling point and the latent heat of vaporization of water (100°C and $2.26 \cdot 10^6 \text{ J/kg}$), which makes it ideal to use.

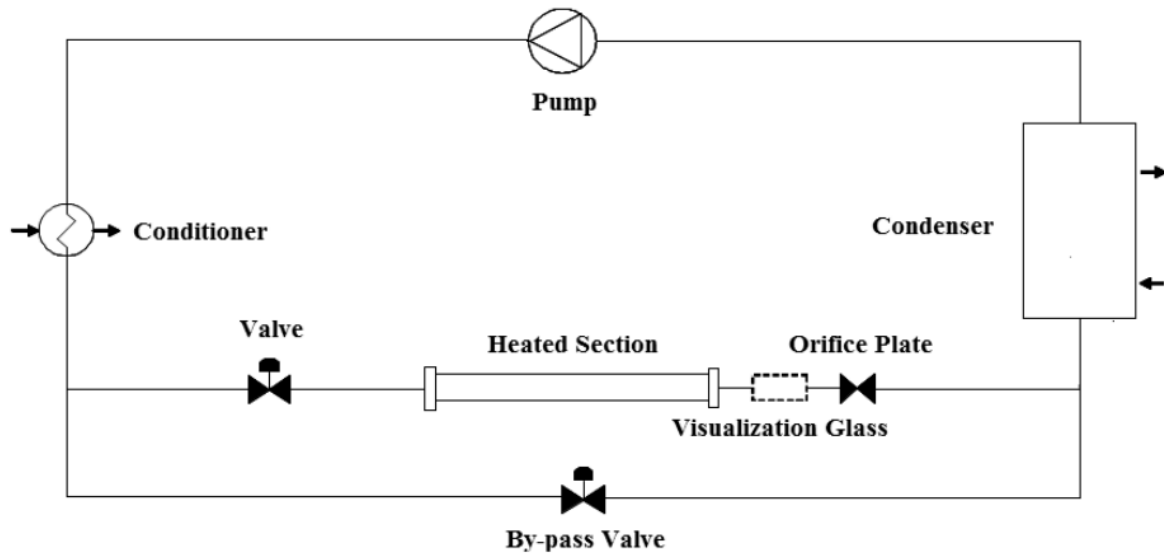


Figure 48: Simplified scheme of the facility.

A gear pump with a magnetic drive coupling is used to circulate the fluid through the system, allowing a large pressure increase. The conditioner in the scheme is a plate-fin heat exchanger that controls the inlet temperature of the heated section. The heated section is a stainless steel tube with an inner diameter of 5 mm, an outer diameter of 8mm and length of 2 meters. The heated section has seven pressure taps for differential pressure drop measurements and ten external thermocouples measuring along the channel. The valve in the inlet provides a local pressure drop at the inlet, given by the value of K_i . At the exit, an orifice plate is installed that may be modified to vary the outlet restriction K_e . The inlet and outlet restriction in all the gathered experiments are $K_i=2.63$ and $K_e=2.70$. The entire section is covered by an isolating material and the thermal losses of the experiments are never above 8 %. These losses are included in the calculation of the actual heat transferred to the fluid [Ruspini, 2013]. The visualization glass is used to perform photographic analysis of the flow pattern by using a high speed camera. To make the assumption of constant pressure drop over the channel true, a by-pass valve is installed in parallel with the heated section. To condense the working fluid coming out of the heated channel a shell and tube heat exchanger is used, where the working fluid passes on the shell side and a mixture glycol and water acts as a coolant on the tube side.

The software interface in the lab (LabVIEW) is shown in figure 49 below. From here the power to the heated section is controlled, the velocity of the pump is set and the reference temperature in the condenser and conditioner (K6 and K9, respectively in figure 49) is determined. LabVIEW also acquires the data and acts as a safety system by shutting down if temperature exceeds 190

°C, if the current is exceeds 200 A or if the pressure is above 1500 kPa.

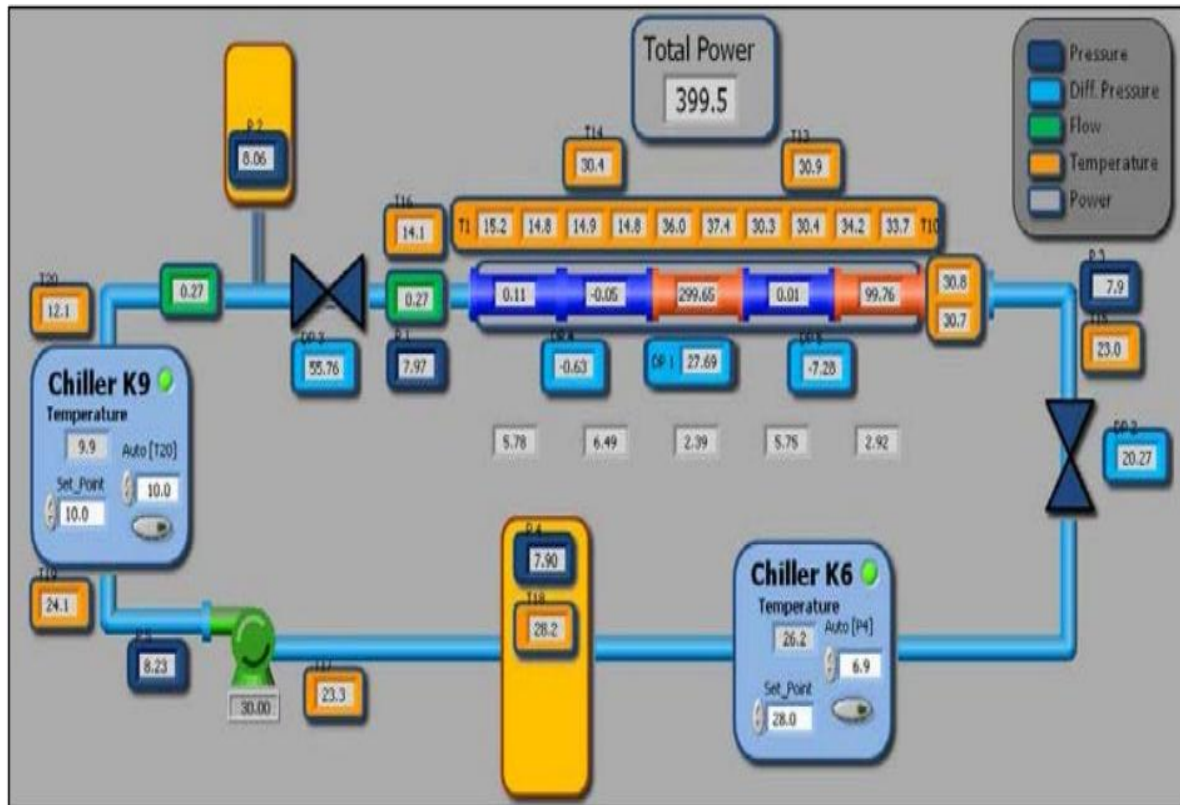


Figure 49: Example of the LabVIEW interface.

5.2 Procedure and validation

As explained in the start of the chapter, effects of changing parameters will be studied by extracting the amplitude and frequency of experiments. Because of the nature of the high frequency DWO, where the real period and amplitude of the signal can be hard to extract because of the frequent disturbances and oscillations, a procedure of how to evaluate the experiments has to be conducted. First a sine wave is created with added random disturbances as a test graph and to validate the evaluation tools. The reason to create a signal, and not use an existing sample from an experiment, is to be sure of the amplitude and frequency of the undisturbed curve and test if it is possible to recreate the undisturbed signal after the disturbances have been added. The sine curve have a frequency of 5 Hz ($y = \sin(2\pi 5t)$) and the disturbances consists of one random value between 0 and 1 adding to the graph, and one value between -1 and 0 subtracted from the y-value for every time step t to simulate the density waves. The horizontal axis is the time axis denoted t , with sample steps of 0.01 seconds. Here it is known that the “true” peak-to-peak amplitude has a magnitude of 2 (sine signal varies from 1 to -1), but the disturbances can make the estimation difficult. In figure 50, the disturbed sine curve is raised up ($y+2$) to be above zero.

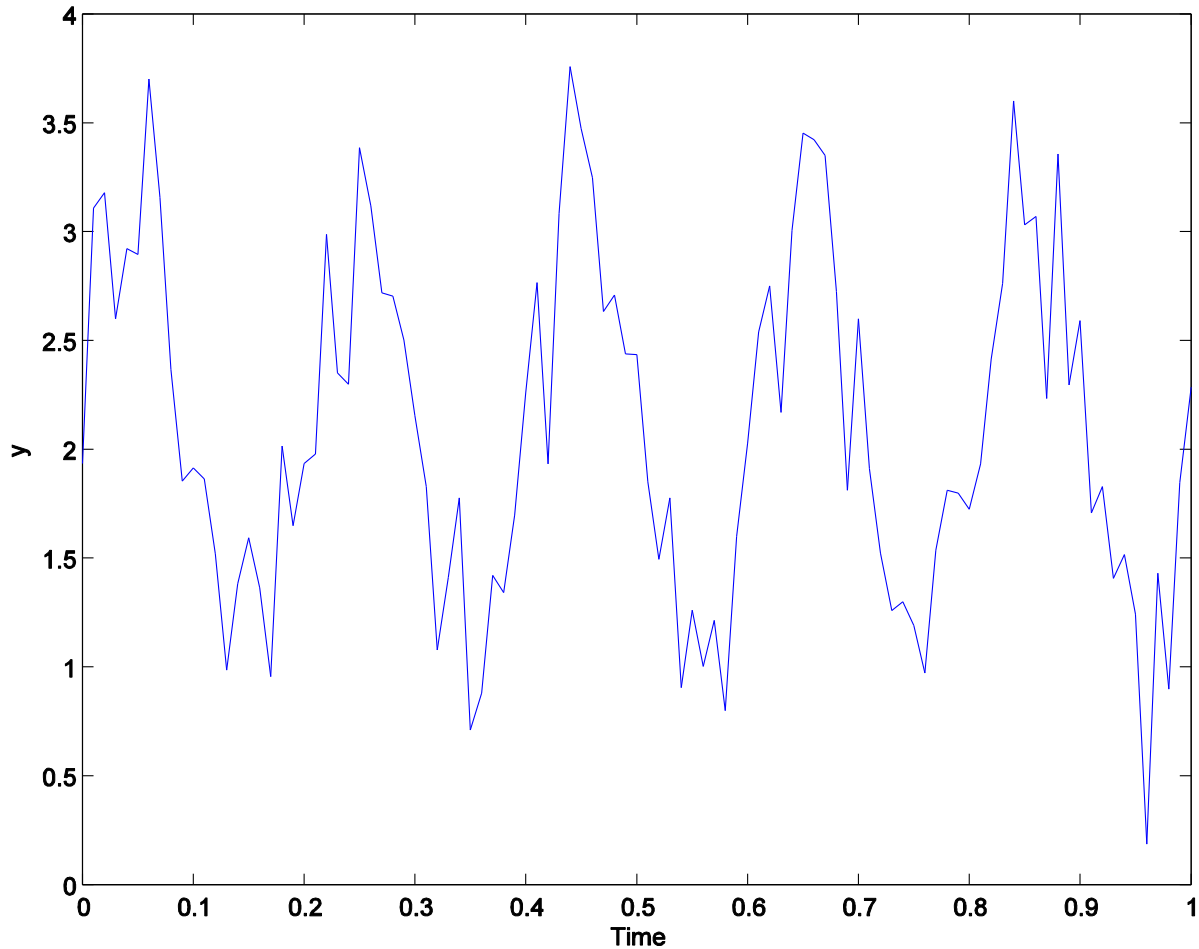


Figure 50: Disturbed sine wave.

To estimate the amplitude of the sine curve several methods have been investigated. The one that gave the most precise results were the function `findpeaks` in matlab, and by the try-and-fail method the best filtration of the signal was to only include peaks above the mean plus 10 % of the difference between the max of the graph and the mean (syntax matlab: `[pcs,locs]= findpeaks (y, 'minpeakheight',(mean(y)+((max(y)-mean(y))/10))`);) and in the end subtract the amplitude by 10 % of the mean to account for the disturbances that add to the true peaks of the sine wave. By doing this, the peaks closest to the mean are filtrated out and the values are adjusted so that the lower peaks above the “true” peaks of the sine wave are diminished. An improvement of this code would be to filtrate out the highest values too, just as the “`findpeaks`”-function does for the values closest to the mean. The peaks are then subtracted by the mean of `y` and multiplied by 2 to get the peak-to-peak amplitudes shown below in figure 51. The mean of these peak-to-peak amplitudes is then calculated and outputted peak-to-peak amplitude. One pitfall of using this function would be if there is one max far above all the other peaks, for example due to measurement failure. For the above case the peak-to-peak amplitude is estimated to 2.0376 (dashed line in figure 51). For 50 runs on differently disturbed sine curves the average estimated peak-to-peak amplitude is 1.963 (but also with values as low as 1.82 and up to 2.25).

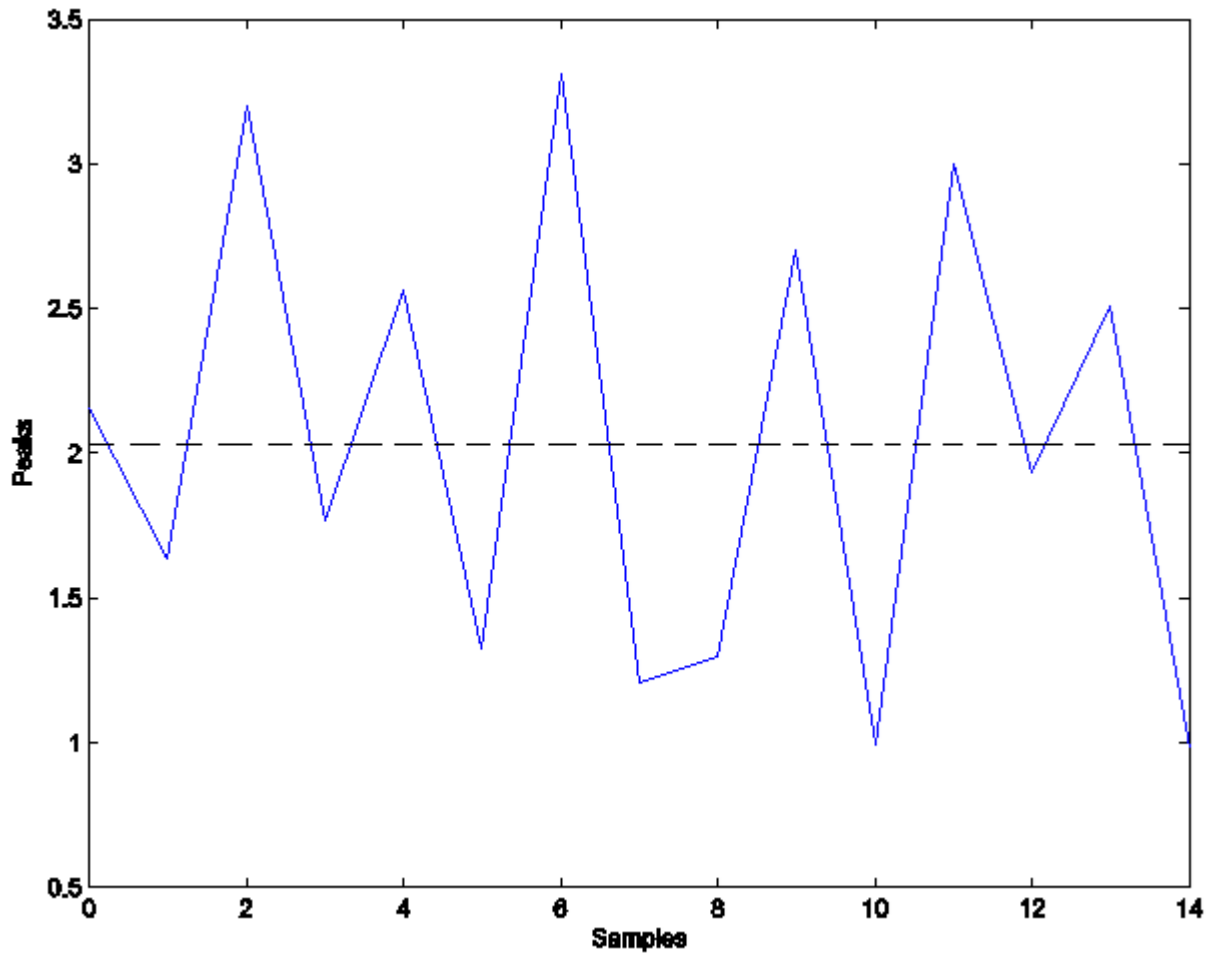


Figure 51: Samples for amplitude calculations in blue and the estimated outputted amplitude illustrated by the dashed black line.

The fast Fourier transform (fft function in matlab) converts the time scale to a frequency scale. This paper has no intentions of explaining all the characteristics of the fft function, but it is used to evaluate the signals that a graph is made up of. For more information the reader is referred to Bergland [1969]. The fft function gives both the magnitude and phase, but here (figure 52) only the magnitude spectrum is plotted along the y-axis. From the time steps of 0.01, the upper frequency corresponds to 100 Hz:

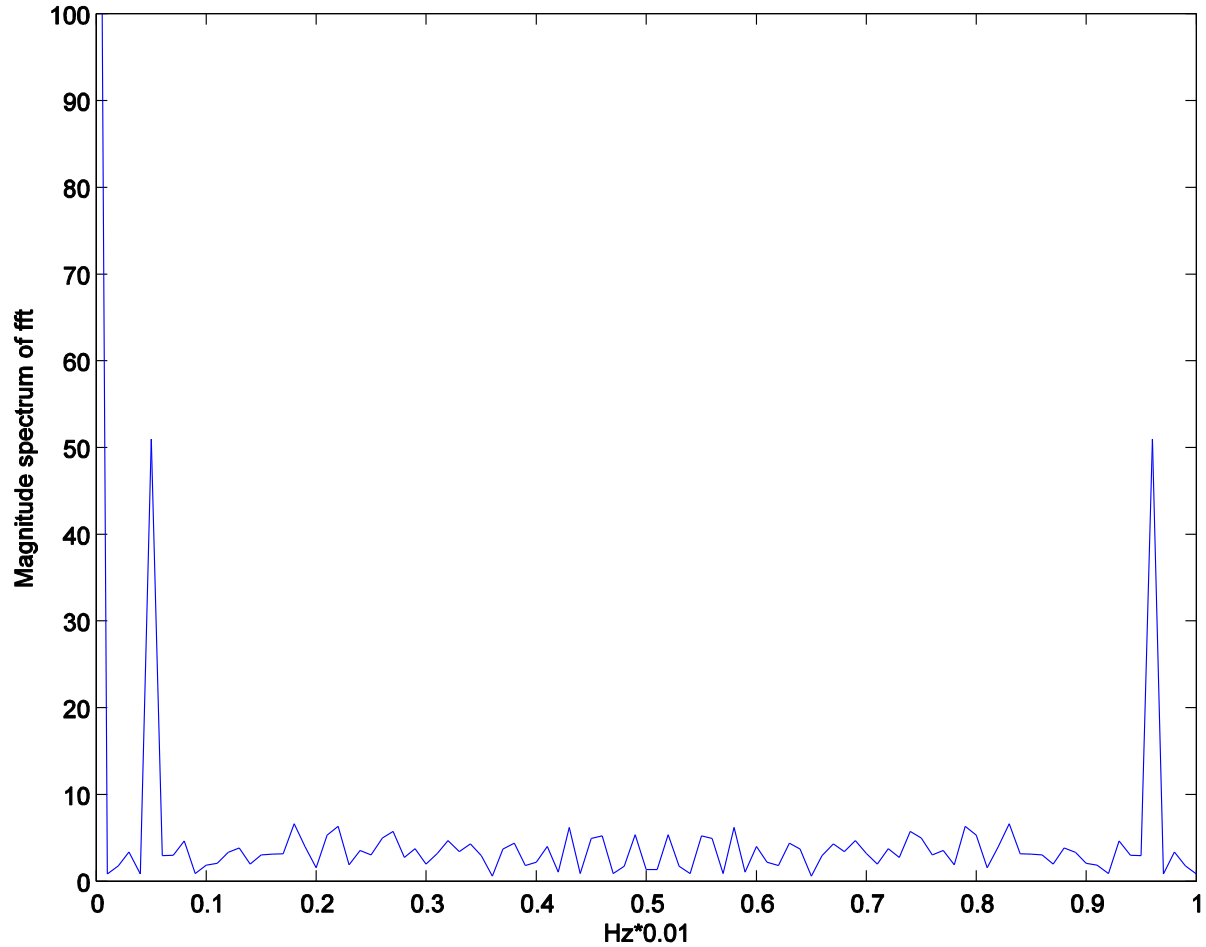


Figure 52: Fast Fourier transform of the disturbed sine wave.

In figure 52 there is a peak at zero due to non-zero mean value of the signal. The second peak occurs at approximately 5 Hz, which is the frequency of the sine signal. The third peak at approximately 96 Hz is the high frequency noise. This can be used in the experiments to calculate the period of the signal not affected by the disturbances, by the relation between period and frequency:

$$period = \frac{1}{frequency} \quad (5.3)$$

When examining the experiments, both premade tools and self-developed analyzing tools are used. To make a clear distinction between a stable and an unstable flow, a limit of at least 10 % on the mean oscillations for the mass flux is set to be seen as unstable for density waves. In other words:

$$Unstable \text{ if: } \quad \frac{\Delta G_{mean}}{G_{mean}} > 0.1 \quad (5.4)$$

5.3 Parameters affecting DWO characteristics

Most of the experiments studied are unstable and have a high equilibrium phase change number, mainly because the setup is used to collect data on density waves. Over a hundred experiments have been looked at and a few of them are rendered to study effects of changing parameters. A large amount of the experiments had to be discarded due to simultaneous change of more than one parameter. The reason for this is to be sure of what parameter that changes the density-wave behavior. To be able to find back the results, the experiments are tagged with the date for the experiment and the experiment number. By amplitude in this section it is always referred to peak-to-peak amplitude. The operating conditions mentioned are the mean values of the illustrated data, as in figure 53 below. The K-values for all the following experiments are $K_i=2.63$ and $K_e=2.70$.

5.3.1 Applied heat

The total power q delivered to the heated section is measured throughout all of the experiments and sometimes varied. To see the effect of the changes done in total power added to the system, some of these samples are looked into. Here three experiments are presented with increasing power input. Increase in power input leads to an increase in the added heat to the pipe, so the terms “power input”, “heat flux” and “applied heat” are used interchangeably. ΔT_{sub} is the difference between the inlet temperature and the saturation temperature.

Experiment 20131127-E019

Operating conditions: $G=300.4 \text{ kg/m}^2\text{s}$, $p_{in}=999.6 \text{ kPa}$, $q=1000 \text{ W}$, $T_{in}=29.5 \text{ }^\circ\text{C}$, $\Delta T_{sub}=10.0^\circ\text{C}$.

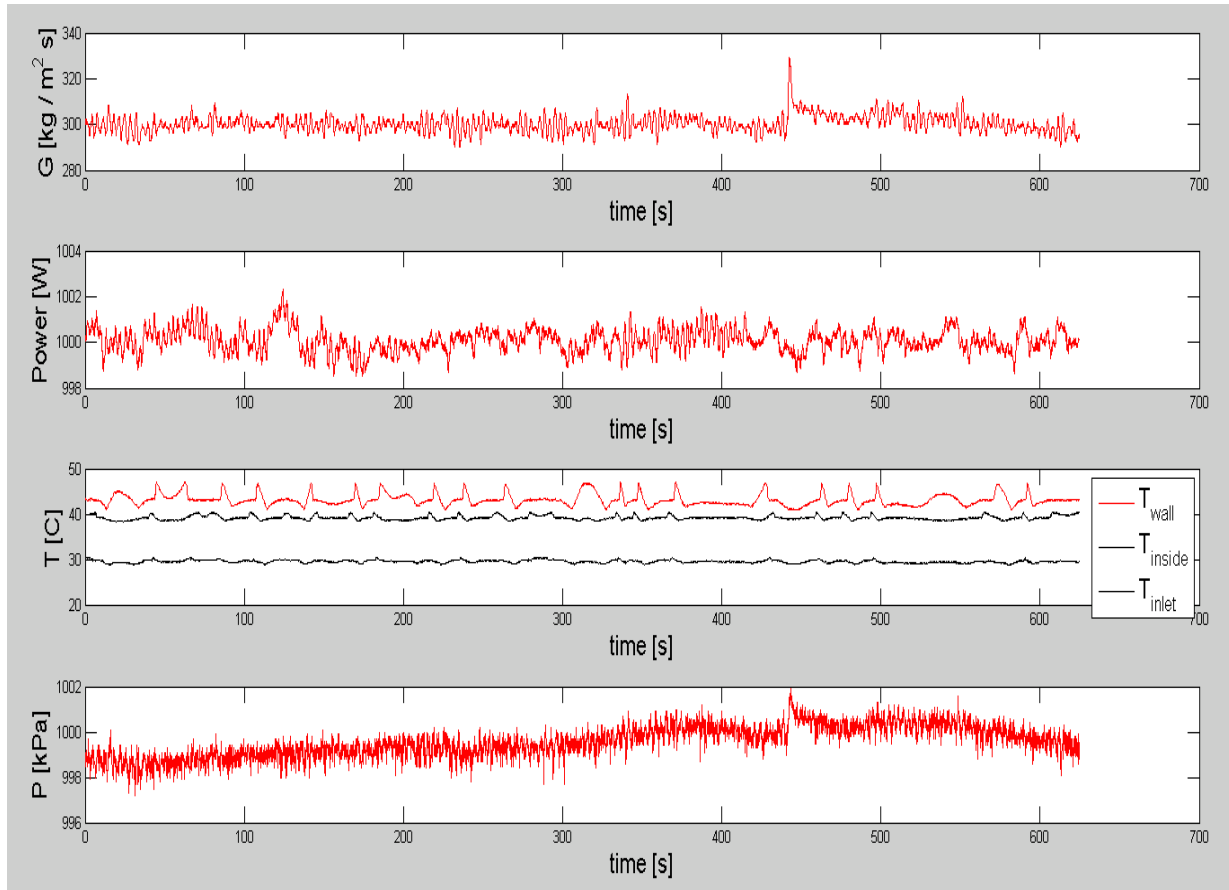


Figure 53: Illustrated data from experiment 20131127-E019.

The figure above is the computed graphs for mass flux in the outlet, total power added to the system, the temperatures at the wall, inside the tube at the outlet (T13 in figure 49) and the temperature at the inlet and the last graph is the measured inlet pressure. All the data is gathered by reconstructing the data acquired by LabVIEW using tools in matlab. The mean total power delivered is 1000 W. In figure 53 the fluctuations of the mass flux are small compared to the total magnitude. By using the tools from section 5.2 to calculate the amplitude and period, and equations 3.1 and 3.2 for the subcooling number N_{sub} and the equilibrium phase change number N_{pch} , respectively, results in:

<i>The amplitude for the mass flux (ΔG) oscillations</i>	<i>11.3 kg/m²s</i>
<i>The period for the mass flux oscillations</i>	<i>3.22 seconds giving a frequency of 0.31 Hz</i>
N_{sub}	1.8
N_{pch}	24.2
$\Delta G/G$	$(11.3/2) / 300.4 = 1.88 \% < 10\%$

Table 22: Estimated results from experiment 20131127-E019.

The system is therefore seen as stable resulting from equation 5.4. Then the power is increased from 1000 to 1050 Watt, while the other given parameters are held (almost) constant:

Experiment 20131127-E001

Operating conditions: $G=300.3 \text{ kg/m}^2\text{s}$, $p_{in}=999.1 \text{ kPa}$, $q=1050 \text{ W}$, $T_{in}=29.5 \text{ }^\circ\text{C}$, $\Delta T_{sub}=10.0^\circ\text{C}$.

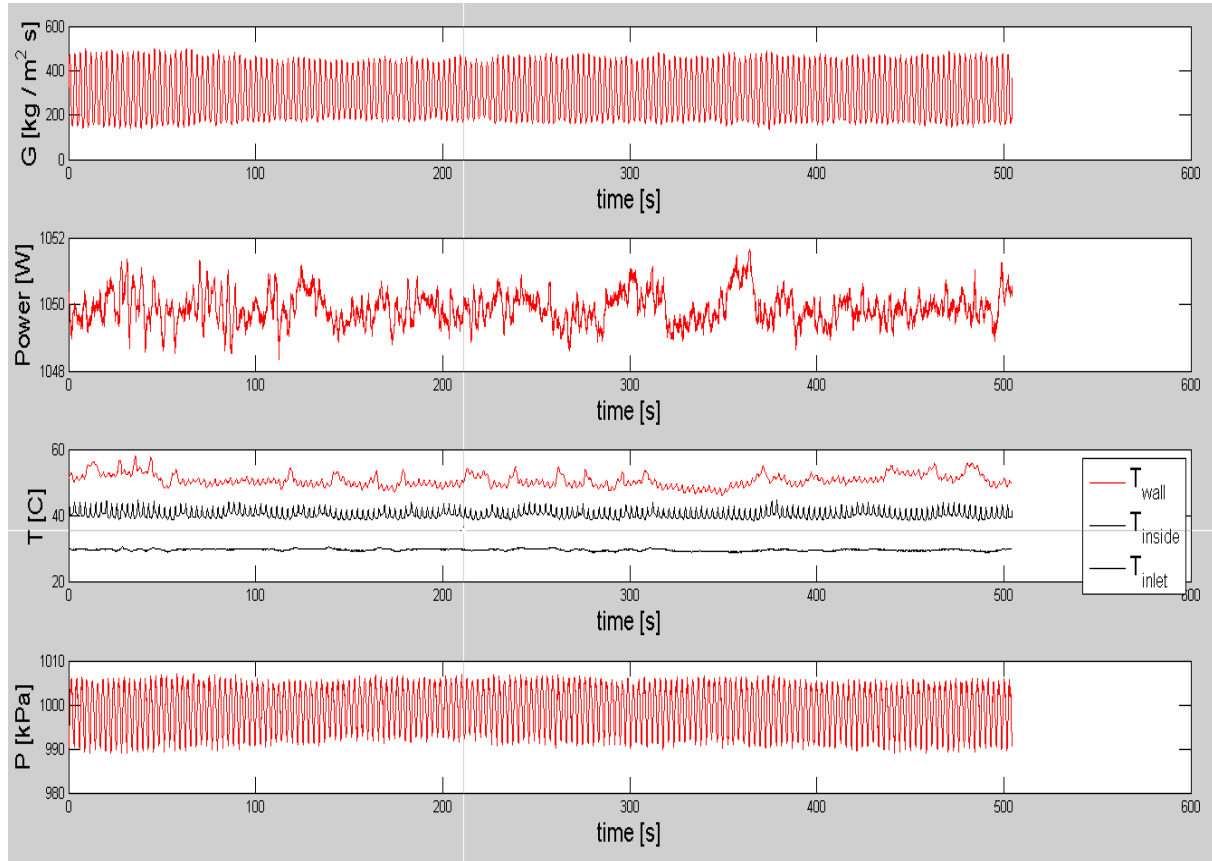


Figure 54: Illustrated data from experiment 20131127-E001.

It is seen that the oscillations have a significant increase for mass flux, power, T_{wall} , T_{inside} and pressure. The estimations are now:

<i>The amplitude for the mass flux oscillations</i>	<i>299.8 kg/m²s</i>
<i>The period for the mass flux oscillations</i>	<i>2.87 seconds giving a frequency of 0.35 Hz</i>
N_{sub}	1.9
N_{pch}	29.2
$\Delta G/G$	$(299.8/2) / 300.3 = 49.9 \% > 10 \%$

Table 23: Estimated results from experiment 20131127-E001.

As a result of the increased oscillations in mass flux, the pressure, the power, the wall temperature T_{wall} and the fluid temperature T_{inside} has also started to oscillate. The subcooling

number is almost unchanged due to approximately the same inlet temperature into the channel. Both the amplitude and frequency of the oscillations are increased. The system is now classified as unstable and it indicates that the increase in added power has a destabilizing effect so that density waves appear. One more experiment is investigated in order to study the effect of an increase in heat within the unstable area. The power input is then increased further from 1050 to 1100 Watt:

Experiment 20131127-E005

Operating conditions: $G=298.9 \text{ kg/m}^2\text{s}$, $p_{in}=1000.0 \text{ kPa}$, $q=1100 \text{ W}$, $T_{in}=29.3^\circ\text{C}$, $\Delta T_{sub}=10.1^\circ\text{C}$.

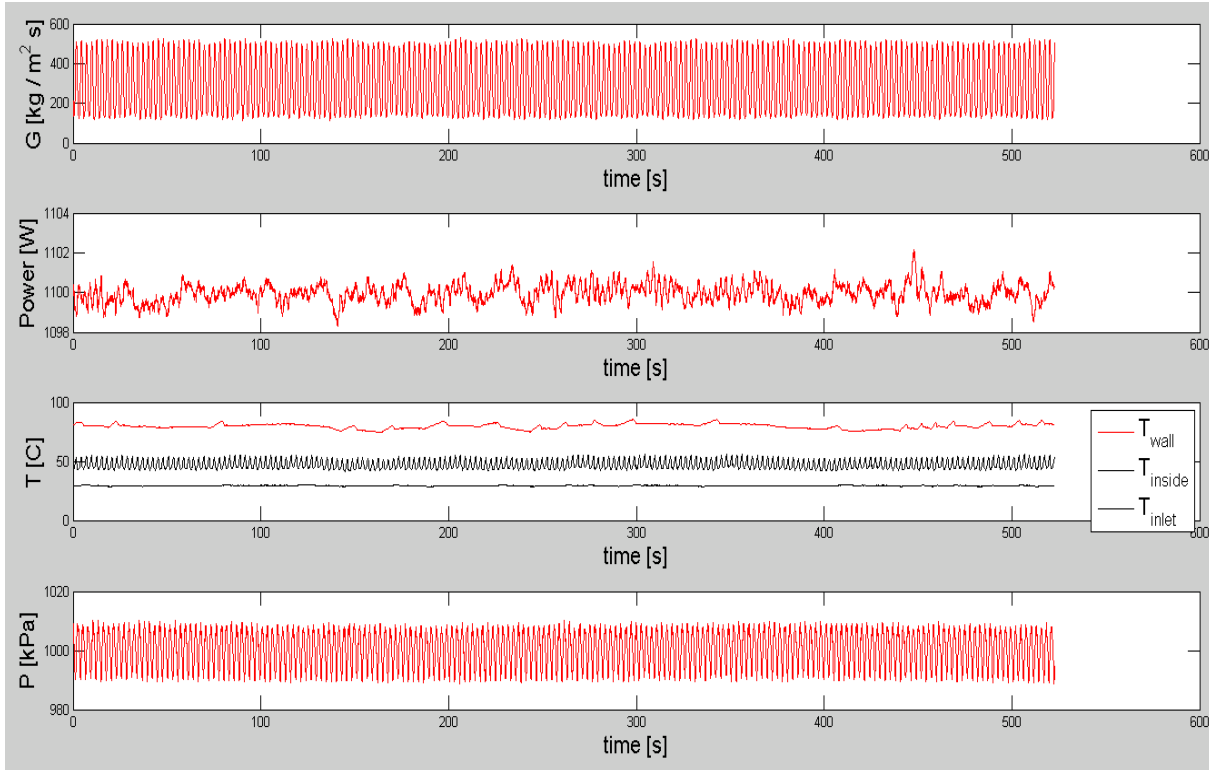


Figure 55: Illustrated data from experiment 20131127-E005.

The key values is:

<i>The amplitude for the mass flux oscillations</i>	<i>392.5 kg/m²s</i>
<i>The period for the mass flux oscillations</i>	<i>2.73 seconds giving a frequency of 0.37 Hz</i>
N_{sub}	2.0
N_{pch}	34.3
$\Delta G/G$	$(392.5/2) / 298.9 = 65.7 \% > 10\%$

Table 24: Estimated results from experiment 20131127-E005.

The increase of heat within the unstable area has increased the amplitude and reduced the period as shown from table 23 and 24. The effects of changing heat indicate the same results as assumed from the literature study.

5.3.2 Inlet subcooling

As mentioned most of the experiments are unstable, but there is still a possibility to look for changes in wave characteristics by studying different operation points within the unstable area. Following are two samples where the only differences in input parameters are the inlet temperatures. To be able to recognize noticing difference only small intervals of the time scale of the following experiments are displayed and only the mass flux is graphed.

Experiment 20130823-E005

Operating conditions: $G=300.2 \text{ kg/sm}^2$, $p_{in}=1100 \text{ kPa}$, $q=1200 \text{ W}$, $T_{in}=31.1 \text{ }^\circ\text{C}$, $\Delta T_{sub}=11.8 \text{ }^\circ\text{C}$ (mean values for the total time interval, not only the timeframe below).

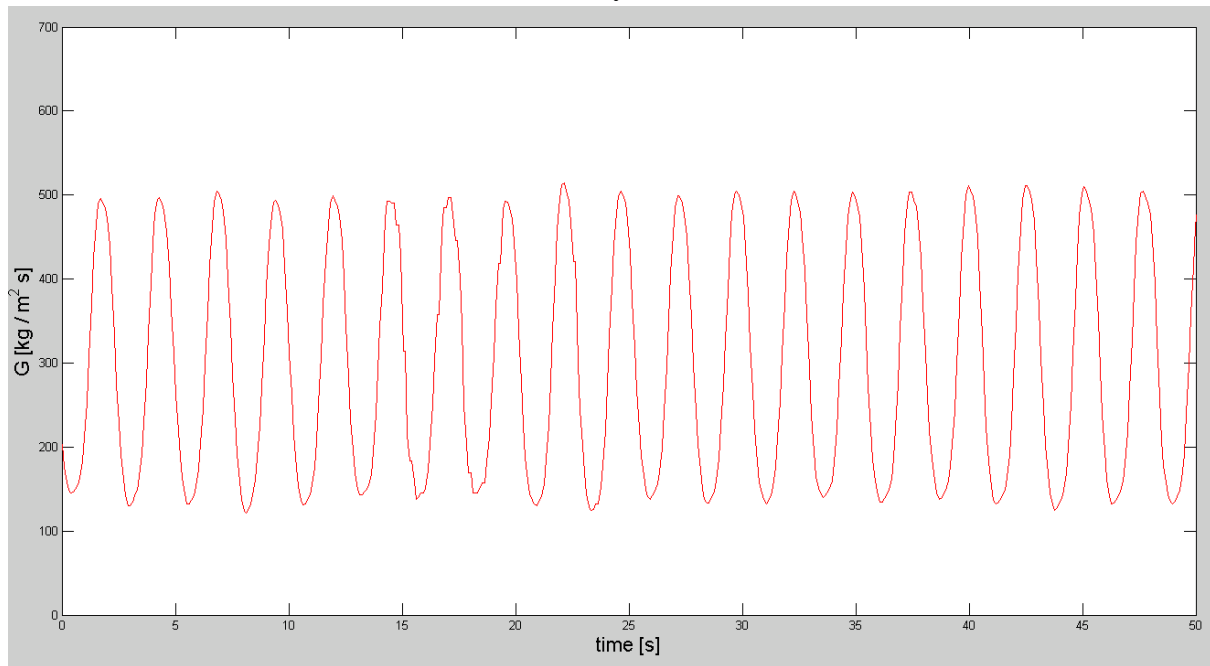


Figure 56: Oscillations for the mass flux in a time interval of the experiment.

The experiment gives:

<i>The amplitude for the mass flux oscillations</i>	$381.6 \text{ kg/m}^2\text{s}$
<i>The period for the mass flux oscillations</i>	$2.57 \text{ seconds giving a frequency of } 0.39 \text{ Hz}$
N_{sub}	2.2
N_{pch}	33.7
$\Delta G/G$	$(381.6/2) / 300.2 = 63.6 \% > 10\%$

Table 25: Estimated results from experiment 20130823-E005.

From the results the system is classified as unstable. The inlet temperature is then lowered by an average of $2.6 \text{ }^\circ\text{C}$ (increased subcooling):

Experiment 20130823-E008

Operating conditions: $G=300.5 \text{ kg/m}^2$, $p_{in}=1099 \text{ kPa}$, $q=1200 \text{ W}$, $T_{in}=28.5 \text{ }^\circ\text{C}$, $\Delta T_{sub}=14.4 \text{ }^\circ\text{C}$

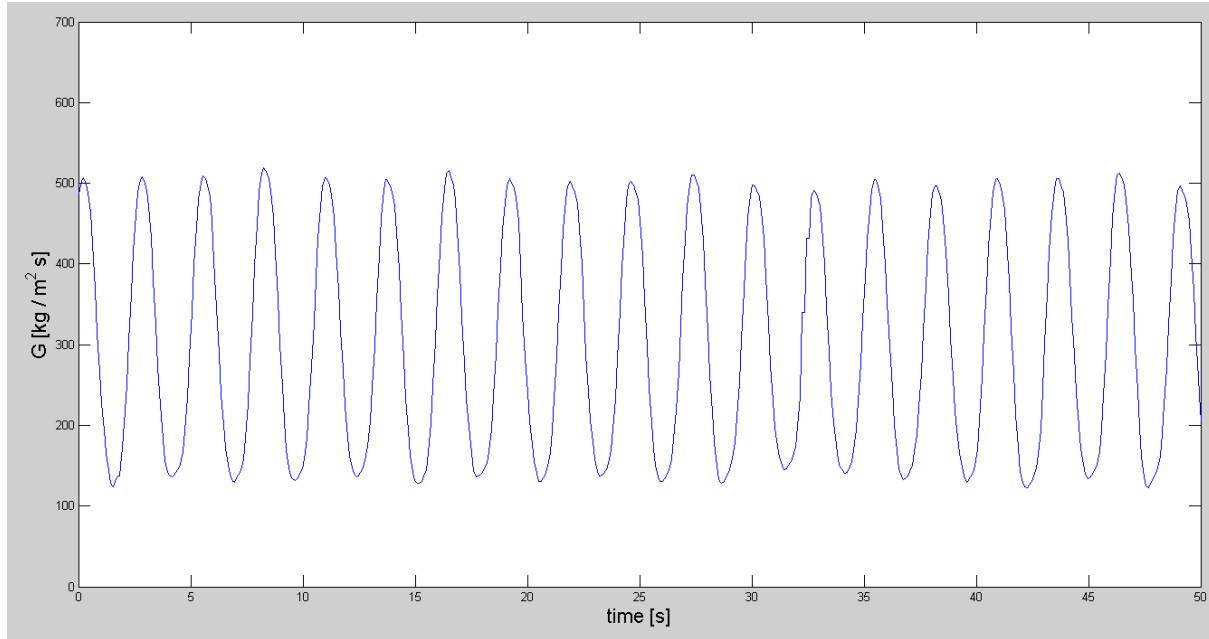


Figure 57: Oscillations for the mass flux in a time interval of the experiment.

The results are:

<i>The amplitude for the mass flux oscillations</i>	$376.5 \text{ kg/m}^2\text{s}$
<i>The period for the mass flux oscillations</i>	$2.74 \text{ seconds giving a frequency of } 0.36 \text{ Hz}$
N_{sub}	2.6
N_{pch}	33.7
$\Delta G/G$	$(376.5/2) / 300.5 = 62.6 \% > 10\%$

Table 26: Estimated results from experiment 20130823-E008.

Both of the samples in experiments are considered unstable. The sample from experiment E008 has a lower inlet temperature and thereby a higher subcooling number, which results in a slightly lower amplitude and frequency than the sample in E005.

Both the experiments are plotted in figure 58 below for another time interval:

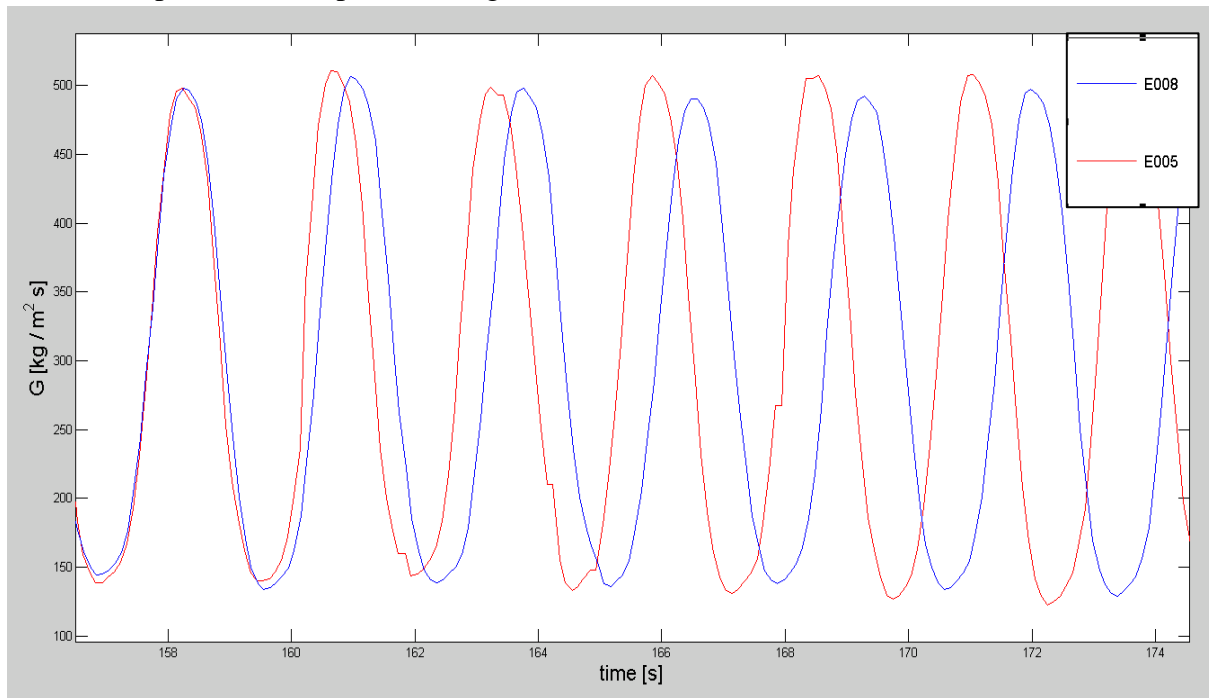


Figure 58: Comparison between experiment E005 and E008, where E005 has a higher inlet temperature.

As shown from figure 58 and the data in table 25 and table 26 it is seen that the lower inlet temperature increased the period and reduced the amplitude, but only with a small amount for this particular case. This is the opposite effect of what has been assumed on the basis of the literature study with regards to amplitude and the same effect regarding period. As discussed in the literature review a few cases of increased subcooling in the study of Strømsvåg [2011] also showed decreased amplitude with increased subcooling, even though the general tendency was shown to be the opposite. Other operating conditions should be investigated in order to find a general tendency between subcooling and amplitude.

5.3.3 Inlet pressure

The inlet pressure can be adjusted in the experimental system. The mass flux curves are only shown together in a limited timeframe to illustrate the changes in amplitude and period.

Experiment 20131009-E005:

Operating conditions: $G=303.2 \text{ kg/sm}^2$, $p_{in}=581.0 \text{ kPa}$, $q=1199 \text{ W}$, $T_{in}=0.6 \text{ }^\circ\text{C}$, $\Delta T_{sub}=19.9^\circ\text{C}$

The key values for the given operating conditions become:

<i>The amplitude for the mass flux oscillations</i>	332.7 kg/m ² s
<i>The period for the mass flux oscillations</i>	2.17 giving a frequency of 0.46 Hz
N_{sub}	6.4
N_{pch}	57.1
$\Delta G/G$	(332.7/2) / 303.2 = 54.9 % > 10 %

Table 27: Estimated results from experiment 20131009-E005.

From equation 5.4 the system is classified as unstable. The inlet pressure is then increased by an average of 52.4 kPa while the rest of the operating conditions are held almost constant.

Experiment 20131009-E002:

Operating conditions: $G=299.0$ kg/sm², $p_{in}=633.4$ kPa, $q=1998$ W, $T_{in}=3.7$ °C, $\Delta T_{sub}=19.6$ °C

The inlet temperature has increased from the previous experiment at the same amount as the change of the boiling point due to the increase of pressure, to keep the subcooling temperature approximately unchanged. The boiling point for the fluid R134a at the inlet pressure of 633.4 kPa is 23.4 °C and at 581.0 kPa (for the previous experiment 20131009-E005) is 20.5 °C, giving a difference of 2.9 °C. The inlet temperature for this experiment is 3.7 °C and the previous was 0.6 °C giving a difference of 3.1 °C, making the subcooling temperatures almost constant.

The key values for the given operating conditions become:

<i>The amplitude for the mass flux oscillations</i>	342.0 kg/m ² s
<i>The period for the mass flux oscillations</i>	2.15 giving a frequency of 0.47 Hz
N_{sub}	5.8
N_{pch}	53.4
$\Delta G/G$	(342.0/2) / 299.0 = 57.2% > 10%

Table 28: Estimated results from experiment 20131009-E002.

The two mass flux curves together for a short timeframe becomes:

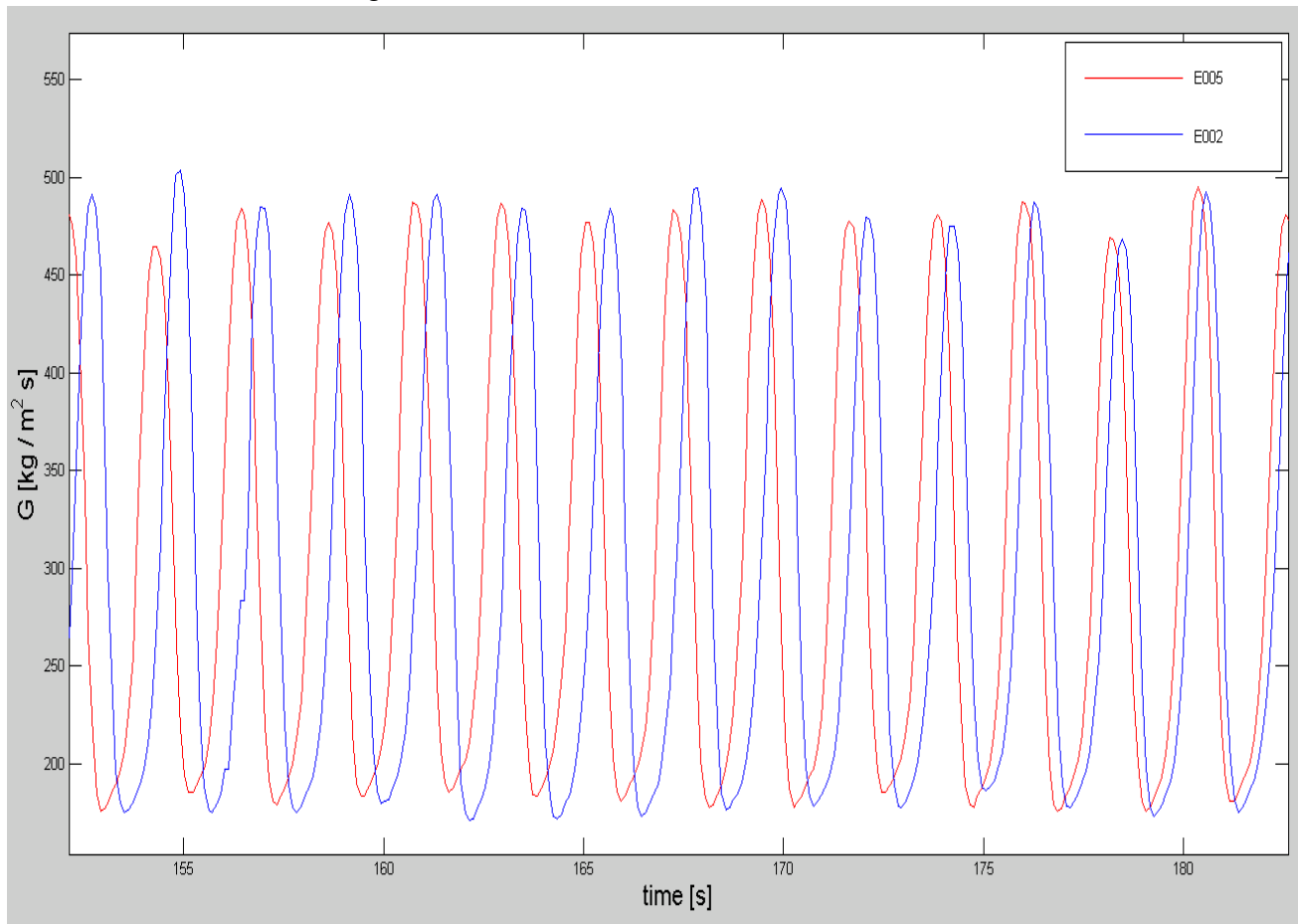


Figure 59: Comparison between experiment E005 (red) and E002 (blue), where E002 has a higher inlet pressure.

As seen when comparing table 27 and 28, the amplitude has increased due to the increased pressure. This leads to the opposite conclusion of the established hypothesis, but is similar to the effects gathered from Sørnum [2013] in figure 20 at similar mass flux. The period is approximately unaffected and thereby acts as assumed in the hypothesis.

5.3.4 Mass flux

The mass flux into the system can be varied. Not many experiments from the used database have adjusted the mass flux without adjusting other parameters simultaneously, but here one sample is presented. The mass flux curves are only shown together for a limited timeframe.

Experiment 20131017-E006:

Operating conditions: $G=304,0 \text{ kg/sm}^2$, $p_{in}=694,0 \text{ kPa}$, $q=1400 \text{ W}$, $T_{in}=16,4 \text{ }^\circ\text{C}$.

The extracted results from the given operating conditions become:

<i>The amplitude for the mass flux oscillations</i>	502.3
<i>The period for the mass flux oscillations</i>	1.69 seconds giving a frequency of 0.59 Hz.
N_{sub}	2.8
N_{pch}	68.0
$\Delta G/G$	$(502.3/2) / 304.0 = 82.6 \% > 10\%$

Table 29: Estimated results from experiment 20131017-E006.

This experiment is considered unstable. The mass flux is then increased from an average of 304 kg/sm^2 to 397 kg/sm^2 :

Experiment 20131017-E023:

Operating conditions: $G=397.0 \text{ kg/sm}^2$, $p_{in}=699.0 \text{ kPa}$, $q=1400 \text{ W}$, $T_{in}=16.8 \text{ }^\circ\text{C}$.

The results are:

<i>The amplitude for the mass flux oscillations</i>	446.2
<i>The period for the mass flux oscillations</i>	1.69 seconds giving a frequency of 0.59 Hz.
N_{sub}	2.7
N_{pch}	41.4
$\Delta G/G$	$(485.9/2) / 397.0 = 56.2 \% > 10\%$

Table 30: Estimated results from experiment 20131017-E023.

Both systems are classified as unstable. Plotted together:

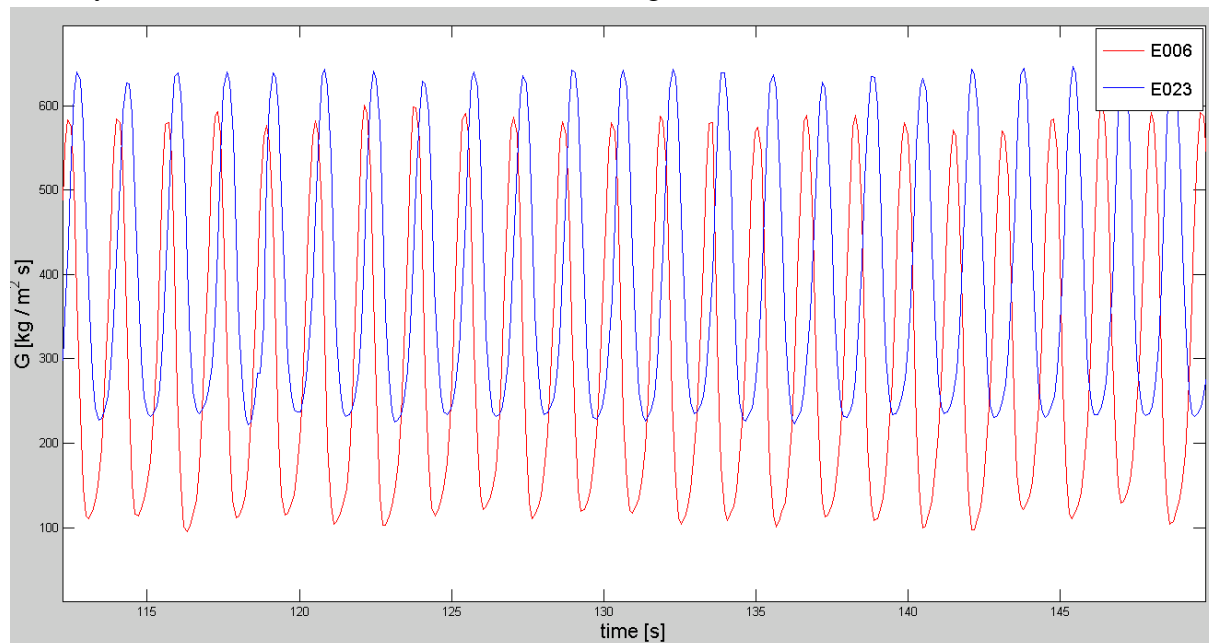


Figure 60: Comparison between experiment E006 and E023, where E023 has a higher mass flux.

From figure 60 it is clearly shown that the amplitude are lower for experiment E023, where the mass flux was the highest and thereby correlates with the assumed effect in the hypothesis. The hypothesis suggested an increase in period due to the increase in mass flux, but for these conditions and from table 29 and 30 showed that the period remained the same.

5.4 Differences and similarities between numerical and experimental tests

The experimental results are by definition correct in sense of characterizing effects and measurement errors are among the few differences between “the real life situations” and the results presented. From section 5.3 it is seen that the experimental results gives marginally stable conditions on both sides of the stability boundary, while chapter 4 showed that the code resulted in converging oscillations on the left side of the stability boundary and diverging oscillations on the right side. This behavior indicates that the numerical code only has a chance of coinciding with the experimental results when operating on the stability boundary, if the same boundary is modeled. Most of the experimental results are as mentioned earlier set up with the intention of producing DWO and includes a very high heat number. If these conditions were to be set up with the numerical model the oscillations would oscillate out of the physical limits after a short amount of time (highly diverging amplitudes) as in section 4.5.2 simulation nr 1. Possible reasons for these differences between the model-predicted flow behavior and the experiments are too many to mention, but it might be due to backflow through the channel as the oscillations increase, inertial effects, user made errors in the simulation code or physical limitations such as the confinement walls. This is left as an assignment for further investigation.

All the found parametric effects become:

<i>Hypothesis</i>	Increased heat	Inc. subcooling	Inc. pressure	Inc. mass flux
Amplitude	Positive	Positive	Negative	Negative
Period	Negative*	Positive	No effect	Positive
<i>Model prediction</i>	Increased heat	Inc. subcooling	Inc. pressure	Inc. mass flux
Amplitude	Positive	Positive	Negative	Inconclusive
Period	Negative	Positive	Inconclusive	Inconclusive
<i>Experimental study</i>	Increased heat	Inc. subcooling	Inc. pressure	Inc. mass flux
Amplitude	Positive	Negative	Positive	Negative
Period	Negative	Positive	No effect	No effect

Table 31: Comparison of characterizing effects from the literature study, the simulations and the studied experiments.

*no opposing effects found in the literature study

Be aware that the listed parametric effects for the experiments are conducted for different operating conditions than the numerically found effects, and might lead to different wave characteristics. The assumption that was made in chapter 4 regarding the effect of increased heat is supported both by the literature study and the experimental study. The effect of increasing heat has to be accurate for the other model predicted parametric effects to be correct. The only

opposing effect regarding inlet subcooling was found experimentally regarding the amplitude. This was a small decrease and more operating conditions should be looked at to find a general tendency between amplitude and increased subcooling. For the increased pressure, both the literature study and the model predicted diminished amplitude. The experimental study showed increased amplitude and this was also found experimentally by Sørum [2013] in the same facility at similar mass flux. Sørum also found decreased amplitude at higher mass flux in figure 21, but this has not been investigated in this report. The experimental study and the literature study both showed diminished amplitude for increased pressure. The effect of increased pressure regarding the period was not found by the model because more than one parameter could have caused the change (heat or pressure). For the same reason the characterizing effects of the mass flux could not be found by the model. The experimental study and the literature study showed decreased amplitude for increased mass flux, while the period was found experimentally to be unchanged with mass flux. Figure 20 from Sørum indicated that this can change with the amount of heat input. This has not been investigated in this report.

6 Conclusion

6.1 Summary

The dynamic instability density wave oscillations have been investigated through a literature study, numerically and by studying experiments. In addition to the given assignment regarding the parametric effects of applied heat, pressure and inlet subcooling, also the mass flux has been investigated numerically and experimentally. The literature study consisted of both numerical and experimental results and a hypothesis based on the literature study was made regarding amplitude and period with heat-, pressure-, subcooling- and mass flux changes.

The code was shown to predict converging mass flux oscillations in the stable area of the stability map and diverging behavior in the unstable area. A procedure to extract the amplitude and period from the modeled mass flux curves was established and a method to reduce the amount of simulations needed to find the marginally stable operating conditions was developed. The numerically obtained stability threshold is predicted to be far to the left of the experimentally obtained threshold found in literature, making the unstable area to the right of the stability boundary larger. This leads the modeled diverging DWO to appear at lower heat numbers. The reason for the difference between the stability thresholds is attributed to backflow through the channel as the oscillations increase, inertial effects, the absence of a pump in the model and physical limitations such as the confinement walls. To be able to compare the numerically obtained results with experimental results from the lab, a procedure for extracting the amplitude and period has also been done for the recreated experimental results. The oscillations in the experiments were found to be marginally stable also within the unstable area of the stability map, making it easier to extract the characterizing effects of changing parameters compared to the model.

In addition to finding the stability boundaries for DWO, the model was also used to perform a parametric study of the variables affecting the characteristics of the oscillations. Although the change of amplitude and period were found for increasing applied heat, pressure, inlet subcooling and mass flux, they did not all coincide with the literature study and the predicted parametric effects. The effect of increasing applied heat is found to increase the amplitude and reduce the period of the oscillations by both the numerical and the experimental results. The modeled results predict the increased inlet subcooling to increase the amplitude and the period. However, the experimental results displays a small decrease in amplitude for increased inlet subcooling for the set operating conditions, while the period shows the same effect as the modeled results. The increased pressure is by the model shown to decrease the amplitude, but the opposite is shown by the experimental results for different operating conditions. The different operating conditions might be the cause of the difference between the model predictions and the experimental results. The effects of mass flux can be caused by both heat variations and change of the mass flux so no conclusion can be made from the model. Similarly, the change of the period when increasing the pressure can also be caused by both the pressure change and the change of applied heat.

The studied experiments shows increased amplitude with increased pressure and decreased mass flux, while the period remains unaffected by pressure and mass flux variations.

6.2 Future work

In order to improve the model it is suggested to implement a pump in between the two reservoirs and to implement the effect of backflow through the channel. The reason for the contradicting parametric effects that is encountered in the experimental results might occur due to different operating conditions. From the literature study it is seen that opposing effects can occur for the period of oscillations when varying mass flux for different heat inputs and it is also implied that the period of pressure depends on the level of mass flux. To study if these effects will be predicted by the numerical model is left as a suggested future assignment. Also a more exact amplitude extraction from the experiments would be useful, by a more “sophisticated” method. The function used in this report will as mentioned filtrate out the lower disturbances, and a function should be developed for to also filtrate out the upper disturbances (section 5.2).

References

- Akagawa, K., Sakaguchi, T., Kono, M., & Nishimura, M. (1971). Study on Distribution of Flow Rates and Flow Stabilities in Parallel Long Evaporators. *Japan Society of Mechanical Engineers Vol.14 No 74*, p. 532.542 : 536.423.
- Aldridge, C., & Fowler, A. (1996). Stability and instability in evaporating two-phase flows. *Surveys on Mathematics for Industry*, 75-107.
- Ambrosini, W., & Ferreri, J. (2006). Analysis of basic phenomena in boiling channel instabilities with different flow models and numerical schemes. *International Conference on Nuclear Engineering*. Miami.
- Ambrosini, W., Di Marco, P., & Ferreri, J. (2000). Linear and Non-Linear Analysis of Density-Wave Instability Phenomena. *International Journal of Heat and Technology*, Vol 18, No 1, pp. 27-36.
- Belblidia, L., & Bratianu, C. (1979). Density-Wave Oscillations. *Annals of Nuclear Energy*, 425-444.
- Bergland, G. (1969). A guided tour of the fast Fourier transform. *Spectrum, IEEE Volume 6, Issue 7*, 41-52.
- Bouré, J., Bergles, A., & Tong, L. (1973). Review of two-phase flow instability. *Nuclear Engineering and Design*, 165-192.
- Chiapero, E. M. (2013). *Two-phase flow instabilities and flow mal-distribution in parallel channels*. Trondheim: Norwegian University of Science and Technology, Department of Energy and Process Engineering, MSc thesis.
- Collins, D., & Gacesa, M. (1969). Hydrodynamic Instability in a full-scale simulated reactor channel. *Proceedings of the Institution of Mechanical Engineers*, (pp. 115-126).
- Colombo, M., Cammi, A., Papini, D., & Ricotti, M. (2012). RELAP5/MOD3.3 study on density wave instabilities in single and parallel channels. *Progress in Nuclear Energy*, 15-23.
- Comakli, Ö., Karsli, S., & Yilmaz, M. (2002). Experimental investigation of two phase flow instabilities in a horizontal in-tube boiling systems. *Energy Conversion and Management*, 249-268.
- Ding, Y., Kakac, S., & Chen, K. (1995). Dynamic Instabilities of Boiling Two-Phase Flow in a Single Horizontal Channel. *Experimental Thermal and Fluid Science*, pp. 327-342.
- Dolgov, V., & Sudnitsyn, O. (1965, December). Hydrodynamic instability in boiling-water reactors. *Teploenergetika Vol 3*.

- Ghiaasiaan, S. (2008). *Two-Phase Flow Boiling and Condensation in Conventional and Miniature Systems*. New York: Cambridge University Press.
- Incropera, F., Dewitt, D., Bergman, T., & Lavine, A. (2013). *Principles of Heat and Mass Transfer*. Singapore: Jon Wiley & Sons, Inc.
- Ishii, M., & Zuber, N. (1970). Thermally induced flow instabilities in two phase mixtures. *Proceedings of the fourth international heat transfer conference*.
- Kakac, S., & Bon, B. (2008). A review of two-phase flow dynamic instabilities in tube boiling systems. *International Journal of Heat and Mass Transfer* 51, pp. 399-433.
- Maerschallck, B. (2003). *Space-Time least-squares spectral element method for unsteady flows—application and evaluation for linear and non-linear hyperbolic scalar equations*, Master Thesis Report. Delft University of Technology, Department of Aerospace Engineering.
- Mathisen, R. (1967). Out of pile channel instability in the loop skalvan. *Symposium on Two-phase Flow Dynamics*.
- Ozawa, M., Nakanishi, S., Ishgai, S., Mizuta, Y., & Tarui, H. (1979). Flow Instabilities in Boiling Channels. *Bulletin of the JSME Vol. 22*, pp. 1113-1118.
- Papini, D., Cammi, A., Colombo, M., & Ricotti, M. (2011). On Density Wave Instability Phenomena -Modeling and Experimental Investigation. *Ahsan, A (Ed.), Two-Phase Flow, Phase Change and Numerical Modeling, InTech publisher, Rijeka*, pp. 257-284.
- Papini, D., Cammi, A., Colombo, M., & Ricotti, M. (2012). Time-domain linear and non-linear studies on density wave oscillations. *Chemical Engineering Science*, 118-139.
- Rizwan-Uddin. (1994). On density-wave oscillations in two-phase flows. *Int. J. Multiphase Flow*, 721-737.
- Ruspini, L. (2013). *Experimental and numerical investigation on two-phase flow instabilities*, Phd Thesis. Trondheim: Norwegian University of Science and Technology, Department of Energy and Process Engineering.
- Saha, P., Ishii, M., & Zuber, N. (1976). Experimental investigation of the thermally induced flow oscillations in two-phase systems. *Journal of Heat Transfer*, 616-622.
- Sørum, M. (2013). *Experimental investigation of the effects of heat flux and mass flow rate in the oscillations characteristic of Density Wave Oscillations*. Trondheim: Norwegian University of Science and Technology, Department of Energy and Process Engineering, Project thesis.

- Strømsvåg, D. (2011). *Fundamental mechanisms of density wave oscillations and the effect of subcooling*. Trondheim: Norwegian University of Science and Technology, Department of Energy and Process Engineering, MSc thesis.
- Thome, J. (2004). *Engineering Data Book 3*. Lausanne: Wolverine Tube, Inc.
- Ugueto, L. (2013). *Experimental study of density waves*. Trondheim: Norwegian University of Science and Technology, Department of Energy and Process Engineering, MSc thesis.
- Wang, Q., Chen, X., Kakac, S., & Ding, Y. (1994). An experimental investigation of density-wave-type oscillations in a convective boiling upflow system. *Int. J. Heat and Fluid Flow* Vol. 14, No 3, pp. 241-246.
- Wattelet, J., Chato, J., Christoffersen, B., Gaibel, J., Ponchner, M., Kenney, P., et al. (1994). *Heat Transfer Flow Regimes of Refrigerants in a Horizontal-Tube Evaporator*. Illinois: Air Conditioning and Refrigeration Center.
- White, F. (1991). *Viscous Fluid Flow*. McGraw-Hill Book Company.
- Yuncu, H. (1990). An Experimental and Theoretical Study of Density Wave and Pressure Drop Oscillations. *Heat Transfer Engineering*, pp. 11:45-56.
- Yuncu, H., Yildirim, O., & Kakac, S. (1991). Two-phase flow instabilities in a horizontal single boiling channel. *Applied Scientific Research*, pp. 48:83-104.